POLITECNICO DI MILANO

Master of Science in
Civil Engineering for Risk Mitigation

Dynamic monitoring and structure assessment of “Gabbia Tower”

Supervisor: Prof. Gentile Carmelo

MSc Thesis of:

Xu Man ID. 780276

Academic Year 2012 – 2013

Content

Abstract

This MSc Thesis deals with long-term dynamic monitoring, modal identification and damage assessment of a masonry tower. The investigated tower, about 54.0 m high and dating back to the XII century, is known as the “Gabbia” Tower and is the major historic tower in Mantua, Italy.

After the earthquake of May 29th, 2012 an extensive research program was planned and performed to evaluate the structural condition of the tower. A metal scaffolding and a light wooden roof have been installed inside the tower later. The results of the investigations clearly highlighted the critical situation of the tower, pointing out the need for structural monitoring and intervention work. A simple permanent dynamic monitoring system (including three highly sensitive accelerometers and one temperature sensor) was installed in the tower, with structural health monitoring and seismic early warning purposes.

After a description of literature review about structure assessment and theory of operational modal analysis, the Dissertation summarizes the information provided by visual inspection and dynamic tests, clearly highlighting the poor structural condition and the high seismic vulnerability of the upper part of the tower. Subsequently, the permanent dynamic monitoring system installed on the tower is described and the results of the monitoring are presented and discussed.

Introduction

The Dissertation is focused on one historic masonry tower in Italy. The “Gabbia” Tower, dating back to the XII century, is located in Mantua, the north of Italy (Figure 0-1). Two severe earthquakes happened in May 2012. Damages were reported on several historic buildings placed in the town of Mantua, where Politecnico di Milano has a large campus. Consequently, “Polo Territoriale di Mantua” and the VIBLAB (Laboratory of Vibration and Dynamic Monitoring of Structures) of Politecnico di Milano was committed to assess the structural condition and to evaluate the seismic performances of the "Gabbia" Tower.

In the first chapter, introduction about the issues related to historic structures is presented. Historic, geometric surveys and visual inspections always draw a clear view of the condition of historic structures: cracks and repair work dating back from different period are the main causes of structure discontinuity, which increase the risk of the structures of being damaged during certain attacks. Ambient vibration tests (AVT) and long-term monitoring are helpful in evaluating structure characteristics. Aging and deterioration phenomena on existing structures provided strong motivations to develop efficient vibration-based damage detection methods, often supported by monitoring systems collecting over time the vibration response of a structure at selected points (Cunha & Caetano 2006).

Within this framework, Operational Modal Analysis (OMA) is nowadays considered as a reliable tool for modal identification from experimental data collected in operational conditions (ambient vibration tests and long-term dynamic monitoring test). The management of data acquired from in-situ tests calls for operational modal analysis methods. The theory of two main operational modal analysis methods is introduced in Chapter 2. In addition, two commercial computer codes are applied for the data management, DADISP and ARTeMIS.

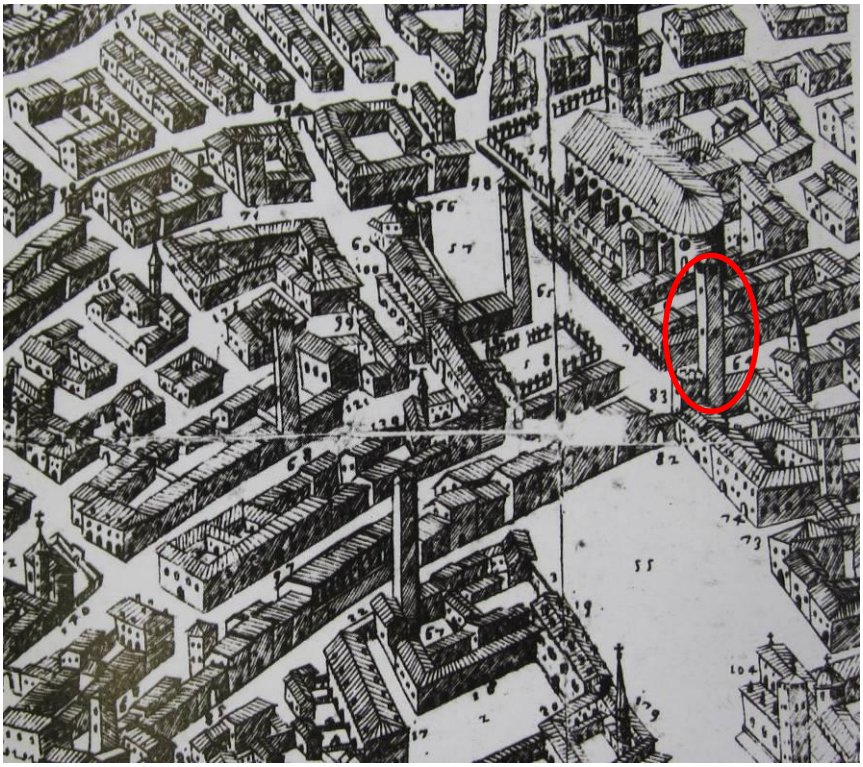

Figure 0-1 G. Bertazzolo (1628) Description of Urban area of Mantua

Figure 0-2 Tower of "Gabbia": overall views and details of the top and the cage

After the earthquake of May 29th, 2012 an extensive research program was planned and performed to evaluate the structural condition of the tower. In Chapter 3, the first part of the research is presented, which includes: (a) historic and documentary

research; (b) geometric survey and visual inspection of the bearing walls; (c) on-site survey of the crack pattern and structural discontinuities; (d) non-destructive and slightly destructive tests of materials on site (i.e. sonic pulse velocity tests and flat-jack tests); (e) dynamic tests in operational conditions (Gentile et al, 2013). Visual inspection of all main bearing walls clearly indicated that the upper part of the tower is characterized by the presence of several discontinuities due to the historic evolution of the building, local lack of connection and extensive masonry decay (Figure 0-3).

The poor state of preservation of the same region was confirmed by the observed dynamic characteristics and one local mode involving the upper part of the tower was clearly identified by applying different output-only techniques to the response data collected for more than 24 hours on the historic building. These results clearly highlighted the critical situation of the upper part of the tower, pointing out the need for structural interventions to be carried out. With this motivation, and in order to allow better indoor inspection of the tower bearing walls, a metal scaffolding and a light wooden roof have been installed inside the tower. Hence, a second dynamic test with the same instrument of the first one was performed, aiming at checking the possible effects of scaffolding and wooden roof on the modal characteristics of the structure.

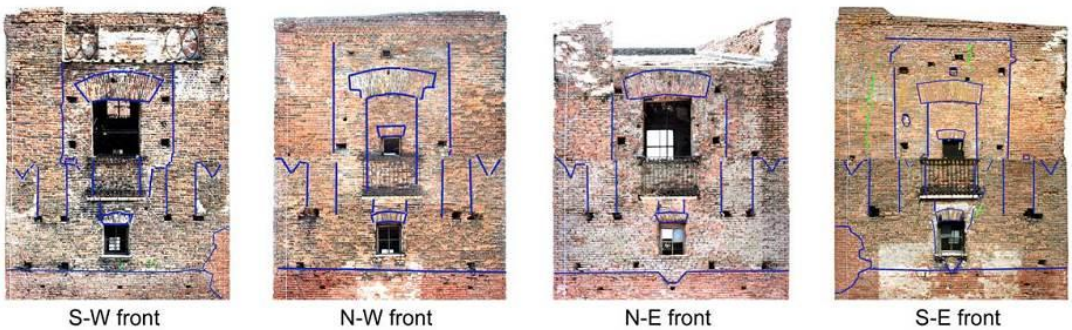

Figure 0-3 Map of the discontinuities on top of the "Gabbia" tower.

There appeared a significant change (Figure 0-4) between the results of 1st and 2nd AVT, pointing out a possibility of damage. A simple permanent dynamic monitoring system (including three highly sensitive accelerometers and one temperature sensor)

was installed (Gentile et al, 2013) in the tower for the structure assessment. Monitoring can play a significant role in diagnosis, and can be applied not only before the intervention to verify if the phenomena are progressing or to obtain global structural properties, but also during and after the works, to control and evaluate their performance (Ramos et al. 2013).

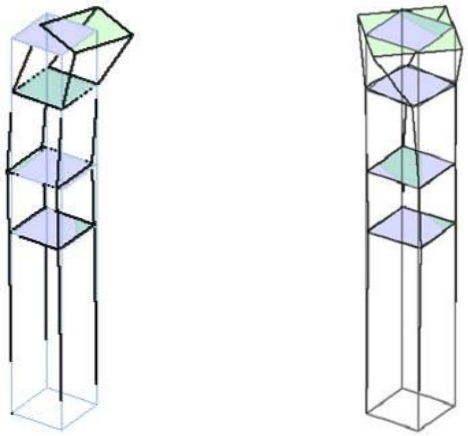

a) $f_5^{T1} = 6.885Hz$ b)$f_5^{T2} = 9.893\ Hz$

Figure 0-4 The natural frequency of local mode (5th mode) from a) 1st AVT; b) 2nd AVT

Dynamic characteristic is the most typical index to explore the service condition of the structures. And according to long-term monitoring, dynamic characteristic can be extracted by Frequency Domain Decomposition (FDD) method, Stochastic Subspace Identification (SSI) method and some other methods. In Chapter 4, details of the long-term dynamic monitoring system are explained. The results of the management of data show well the structure characteristics by natural frequency. The first five natural frequencies are extracted for further analysis. The correlation between natural frequency and temperature (environment effect) is taken into consideration before the assessment of damage. What's more, the earthquake on June 21th, 2013 was well recorded by the dynamic monitoring system. The variation of the frequencies before and after the earthquake was clearly detected.

Chapter 1

Ambient Vibration Testing and Monitoring in the Assessment of Historic Structures

1.1 Introduction

Historic structures play an important role in the cultural heritage. Several historic buildings existing now can trace back to several centuries ago and are meaningful traces and document of the urban development in the history. Nowadays, a large number of problems of aging and degradation can be observed in historic structures. What's more, in seismic zones, earthquakes occur frequently, which increase the demands for safety of historic structures. The general issues about historic structures and their preservation are presented in Paragraph 1.2.

Between historic buildings, churches are present in every town in Italy, and a bell-tower is usually standing beside a church. Furthermore, historic slender military architectures and civic towers are diffused. Therefore, among the historic buildings, towers take a high percentage, very well recognisable in the urban skyline of the historic centres. They are often in strategic position and in same case they became the symbol of the city (e.g. the Tower of Pisa, The Asinelli Tower in Bologna, the Torrazzo in Cremona, etc.). Such building typology shows specific behaviour and damages in case of seismic actions. Because of their position, often in strategic places in the urban centre, and for their massive structural geometry, towers need accurate controls in order to guarantee their safety and preservation. In the thesis, surveys and tests were

focus on the tallest historic tower in Mantua, Italy.

Integrity assessment of historic masonry buildings requires comprehensive knowledge about the structural systems, materials properties, boundary conditions, causes of the damages as well as their vulnerability. Typical steps of the assessment of a historic building include following aspects: historic and documentary research, geometrical surveys, as well as visual inspections which are the starting point of any structural evaluation. Non-destructive and/or slight destructive tests could help in qualifying the materials and some structural detailing or morphology of the masonry. All of these surveys and tests are considered as starting point of the diagnosis, according to which, finite element models can be set up and calibrate on the base of global tests such as dynamic testing. These diagnostic approaches are presented in Paragraph 1.3.

The uncertainties of parameters can't be avoided during the numerical modelling. Hence, calibration of numerical models is essential. Since it's not practical to set up thousand non-destructive tests all over the structure in order to provide all the parameters, an overview of the behaviour of the structure is more useful for the calibration. Experimental data obtained from ambient vibration tests could be effectively used to identify structural dynamic characteristics for the FEM calibration. In Paragraph 1.4, the theory and applications of ambient vibration tests are introduced. Long period acquisition systems (monitoring) can be installed to detect the eventual evolution of the structural behaviour due to ageing or to aggressive actions like strong winds or seismic events. The arrangement and function of long-term monitoring system is introduced in Paragraph 1.5.

1.2 Typical issues related to historic structures

With the passage of time many historic structures collapsed or were damaged due to unexpected actions, such as strong wind, earthquakes and so on. Nevertheless, not only exceptional events affect historic structures. Fatigue and strength degradation, accumulated damage due to material decay, environmental actions, soil settlements

and the lack of structural understanding could affect historic buildings.

Masonry material was common used, taking advantage of the stability and durability of the material. Masonry building represents a box-type structural system composed of vertical structural elements - walls - and horizontal structural elements – floors and roofs. Vertical loads are transferred from the floors, acting as horizontal flexural members, to the bearing walls, and from the bearing walls, acting as vertical compression members, to the foundation system.

As known, when a building is subjected to an earthquake motion, the inertia force, proportional to the masses of the structural system has to be taken into account. Those action effects depend on various parameters, such as the mass and the stiffness of the structure and their distribution, the magnitude of the imposed actions, the number of cycles of the earthquake motion, the characteristics of the foundation soil, etc.

Since the ground motion is in general three-directional both vertical and horizontal inertia forces will be acting on the structure, inducing displacements, changing in-time (both in magnitude and in sign), and resulting in the three-dimensional vibrations of the building.

Horizontal inertia actions are transferred from the floor structures, which should act as rigid horizontal diaphragms, into the bearing walls, causing shearing and bending effects, and from the bearing walls into the foundation system. Additionally, due to the distributed mass of wall elements, distributed inertia forces are induced resulting in out of plane bending of walls.

Experimental testing and observation of damage modality of real structures have shown that masonry walls are less resistant to actions perpendicular to their medium plane (out-of-plane actions) than to actions parallel to this plane (in-plane actions). In the first case, the stiffness of the wall is far less than in the other. For a good load bearing behaviour, all walls of a masonry building should resist actions parallel to them, avoiding inflection and overturning. This philosophy considers the behaviour of the building as a box. The walls should be connected, by stiff constraints to the floor,

because the floor should be able to distribute the seismic actions between the walls as a function of their stiffness.

It is generally recognized that a satisfactory seismic behaviour is attained only if out-of plane collapse is prevented and in-plane strength and deformation capacity of walls can be fully exploited.

The seismic vulnerability of masonry buildings depends on several parameters, such as in-plan and/or in-height irregularity, discontinuity of walls/piers along the height of the building, alteration of the initial structural scheme during the lifetime of the building, inadequate interventions after previous seismic events, low quality construction type of masonry and/or low quality of materials, inadequate connections among vertical elements or between horizontal and vertical elements, lack of any diaphragm action of horizontal bearing elements, etc.

Box action results in limiting the deformations imposed to masonry during an earthquake and, hence, prevents extensive damages and collapse.

The observations of masonry buildings when subjected to earthquakes have shown that the behaviour is strongly dependent on how the walls are interconnected and anchored and to floors and roofs. In old structure the unfavourable effect of insufficient anchorage between walls and between walls and floors was often observed. Irregular structural layout in plan, large openings and lack of bearing walls in both directions often caused severe damage or even collapse. A good quality of the connections between floors and walls, between roof and walls and between perpendicular walls is also crucial to reach a good global seismic behaviour of the building. Good quality connections will drive the collapse of the construction to a configuration that requires a stronger seismic action.

Other contributing factors include (1) original configuration and craftsmanship of the masonry; (2) modifications made over time, such as buttresses and ties (which improve the general performance) and additional storeys (which tend to compromise the performance); (3) the characteristics, quality, and condition of the masonry; (4)

the appropriate thickness of the bearing and non-bearing walls and discontinuities; (5) the method and configuration of the connection of the floors and roof to the walls; and (6) the materials and design of the floors and roofs themselves. The most important factors tend to differ with the building typology.

Damage to masonry buildings can be essentially interpreted on the basis of two fundamental collapse mechanisms. According Giuffrè definition (Giuffrè 1993), the "First Damage Mode" is produced by seismic actions perpendicular to the wall (out-of-plane) that cause the overturning of the whole wall panel or of a significant portion of it. A signature of such damage, short of collapse, can be the shedding of a portion of the exterior leaf of masonry. Another can be the formation of vertical cracks at the corners of a building where the wall began to form a hinge from the swaying.

The construction type, quality and state of preservation of masonry play a fundamental role in determining the capacity of a construction to sustain seismic actions.

A good performed masonry wall should behave monolithically, and reach the collapse, for instance, under seismic loads through the formation of cylindrical springs, whereas the portions of the wall which do not crack maintain a "rigid body" like behaviour (Figure 1-1). Such a mechanism of collapse has the advantage to be predictable and possibly preventable through suitable interventions. The worst defect of a masonry wall is to be not monolithic in the lateral direction. This makes the wall to become more brittle particularly when external forces act in the horizontal direction and vertical when loads act eccentrically (Figure 1- 2).

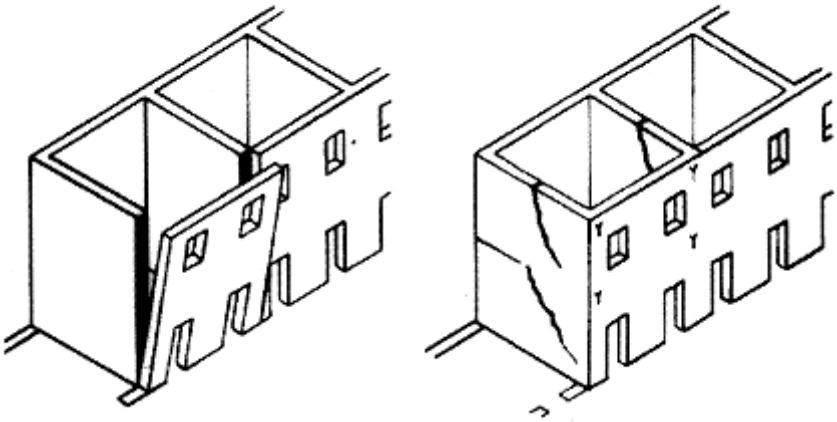

Figure 1-1 Example of predictable mechanisms of collapse (Giuffrè1993).

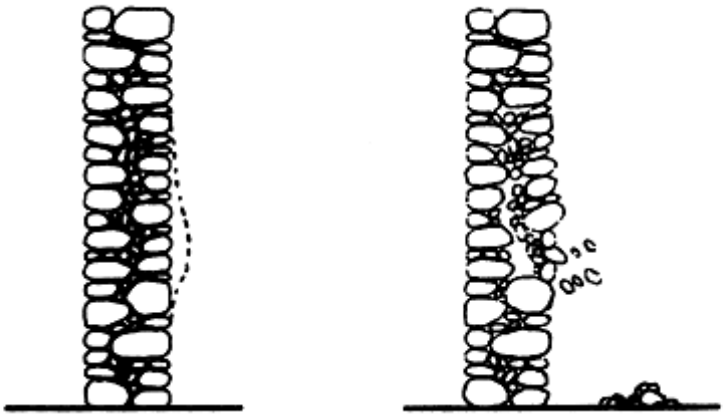

Figure 1-2 Deformation and failure of a two-leaf wall. From (Giuffrè1993)

It is worth to remark that peculiar damages could affect a specific building typology. Such an example, in chimneys can be observed out of plumb, longitudinal cracking, general deterioration of the crowns and etc. The damage of being out of plumb usually is due to faulty construction methods, foundation problems, or, more frequently, differences in mortar drying on different sides due to the action of the prevailing wind. And the type of damage consists of longitudinal cracking (Figure 1-3) and general deterioration of the crowns normally gives rise to partial loss of material (Pallarés et al. 2011).

The analysis of historic masonry structures is a complex task, and including slight and non-destructive in-situ testing, adequate laboratory testing and development of

reliable numerical tools.

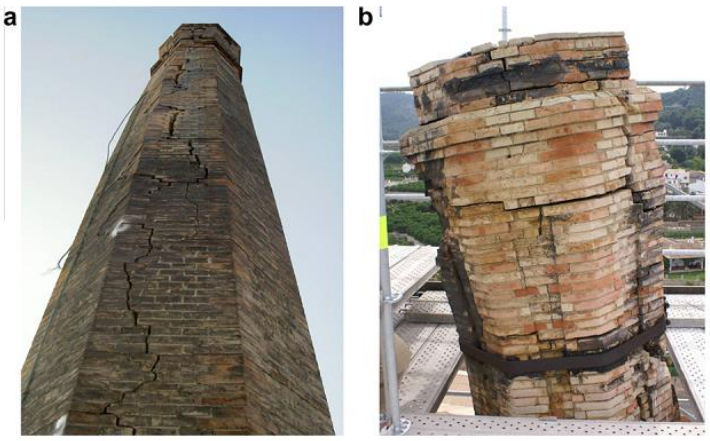

Figure 1-3 a) Longitudinal cracking caused by thermal gradient; b) Damaged crown (Pallarés et al. 2011)

An appropriate and rational use of structural analysis can help in defining the eventual state of danger and in forecasting the future behaviour of the structure. To this aim, the definition of the mechanical properties of the materials, the implementation of constitutive laws for decayed materials and of methods of analysis for damaged structures and the improvement of reliability criteria are needed (Binda et al. 2000). Nevertheless the question is still open.

1.3 Traditional diagnostic approaches

The first step of assessing a structure is to carry out a fundamental survey to have an overview as well as the service condition of the material of the structure. Historic study gives general information on the structure, including some significant events in its history and evolution, or the presence of past intervention. Geometry survey detects the geometrical characteristic of the structure. The surface damage of the structure, such as cracks, can be introduced in crack pattern survey. Material characteristic is obtained by slight or non-destructive tests. Numerical modelling, but only after an accurate model tuning, could be helpful to predict the structural behaviour to some particular actions.

1.3.1 Historic study

During years, the historic structures could be decayed due to aggressive environment or pollution or damages by natural actions such as earthquake or strong winds. At the meantime, in plenty of masonry structures, several repair interventions or structural variations has been done. Historic studies are the basic way to get a general view of the masonry structure condition. And in some cases, the historical evolution of the structure has to be known in order to explain the signs of damage detected on the building, to detect eventual discontinuities or lack of connections between the different masonry portions or to recognise changes in the building typologies and materials.

1.3.2 Geometry survey

Geometry surveys provide the information about the dimensions and the shape of the masonry structures, and the basic geometry parameters, and the buildings surrounding situations.

A preliminary in-situ survey is useful in order to provide details on the geometry of the structure and in order to identify the locations where more accurate observations have to be concentrated. Following this survey a more refined investigation has to be carried out, identifying irregularities vertical deviations, rotations, etc. (Binda et al. 2000). A survey of a masonry texture is shown in Figure 1-4.

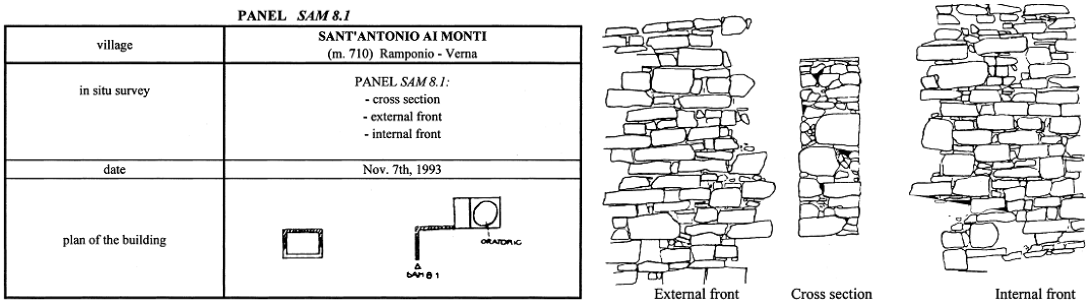

Figure 1-4 Example of masonry survey (front texture and section) at S. Antonio ai Monti (Ramponio-Verna) oratory (Binda et al. 2000)

1.3.3 Visual inspection and Crack pattern survey

The general observation of the wall surface, the change of material on the surface, the location and condition of crack, discontinuities or repair work and some other situations are the main content of the visual inspection.

Another especially important survey is drawing the crack patterns. The interpretation of the crack pattern can be of great help in understanding the state of damage of the structure, the possible causes and the type of survey to be performed, provided that the historic evolution of the building is already known. An example is shown in Figure 1-5. The crack pattern could be easily interpreted knowing that the large room A was inserted three centuries after the construction of the building and the large masonry vault had no rods or buttresses balancing the thrusting

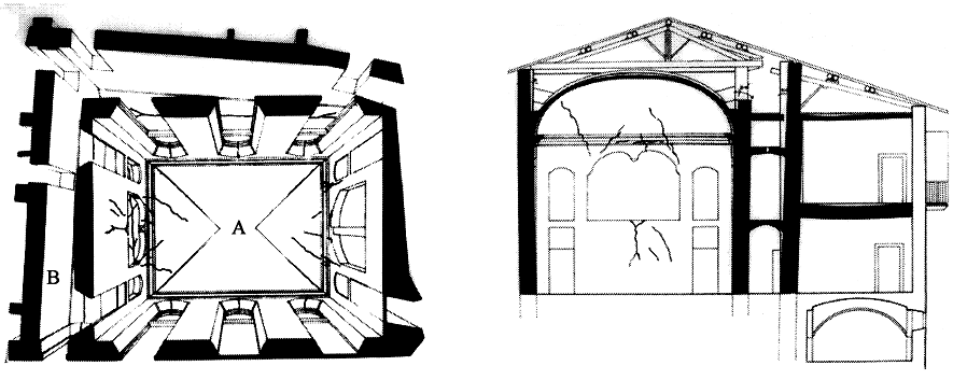

Figure 1-5 Villa Crivelli, Inverigo, Italy. Drawing of main crack on
a) the perspective of room A; b) wall B (Binda et al. 2000)

1.3.4 Characteristic of the materials

After the geometric, material, damage surveys of historic structures, a first evaluation of the structure could be hypothesised, knowing that the information is more focus on the description of the surface characteristics. In order to get more information about the property and condition of the characteristic of the material, non-destructive tests and slight destructive are introduced.

Slight destructive tests usually carried out on the structure surface directly. Being slight

destructive tests, their number have to be limited. Material sampling, surface hardness tests, pull out tests and flat jack tests are all common performed to evaluate the material characteristic. In this section, specimen tests and flat jack tests are described in details.

On the other hand, NDT can be helpful in finding hidden characteristics (internal voids and flaws and characteristics of a wall section) which cannot be determined by destructive tests. In ND tests, a correlation between the measured and physical parameters is usually difficult to set up, but provides an overall qualitative response. Sonic tests, radar tests and some other techniques are common used for Non-Destructive tests. Here, more details about sonic tests are presented.

Sampling

The idea of this test is: firstly, take appropriate specimens sampling directly from the masonry structure; secondly, carry out some tests on the specimens, such as mechanic tests, compressive, tensile or Brazilian tests, water absorption or other physical tests and so on; thirdly, obtain meaningful parameters to feed the structural model.

Sampling is a strategic but critic step, affecting the meaningful of the following test results. This phase has to be accurate designed, both on the localisation and on the procedure, on the base of the preliminary onsite and documentary research.

In spite of the disadvantages, by making use of the specimens, several tests can be carried out. The evaluation of the material properties could be relatively accurate despite the no-standardised material dimensions and test procedures.

Flat jack test

The method was originally applied to determine the in-situ stress level of the masonry. The firsts applications of this technique on some historical monuments (Rossi 1982), clearly showed its great potential. The test is carried out by introducing a thin flat-jack into the mortar layer, in masonry with regular and thin joints. The test is only slightly destructive (ASTM 1991a, b, Binda & Tiraboschi 1999b, Binda et al. 2007b).

The determination of the state of stress is based on the stress relaxation caused by a cut perpendicular to the wall surface; the stress release is deter-mined by a partial closing of the cutting, i.e. the distance after the cutting is lower than before (ASTM 1991a). A thin flat-jack is placed inside the cut and the pressure is gradually increased to obtain the distance measured before the cut. The displacement caused by the slot and the ones subsequently induced by the flat-jack are measured by a removable extensometer before, after the slot and during the tests. Pf corresponds to the pres-sure of the hydraulic system driving the displacement equal to those read before the slot is executed.

The value of the stress state is calculated with the following equation:

$$\sigma_m = P \cdot K_a \cdot K_m \tag{1.1}$$

Where, P = pressure of the jack that allows to restore the initial distance between the bases, as measured in bar; K_a = dimensionless constant which represents the ratio between the area of the jack and the area of the cut in the masonry; K_m = dimensionless constant, dependent on the geometry and rigidity of the cylinder, shown on the calibration certificate of the jack itself.

The cut in the masonry has been realized by means of a circular saw to eccentric disk in a course of mortar. Example of the testing layout is shown in Figure 1-6a).

The test described can also be used to determine the deformability characteristics of masonry used (ASTM 1991b). A second cut is made, parallel to the first one and a second jack is inserted, at a distance of about 40 to 50 cm from the other. The two jacks delimit a masonry sample of appreciable size to which a uniaxial compression stress can be applied. Measurement bases for removable strain-gauge or LVDTs on the sample face provide information on vertical and lateral displacements. In this way a compression tests is carried out on an undisturbed sample of large area. Several loading can be performed at increasing stress levels in order to determine the deformability modulus of the masonry in its loading and unloading phases. It is interesting to compare these last results to the stress level measure in order to verify

the present state of the masonry in relation with its last potentialities (Binda & Tiraboschi 1999b, Binda et al. 2007b).

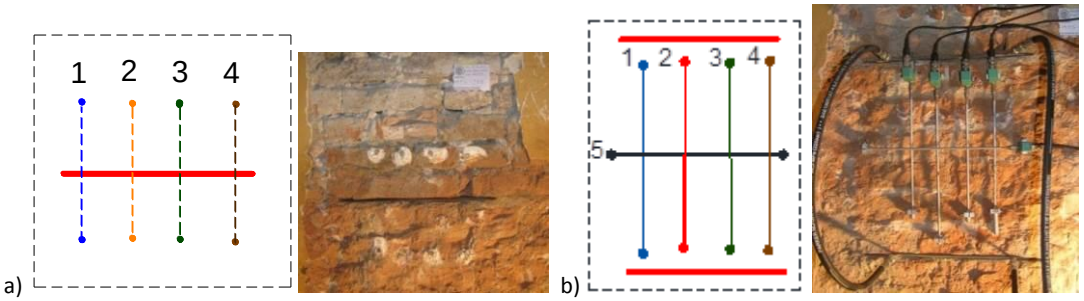

Figure 1-6 Arrangement of a) single; b) double flat jack test

Sonic test

The principle of pulse sonic tests is based on certain relationships between the speed of propagation of elastic waves in a material medium and the elastic properties/density of the medium itself. The speed of propagation of elastic waves is, in fact, directly correlated to the elastic properties and the density of the medium itself, but only if the medium traversed is elastic, homogeneous and isotropic.

When it hits a solid surface, the elastic waves propagate inside the material along longitudinal trajectories (compression waves) and transverse (shear waves), give the greater speed of longitudinal waves and the characteristics of the instruments.

For infinitely homogeneous, elastic and isotropic, the velocity of the compression waves is equal to the following relationship:

$$V = \sqrt{\frac{K \cdot E_d}{\rho}} \tag{1.2}$$

Where, V = speed of compression waves; Ed = Dynamic Elastic Modulus (KN/mm^2); $K = (1-\nu)/[(1+\nu)\cdot(1-2\nu)]$, r = Density (kg/m^3), ν= Poisson's Ratio

The testing methodology is based on the generation of sonic or ultrasonic impulses at a point of the structure. An elastic wave is generated by a percussion or by an electrodynamics or pneumatic device (transmitter) and collected through a receiver, usually an accelerometer, which can be placed in various positions.

The elaboration of the data consists in measuring the time the impulse takes to cover the distance between the transmitter and the receiver. The use of sonic tests for the

evaluation of masonry structures has the following aims:

--to qualify masonry through the morphology of the wall section, to detect the presence of voids and flaws and to find crack and damage (Binda et al 2001, 2007a);

--to control the effectiveness of repair by injection technique in others which can change the physical characteristics of materials (Binda et al 2001).

The first applications of ultrasonic tests to the evaluation of masonry materials and structures have been carried out on long time ago in the sixties (Aerojet 1967). Several efforts have been put in the tentative of interpretation of the data from sonic and ultrasonic tests (Binda et al 2001, 2003b, 2007a).

The limitation given by ultrasonic tests in the case of very inhomogeneous material made the sonic pulse velocity tests more appealing for masonry. Efforts have been made by the authors to correlate the sonic parameter to the mechanical characteristics of the material, but this correlation seems difficult.

The fundaments of wave propagation through solids allow to recognise the theoretical capabilities and limitations of the technique. The velocity of a stress wave passing through a solid material is proportional to the density ρ, dynamic modulus E, and Poisson's ratio ν of the material. Resolution in terms of the smallest recognisable features is related to the dominant wave-length (as determinate by the frequency) of the incident wave and also to the size of the tested element.

Wave-length λ , is determinate by a simple relationship between velocity, v and frequency f: $\lambda = v/f$.

Hence for a given velocity as the frequency increases the wave length decreases, providing the possibility for greater resolution in the final velocity reconstruction. It is beneficial, therefore to use a high frequency to provide for the highest possible resolution. However there is also a relationship between frequency and attenuation of waveform energy. As frequency increases the rate of waveform attenuation also increases limiting the size of the wall section, which can be investigated. The optimal

frequency is chosen considering attenuation and resolution requirements to obtain a reasonable combination of the two limiting parameters. In general it is preferable to use sonic pulse with an input of 3.5 kHz for inhomogeneous masonry.

The velocity and waveform of stress waves generated by mechanical impacts can be affected by:

--Input frequency generated by different types of instrumented hammers and transducers;

--Number of mortar joints crossed from the source to the receiver location; the velocity tends to decrease with the number of joints.

--Local and overall influence of cracks.

Input frequency changes with the characteristics of the superficial material (e.g. presence of thick plaster or cracks). The sonic test in this case shows a very important limit. Due to the wall structure or to the presence of a thick plaster (with fresco) the high frequency components could be filtered.

It is important to stress that the pulse sonic velocity is characteristic of each masonry typology and it is impossible to generalise the values. The tests, then, have to be calibrated for the different types of masonry directly on site.

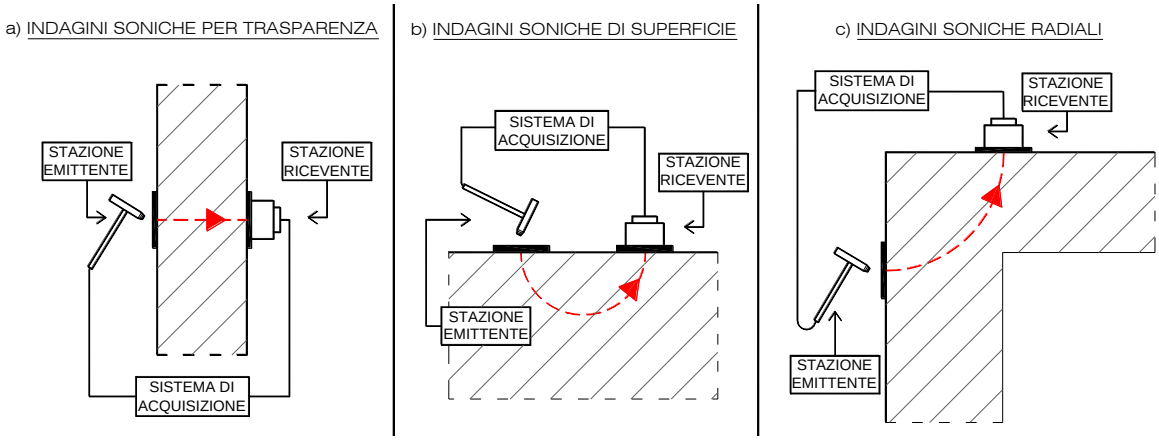

Figure 1-7 Diagrams depicting the main test mode used for sonic surveys

1.3.5 Finite Element Modelling

Finite element modelling is the 2nd level diagnosis of the structure. Information

obtained from the 1st level diagnosis, which includes the results of geometric survey, visual inspection, slight and non-destructive tests, is used in the modelling process. Common used finite element models are two kinds of 3-D models: 3-D solid element solid model (the external shell is set up as a several layered wall); 3-D composite beams model (3 dimensional tapered beam elements of three nodes).

The different types of analysis performed can be divided into two main steps: (a) validation of the analysis tools; and (b) special analysis according to different objectives, for example, evaluation of the seismic behaviour of the tower.

In the first group we have the eigenvalue and self-weight analyses. The calculus of the frequencies and modal shapes allow one to validate the models in the elastic field; while the self-weight analysis allow one to verify the correct geometrical description of the structure and the properties of the materials. Then, in the second step, analysis of different objectives is introduced. In the analysis of seismic action, for example, the non-linear static (pushover) and dynamic analyses are considered.

An example of FE modelling is introduced in the following. The numerical model is based on the geometry survey of the Holy Metropolitan Cathedral Basilica of Saint Mary in Valencia, Spain (Dura et al. 2012).

Based on the graphic geometric survey, a 3D model was generated by CAD applications and the numerical model is shown in Figure 1-8.

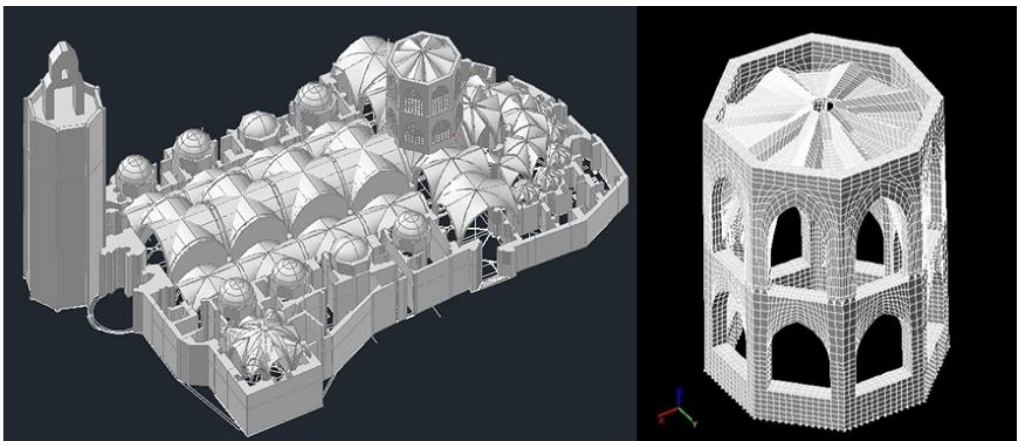

Figure 1-8 3D model of the Cathedral and the solid finite elements mesh model (Dura et al. 2012)

A linear static analysis was first carried out to evaluate the stresses in the masonry, leaving the existing cracks out of consideration, and concentrating only on the self-weight hypothesis. The important mechanical properties used in the numerical model was obtained from previous tests carried out on masonry from the Trinity Bridge in Valencia, which was of similar characteristics and had been obtained from the same quarry (Table 1-1). Non-linear analyses were used in this study by applying a value of 0.05 N/mm^2 tensile strength.

Table 1-1 Parameters used in numerical code (Dura et al. 2012)

Density	Module of deformation	Poisson's ratio	Compressive Force	Tensile Strength
1.918 T/m^3	1.425 N/mm^2	0.2	7.90 N/mm^2	0.15 N/mm^2

1.4 Ambient Vibration Tests

The structure has a response to dynamic load applied. The response, which can be recorded and measured during vibration tests, can be seen as the superposition of the response of each modal coordinate to the applied load. Hence, the response to any dynamic load contains information on the dynamic characteristics of the structure, i.e., natural frequencies, mode shape and damping ratios.

The vibration tests are classified as Experimental modal analysis and Operational modal analysis according to different excitation resources. The test that based on the ambient vibration is called as Ambient Vibration test (AVT). The vibration of Operational modal analysis is forced by ambient, such as wind, earthquake and traffic. In order to obtain good results of natural frequencies and mode shapes, the excitation is assumed to be a white noise. It is generally agreed that the time window of one dataset should be no less than 2000 times the fundamental vibration period of the structure.

Ambient vibration survey has been generally preferred for testing an historic structure because no excitation equipment is needed since the natural or environmental excitations are always present and hence the test implies a minimum interference with

the normal use of the structure (Gentile & Saisi. 2007).

1.4.1 Applications of AVT

The results obtained from the ambient vibration tests are helpful in many aspects of the assessment of structures. The most common application is to calibrate the numerical model through the dynamic characteristics identified by the tests. Besides, according to the dynamic characteristics from the results, fundamental period can also be extracted for the evaluation of the seismic vulnerability of the structure. What's more, in some cases, two AVT tests are carried out to assess the strengthening work. By the comparison of the results obtained from the dynamic tests before and after the retrofitting work, it is able to assess the structure condition after the strengthening work. The details of the applications are explained in the followings.

1.4.1.1 Evaluate the seismic vulnerability

According to EN 1998-1, during the earthquake, the ground motion is described by the elastic ground acceleration response spectrum S_e, denoted as the "elastic response spectrum". The basic shape of the horizontal elastic response spectrum, normalised by a_g, is as presented in Figure 1-9.

As described before, dynamic characteristics such as natural frequencies, mode shapes and damping ratios can be obtained from the ambient vibration test. Hence, the fundamental period of the structure, as the reciprocal of the first natural frequency of the structure, can be extracted as well.

By substituting the fundamental period into the curve shown in Figure 1-9 as the value of horizontal ordinate, the value of elastic spectrum of the structure can be obtained, which indicates the seismic vulnerability of the structure. For example, if the fundamental period is $T = 0s$, the structure is totally rigid, which means the structure will vibrate with the ground together.

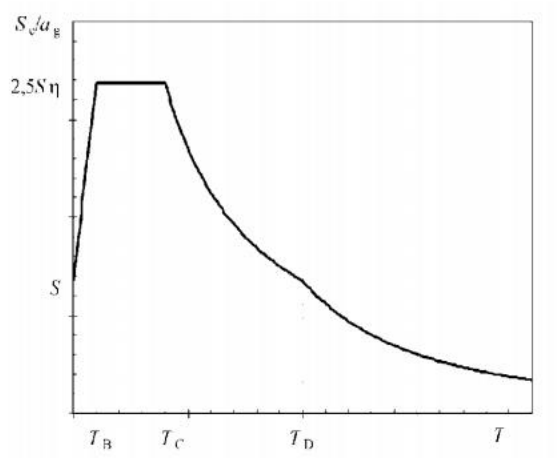

Figure 1-9 Basic shape of the elastic response spectrum in EN 1998-1

1.4.1.2 Calibration of the numerical models

Finite element modelling is a common method to realize the numerical analysis of historic structures. According to the information from 1st level diagnosis (historic study, geometry survey, visual inspection and crack pattern survey), the numerical model is able to set up to represent the structure characteristics.

Nevertheless, there are still plenty of uncertainties of the parameters. For example, the elastic modulus of the material varies in different parts of the structure, considering the degradation and different construction periods. Tests for the mechanic characterisation of the materials can not be carried out everywhere.

Therefore, AVT tests could be help in the identifying the overall structural behaviour of the building. With the help of operational modal analysis, the structure characteristic, such as the modes and natural frequencies can be extracted and used as reference parameters of the numerical models.

Application on a bell-tower in Monza (Gentile&Saisi. 2007)

A meaningful case-history is reported in (Gentile&Saisi. 2007). Ambient vibration tests were conducted on the tower at the beginning of July 2001 to measure the dynamic response in 20 different measurement points (Figure 1-10 a)), with the excitation being associated to environmental loads and to the bell ringing.

Due to the low level of ambient vibrations that existed during the tests, the use of the

velocity responses in the OMA provided better mode shapes estimates, especially for the lower vibration modes. After the data processing, the structure characteristics can be extracted. A total of five vibration modes were identified from ambient vibration data in the frequency range of 0–8 Hz. Table 1-2 and Figure 1-10 b) present the value and mode shape of the first five natural frequencies.

Table 1-2 Modal parameters identified from ambient vibration tests (Gentile&Saisi. 2007)

Mode No.	Mode Type	$f_{PP}(Hz)$	$f_{FDD}(Hz)$	$D_F(\%)$	MAC
1	Bending E-W/N-S	0.586	0.598	2.05	0.9984
2	Bending N-S/E-W	0.708	0.708	0.00	0.9989
3	Torsion	2.456	2.417	1.59	0.9929
4	Bending E-W/N-S	2.731	2.722	0.33	0.9597
5	Bending E-W/N-S	5.706	5.713	0.12	0.9923

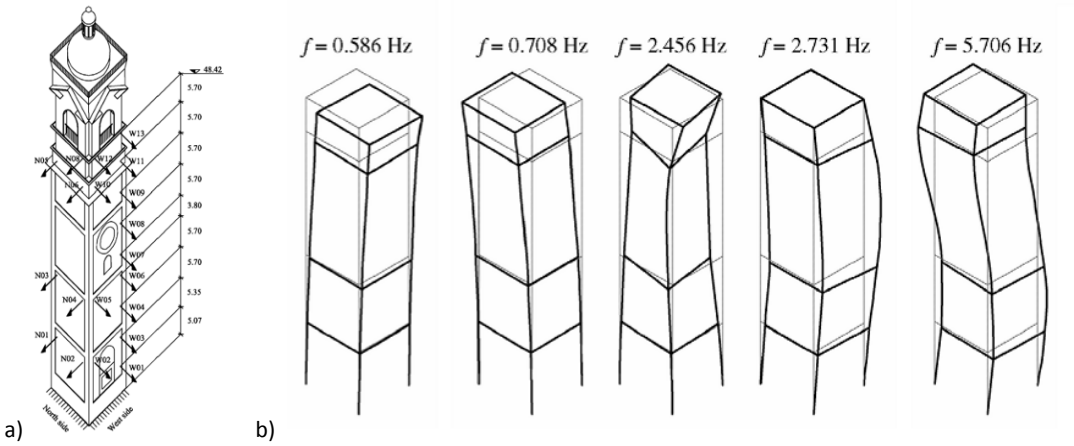

Figure 1-10 a) Sensor locations and directions for the tower test (m); b) Vibration modes identified from ambient vibration measurements (PP) (Gentile&Saisi. 2007)

The experimental investigation was preceded by the development of a 3D finite element model (Figure 1-11 a)), based on the geometric survey. The tower was modelled using 8 node brick elements while the dome was represented by 4 node shell elements. The model results in a total of 4944 nodes, 3387 solid elements and 80 shell elements with 14,286 active degrees of freedom.

The correlation between mode shapes (Figure 1-11 b) and Table 1-3) shows very good agreement with the experimental results for the first two modes (with the MAC being greater than 0.97); for higher modes, the MAC is in the range 0.86–0.87 so that appreciable average differences are detected. Such differences are probably related

either to the simplified distribution of the model elastic properties (which were held constant for large zones of the structure) or to a relative lack of accuracy in the experimental evaluation of the higher mode shapes.

Table 1-3 Comparison of the natural frequencies from FEM and AVT

Terms	1st mode	2nd mode	3rd mode	4th mode	5th mode
$f_{FEM}(Hz)$	0.585	0.709	2.455	2.726	5.698
$f_{PP}\ (Hz)$	0.586	0.708	2.456	2.731	5.706
MAC	0.987	0.975	0.861	0.860	0.872

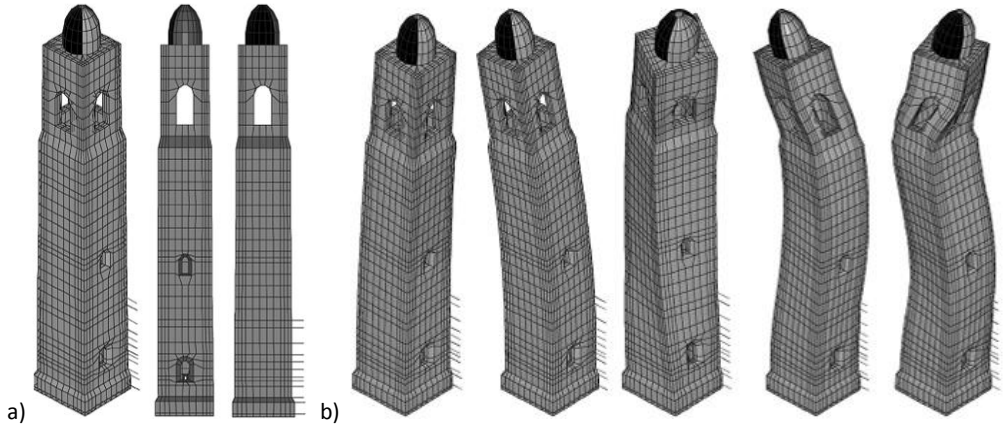

Figure 1-11 Finite Element Model of the bell-tower a) 3D and 2 plan view; b) Vibration modes

Application on historic chimneys

The dynamic tests of the chimneys in this study were carried out by a calibration hummer. The position of seismic accelerometers at four points on a chimney stack to determine mechanical properties by non-destructive testing is shown in Figure 1-12 a). During the test, either vibrations produced by environment or from a calibrated hammer, both detected by seismic accelerometers, the registered values of acceleration can be seen in Figure 1-12 b). The impulse force shown was introduced by the calibrated hammer at 1.5 s and applied at ground level.

The frequencies identified are shown in Figure 1-13 after the application of the Fast Fourier Transform, together with two vibration modes (numerically obtained through an updated model) (Benedettini & Gentile. 2011).

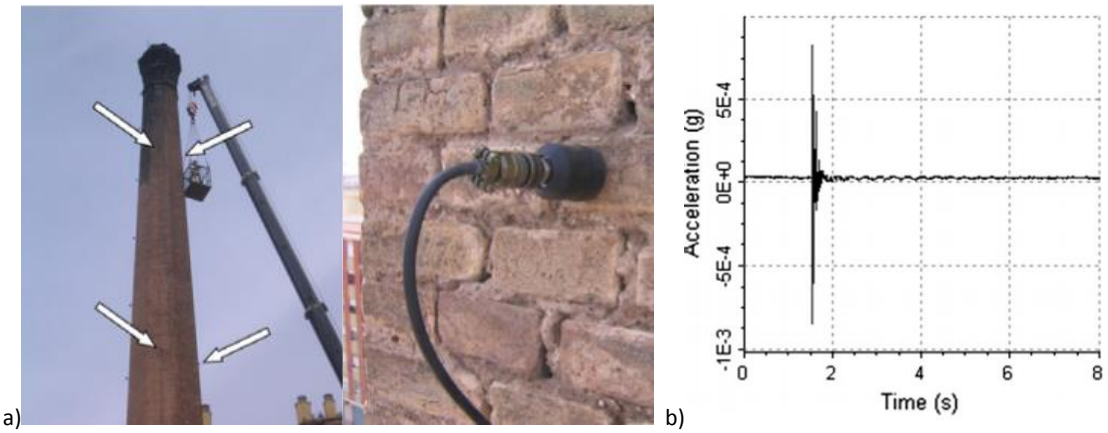

Figure 1-12 a) Position of accelerometers of the chimney; b) the register values of acceleration (Pallarés et al. 2011)

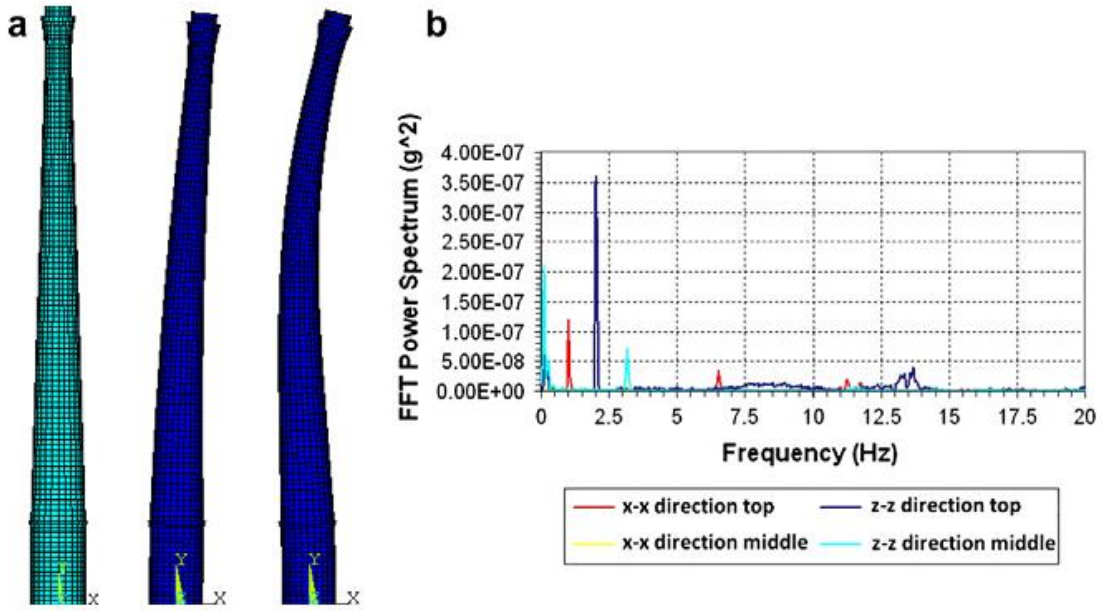

Figure 1-13 a) Numerical model and two mode shapes b) Frequency spectrum from AVT (Pallaré es et al. 2011)

1.4.1.3 Assessment of the effects of strengthening work

In some cases, two ambient vibration tests are carried out on the structure before and after retrofitting work to assess the statement of strengthening work of the structure. Dynamic structure characteristic is the main index of the assessment. An example of this kind of application is introduced in the following section.

Application on the Mogadouro Clock Tower

The Mogadouro Clock Tower is located inside the castle perimeter of Mogadouro, a small town in the Northeast of Portugal. The tower was built after the year 1559. It has

a rectangular cross section of $4.7 \times 4.5\ \mathrm{m}^2$ and a height of 20.4m. Large granite stones were used in the corners and rubble stone with thick lime mortar joints were used in the central part of the walls. The thickness of the walls is about 1.0m.

In 2004, the tower was severely damaged, characterized by large cracks, material deterioration and loss of material in some parts. A geometrical survey of the structure was performed and the existing damage was mapped.

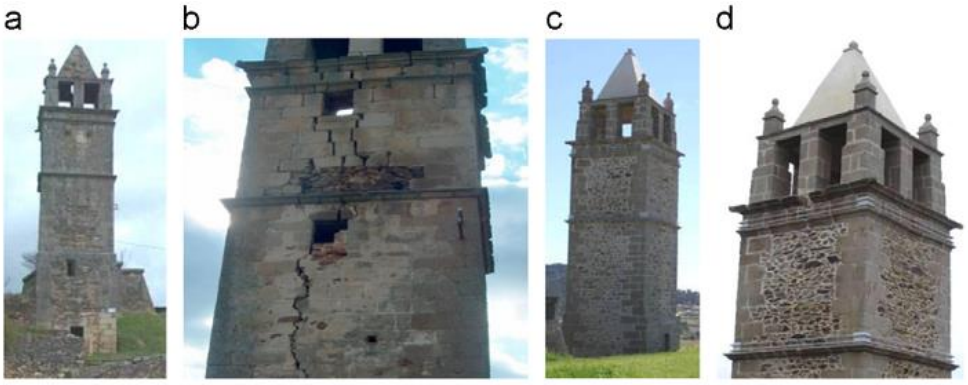

Figure 1-14 Mogadouro Clock Tower: (a,b) before; (c,d) after rehabilitation works (Ramos et al. 2010)

Two dynamic modal identification tests were performed before and after the rehabilitation works. The same test planning was adopted in the two conditions by using the same measuring points, see Figure 1-15 present images of the execution of the ambient dynamic tests carried out before and after the works.

According to the two dynamic tests, the dynamic characterization of the tower can be carried out as shown in Figure 1-16, where the first 7th mode shapes and frequency are exposed. On average the frequencies increased 50% with the consolidation works, while the damping decreased 40% for all modes, with exception of sixth mode. As expected, by closing the cracks the stiffness increased and the energy dissipation decreased, directly affecting the frequencies and damping, respectively. Concerning the modal displacements, local protuberances can be observed in the areas close to the cracks and in the upper part of the tower, before the works. This is due to the presence of severe damage. On the contrary, the structure behaves monolithically

after the rehabilitation.

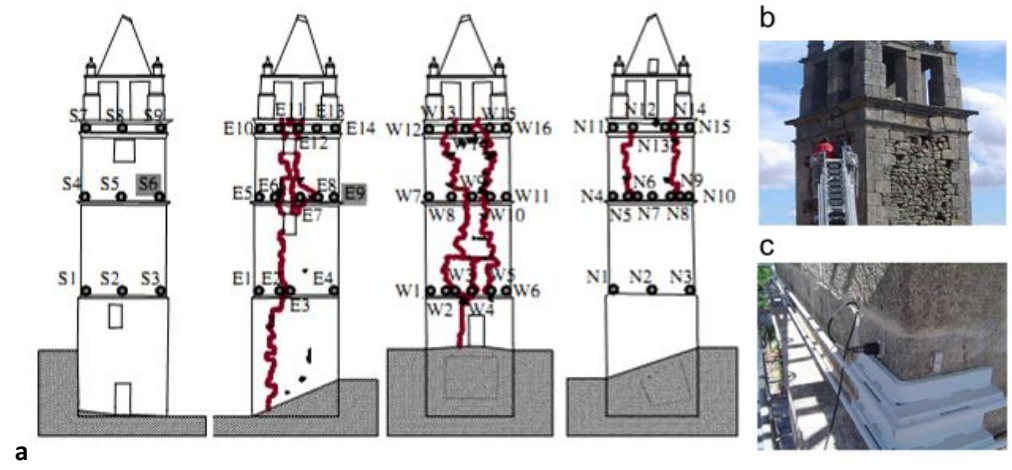

Figure 1-15 Example of sensor locations: (a) south, east, west and north facade measuring points, respectively; (b) measurements before rehabilitation works and (c) after rehabilitation works (Ramos et al. 2010)

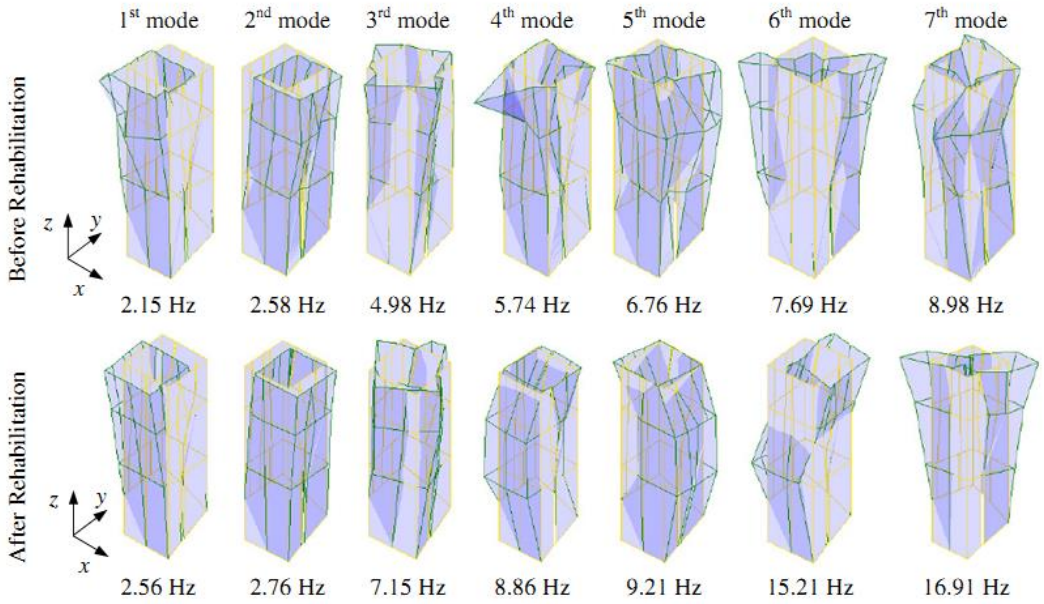

Figure 1-16 Experimental mode shapes and MAC values before and after rehabilitation works (Ramos et al, 2010)

1.5 The monitoring systems

Among the essential investigations, the analysis of potential damage and crack evolution is crucial in finding any relationship between lack of stability and external suffered by the building during time. In order to reconstruct the historical evolution of a collapse mechanism and structure characteristics, long-term monitoring systems

have to be carried out.

1.5.1 Static monitoring

The identification and dating of any repair or strengthening intervention is important, as the knowledge of the traumatic events suffered during centuries (earthquakes, fires, wars, etc.) and the dating of consequent restoration works, together with the presence of spies. This very rough process is called “historical monitoring” (Blasi & Ottoni. 2012), which is one kind of static monitoring and can be completed by modern high precision monitoring system, giving the global graph of the building behaviour from the past to date.

Simple monitoring systems can be applied to some important cracks in masonry walls, were the opening of the cracks along the time can be measured by removable extensometers with high resolution. This system can give very important information where an important crack pattern is detected and its progressive growth is suspected due to soil settlements, temperature variations or to excessive loads. The measure of displacements in the structure as function of time has to be collected. These systems are able only to measure the actions that disturb locally the buildings, without a clear distinction between pathological and recursive behaviours: thermal changes, wind, earthquakes, changes in level and changes in groundwater. They can also provide alarms if certain thresholds are exceeded.

1.5.2 Dynamic monitoring

1.5.2.1 Issues about dynamic monitoring system

Current practices of structural health condition are based mainly on periodic visual inspections or condition surveys but, during the last decade, software and hardware developments made continuous monitoring possible (Marques et al. 2010).

The equipment and the theoretical background of the dynamic monitoring are similar with AVT. Besides the accelerometers used also in AVT, temperature sensors are always

installed in dynamic monitoring systems to assess the environment effects. What's more, in some cases, humidity and wind speed are also taken into consideration.

Dynamic monitoring provides the evolution of dynamic structure characteristics with time, considering the influence of environment effects.

The design constitute part of an integral dynamic structure monitoring system needs to incorporate data acquisition and transmission tools with appropriate automatic feature extraction routines.

Sensors are the common tools to collect data, including the accelerometer, thermometer, humidity sensor, anemometer and etc. Nevertheless, some limitations of the system can not be ignored. One of the main difficulties when implementing these systems is the large amount of recorded data. Thus, the feasibility of a proper implementation of long-term monitoring schemes, as well as real-time interpretations, relies on the use of processes for automatic feature extraction. Such implementation is not a trivial task, since traditional modal identification techniques require constant user interaction and experience from the user (Ramos et al. 2013).

1.5.2.2 Environment effects

The modal parameters are often sensitive to changing environmental conditions such as temperature, humidity, or excitation amplitude. Environmental conditions can have as large an effect on the modal parameters as significant structural damage, so these effects should be accounted for before applying damage identification methods (Moser & Moaveni 2011).

Vibration-based Structure Monitoring methods often rely on changes in the modal parameters for damage identification. However, modal parameters are usually sensitive to other factors as well as damage in-situ. Interaction of the structure with surrounding air currents can produce changes in structural dynamics as wind speeds change (Minh et al. 2000). All these factors can influence the modal parameters of a structure while temperature is the most commonly considered environmental variable.

Changes in natural frequency in the order of 10% from environmental or operational sources are not unusual. This presents a challenge for dynamic monitoring system methods because changes from environmental effects can be larger than changes due to significant damage.

1.5.2.3 Application on a masonry church

Saint Torcato church is located in a small village near Guimaraes. The building exhibits moderate to severe damage, with a major crack in the main facade. A dynamic monitoring system was installed in the church in 2009. The measurement points were placed at their top as shown in Figure 1-17 a). The monitoring system consisted of four piezoelectric accelerometers with 10 V/g sensitivity and dynamic range of 70.5g, one portable DAQ unit model with 24 bits resolution able to acquire 4measurement channels, one Uninterruptible Power Supply, and one computer with embedded processor Pentium IV as remote station. (Figure 1-17 b) &c)).

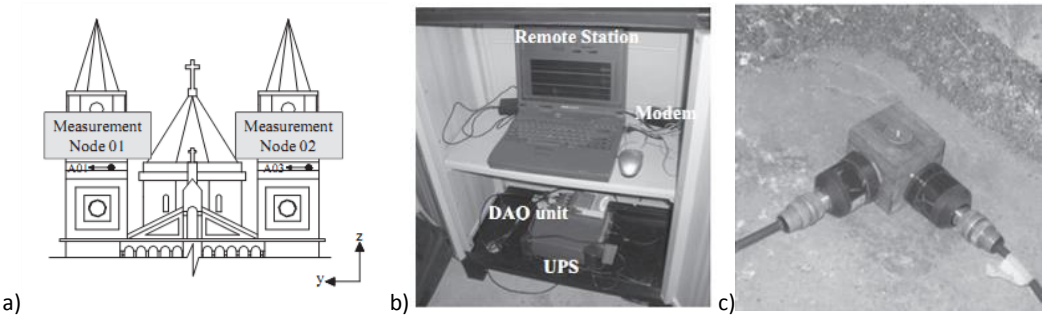

Figure 1-17 Design of the dynamic monitoring system: a) location of the measurement sensors; b) data acquisition station; c) biaxial measure node (Ramos et al. 2013)

A conservative sample time of 10 min with a sample frequency of 50 Hz was considered. The acquisition process was repeated using intervals of 60min, starting from November 2009. In the end, five monitoring campaigns were carried out where 3495 events were registered.

The information presented in Table 1-4 shows the mean values and the standard deviation of the estimated natural frequencies, damping coefficients and that for the MAC values. The variations of frequencies might be due to the changes on the

environmental conditions (temperature and humidity).

The analysis results concluded that the environmental effects significantly change the dynamic response of the structure. Mainly, the water absorption of the walls in the beginning of the raining seasons changes the frequencies about 4%. The series in Figure 1-18 a), b) is linked to the first strong raining event at the site. As no damage was observed in the structure, the humidity influence can be observed by a shift in the linear relation between frequency and temperature by a transition series.

Table 1-4 Automatic modal identification results (Ramos et al. 2013)

Mode Shapes	f ave(Hz)	f std. dev(Hz)	ξ ave(%)	ξ std. dev(%)	MAC ave(%)	MAC min(%)
Mode 1	2.098	0.043	1.414	0.816	99.388	80.169
Mode 2	2.568	0.041	1.848	0.949	99.334	80.081
Mode 3	2.772	0.049	2.071	1.135	98.916	80.123
Mode 4	2.924	0.052	2.085	1.144	98.690	80.101

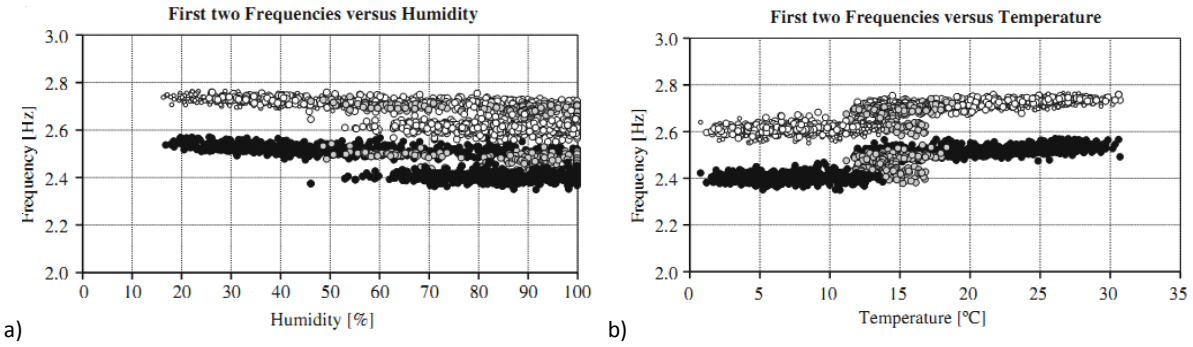

a) b)

Figure 1-18 Environment effects: a) temperature; b) relative air humidity (Ramos et al. 2013)

Chapter 2

Operational Modal Analysis: Theoretical Background

2.1 Introduction

Operational Modal Analysis (OMA) is nowadays considered as a reliable tool for modal identification from experimental data collected in operational conditions (i.e. with the excitation being associated to loads that are always present, such as micro-tremors, traffic, anthropic actions, wind, etc.).

The OMA methodology consists of two main steps: modal testing carried out in operational conditions by using suitable equipment; modal analysis performed by reliable and robust identification procedures.

OMA is based on ambient response data where the dynamic responses were induced by ambient vibration sources, such as micro-tremors or wind. This is different from the more traditional Experimental Modal Analysis (EMA) in which artificially controlled input forces were introduced by actuators so that modal analysis is performed by identifying the relationship(s) between the known input(s) and the measured output(s).

In the last decades, progresses in Digital Signal Processing (DSP) and the development of some new powerful identification techniques such as the Stochastic Subspace Identification (SSI) technique (Van Overschee & De Moor 1996), the Frequency Domain Decomposition (FDD) technique (Brincker et al. 2001) and the poly-Least Square Complex Frequency (p-LSCF) technique (Peeters & Van der Auweraer 2005) have allowed OMA to gain the role of a reliable tool, capable of providing accurate

information on the modal behavior of a mechanical system. As a consequence, nowadays, OMA is often automated to use it as an “engine” to extract modal parameters over time within the framework of several dynamic monitoring programs (Cunha et al. 2011, Rainieri et al. 2011, Magalhães et al. 2012).

In this Chapter, firstly, some basic aspects of OMA are presented and discussed (Paragraph 2.2) by a comparison with EMA, in order to highlight advantages and possible limitations of the OMA methodology. Subsequently, the basis of OMA is presented in Paragraph 2.3 in order to outline the methodology and provide the essential theoretical information that is behind the identification procedures subsequently presented in Paragraph 2.4. The description of modal identification techniques working in both the frequency domain and the time domain are summarized in Paragraph 2.5.

Since application of OMA identification techniques used in this Dissertation are based on two different commercial softwares, namely DADiSP and ARTEMIS, Paragraph 2.6 provides an introduction of the two computer codes.

2.2 Operational versus Experimental Modal Analysis

Identification of modal parameters (resonant frequencies, modal damping ratios and mode shapes) of mechanical systems by experimental tests is a research topic started in the 1960s (Brincker 2010b, Magalhães & Cunha 2011). The first experiences highlighted the usefulness of experimental modal testing both for developing analytical models of the system tested and in estimating parameters describing the dynamic response of reduced-scale physical models as well as full-scale prototypes (Ewins 2000). This practice has become known over years as Experimental Modal Analysis (EMA), where modal testing is mainly based on Forced Vibration Testing (FVT) and the subsequent modal identification is carried out by relating the applied input (excitation) and the measured output (response) of the system. A wide variety of input-output modal identification methods relies on the estimation of a set of

Frequency Response Functions (FRFs) or on the corresponding Impulse Response Functions (IRFs) in the time domain obtained by the Inverse Fourier Transform (IFT) of the FRFs. Modal identification methods may be classified according to the following criteria:

- Domain of application (time or frequency domain);
- Type of formulation (indirect or modal and direct);
- Number of modes analyzed (SDOFS or MDOFS);

The accurate estimation of modal parameters from FRFs strongly depends on carrying out FVT or, in other words, the estimation of the FRFs requires the use of a proper instrumentation chain for structural excitation, data acquisition and signal processing. Focusing attention on the excitation, the device used should provide a wide-band input, including the frequency range of interest, and excite the structure in a lower frequency range with high frequency resolution. EMA was initially developed in the field of Mechanical Engineering, especially in aerospace and automotive areas and only later it had been used in Civil Engineering to test, usually, special structures such as large-scale bridges and high-rise buildings. However, these first experiences allowed to observe that application of EMA - on large size structures - was not straightforward but some challenges arisen. In fact, heavy and expensive devices had to be used to excite artificially large-scale structures in the low frequency range and results were not always successfully. Hence, in Civil Engineering the main general aspects of a different practice called Operational Modal Analysis (OMA) have been outlined.

In particular, it was observed since 1970s that ambient (e.g. wind and microtremors) or operational forces (e.g. road traffic) provided enough energy to effectively excite large structures in the low frequency range without any disturbance to normal operating conditions.

The practice based on Ambient Vibration Tests (AVTs) and subsequent modal identification by output-only techniques (since the excitation is unmeasured) has become known over years as OMA. General aspects of OMA can be summarized as：

a) Environmental and operational loadings are considered as freely available natural sources of ambient excitations in order to investigate the dynamic properties of a mechanical system;
b) AVTs are carried out in order to measure the system response at points of interest. Output-only data are measured while the input remains unknown and so input-output relationships such as FRFs are not estimated in OMA;
c) The unknown input (environmental and operational loadings) is considered as a realization of a white noise and stationary (or close to it) random process;
d) Modal identification in OMA is based on the determination of the linear time invariant model that fits the measured response of a structure, subject to white noise excitation.

Modal identification in step (d) can be performed by a variety of techniques, different, for theoretical background and identification procedures. A common classification distinguishes the techniques in the frequency or time domain even if some techniques may involve both of them. Furthermore, OMA techniques, both in frequency and time domain, can be parametric or non-parametric.

Application of OMA, especially in vibration-based Structural Health Monitoring, is increasingly used but some general limitations of the methodology have to be considered:

1) Since the ambient excitation is generally low, a proper choice of sensitivity - with very low noise levels - has to be generally done in selecting sensor devices. However, in some cases very low signal to noise ratio might not be avoided, so that estimating the modal properties could be uncertain and/or difficult;
2) The frequency content of ambient excitation may not cover the whole frequency band of interest. This is especially the case of stiff structures, that are characterized by vibration modes in the high frequency range;
3) Since OMA is based on output-only information (responses), modal masses cannot be estimated or, in other words, the mode shapes are not scaled in

absolute sense.

Notwithstanding these relative limitations, OMA is considered an effective tool for modal identification and its application in vibration based structure monitoring has opened a promising research field in which one of the main challenge is automating the identification procedures.

2.3 Fundamentals of Operational Modal Analysis

2.3.1 Excitation process and structural system

When an AVT is performed on a real structure, since in general it is globally excited, a multiple-input model should be considered.

In order to exemplify some main concepts, let us consider the model in Figure 2.1. For a real structure, a schematic representation of such a model should include the presence of input and output noise, denoted in Figure 2.1 as *m(t)* and *n(t)*, respectively.

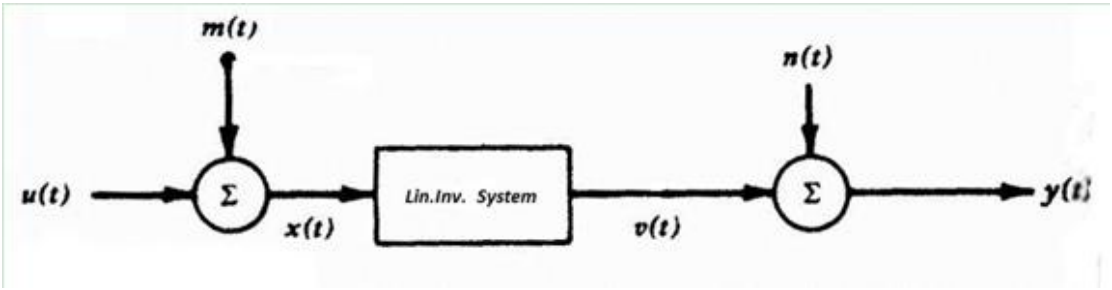

Figure 2-1 Model in an Ambient Vibration Test

In OMA, the unknown input forces or "excitation process" *u(t)* have to rely on some basis hypothesis as well as the "structural system". On one hand, the excitation should ideally be represented by a white noise, stationary, zero mean and Gaussian stochastic process or at least close to it (Brincker 2010b). On the other hand, the mechanical system excited by x(t) should be linear and time-invariant. Thus, the response y*(t)* is finally measured in order to identify the modal parameters of the system.

2.3.2 General aspects concerning identification techniques

As previously stated, OMA is based on some ideal assumptions: a linear, time-invariant

structural system excited by a white noise, stationary, zero mean, Gaussian stochastic process. Even if, such assumptions are rarely fulfilled in reality, they represent sound basis for the theoretical development that is behind the identification technique.

Concerning the response stochastic process it can be observed that (Brincker 2010b):

a) Generally, responses due to natural loadings, according to central limit theorem, are approximately Gaussian, thus all information is carried in the first and second order properties;
b) First order properties of the stochastic response are normally not used since large measurement errors occurred in their estimation;
c) Second order properties of the stochastic response process are used such as those contained in the correlation matrix $\mathrm{C}_{yy}(\tau)$. Consequently, also the spectral matrix $G_{yy}(f)$ obtained by applying the FT to $\mathrm{C}_{yy}(\tau)$ can be used. In fact, either $\mathrm{C}_{yy}(\tau)$ or $G_{yy}(f)$ matrices often represent starting points of several identification techniques.

The OMA procedures normally rely on two steps, as shown in Figure 2-2, although one of them may be missing in some identification techniques. For example, the FDD (Brincker et al. 2007) technique does not need a fitting step in identifying the modal parameters.

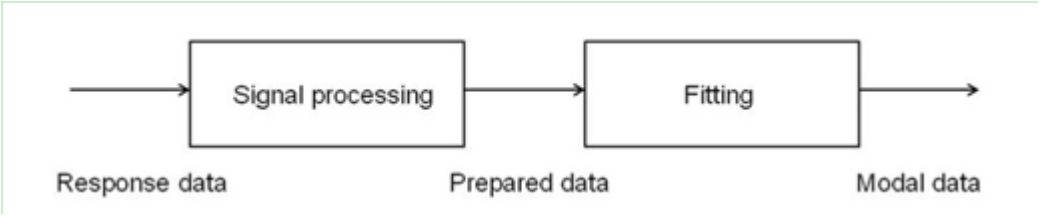

Figure 2-2 OMA procedures: general scheme of identification (Brincker 2010b)

2.4 Theoretical background of OMA techniques

Modal identification from output-only data is mainly based on the following two steps:

a) identify a model representing the vibrating structure from measured data;
b) extract the modal parameters from such a model.

In the general context of system identification, several models have been

formulated with the purpose of obtaining a good representation of a vibrating structure.

In OMA, models describing output-only discrete-time relations are those of interest since in reality output measurements are taken at discrete time instants. Those models are formulated in both time domain and frequency domain.

In the following, the theoretical background even if starting from a general approach will be progressively addressed on the contents of major interest.

The starting point will be a structural system represented by a discrete linear time invariant model whose dynamic equilibrium is described by the following set of N_n second-order differential equations:

$$\mathbf{M}\ddot{\mathbf{y}}(\boldsymbol{t}) + \boldsymbol{C}\dot{\boldsymbol{y}}(\boldsymbol{t}) + \boldsymbol{K}\boldsymbol{y}(\boldsymbol{t}) = \mathbf{f}(\mathbf{t}) = \mathbf{B}\mathbf{u}(\mathbf{t}) \tag{2.1}$$

Where, **M**, **C** and $\mathbf{K} \in \Re^{N_n \times N_n}$ are respectively the mass, damping and stiffness matrices; $\ddot{\mathbf{y}}(\boldsymbol{t})$, $\dot{\boldsymbol{y}}(\boldsymbol{t})$ and $\mathbf{y}(t) \in \Re^{N_n \times 1}$ are respectively the acceleration, velocity and displacement column vectors concerning and $\mathbf{f}(t) \in \Re^{N_n \times 1}$ is the column vector of the unknown input.

However, normally not all the DOFSs are excited so that the load vector **f**(*t*) can be replaced by another line vector **u**(*t*) of smaller dimension $N_i < N_n$ - containing the time evolution of the N_i applied inputs - pre-multiplied by the matrix $\mathbf{B} \in \Re^{N_n \times N_i}$ containing the inputs positions (Eq. 2.1).

2.4.1 The modal model

Applying the Laplace transform and neglecting the initial conditions, Eq. 2.1 is equivalent with the following frequency-domain equation:

$$\left[\mathbf{M}s^2 + \mathbf{C}s + \mathbf{K}\right]\mathbf{Y}(s) = \mathbf{F}(s) \tag{2.2}$$

with $s = i\omega$. Eq. 2.2 can be rewritten as:

$$\mathbf{Z}(s)\mathbf{Y}(s) = \mathbf{F}(s) \tag{2.3}$$

where $\mathbf{Z}(s)=\mathbf{M}s^2+\mathbf{C}s+\mathbf{K}$ is the dynamic stiffness matrix. Inverting Eq. 2.3, yields:

$$\mathbf{Y}(s) = \mathbf{H}(s)\mathbf{F}(s) \tag{2.4}$$

$$\mathbf{H}(s) = \mathbf{Z}^{-1}(s) = \left[\mathbf{M}s^2 + \mathbf{C}s + \mathbf{K}\right]^{-1} \tag{2.5}$$

where $\mathbf{H}(s)$ (i.e. the inverse of $\mathbf{Z}(s)$) is generally called the transfer function matrix since it relates the output or "response" $\mathbf{Y}(s)$ and the input or "excitation" $\mathbf{F}(s)$. Each element of $\mathbf{H}(s)$ is a complex valued function and the values s at which the elements of $\mathbf{H}(s)$ present infinite values are designated as "poles". Poles, denoted as λ_i, appear in complex conjugate pairs.

2.4.1.1 Proportional damping

Let us consider the Newton's equation of motion (Eq. 2.1) under the assumption of proportional damping. Any system response can be expressed in terms of modal coordinates q(t); hence assuming that $\mathbf{\Phi} \in \Re^{N_n \times N_n}$ is the matrix containing the N_n mode shapes $\mathbf{\Phi}$, $\mathbf{y}(t)$ can be expressed as follows:

$$\mathbf{y}(t) = \phi_1 q_1(t) + \phi_2 q_2(t) + \ldots = \mathbf{\Phi q}(t) \tag{2.6}$$

Pre-multiplying Eq. 2.1 by $\mathbf{\Phi}^T$ and introducing Eq. 2.6, yields to:

$$\Phi^T M \Phi \ddot{q}(t) + \Phi^T C \Phi \dot{\mathrm{q}}(t) + \Phi^T K \Phi \mathrm{q}(\mathrm{t}) = \Phi^T f(t) \tag{2.7}$$

where $(\bullet)^T$ is the transpose operator. It can be proven that the following orthogonality conditions hold (see e.g. Newland 2006):

$$\mathbf{\Phi}^T \mathbf{M} \mathbf{\Phi} = diag\left[m_i\right] \tag{2.8}$$

$$\mathbf{\Phi}^T \mathbf{C} \mathbf{\Phi} = diag\left[2\xi_i \omega_i m_i\right] = \mathbf{D}\, diag\left[m_i\right] \tag{2.9}$$

$$\mathbf{\Phi}^T \mathbf{K} \mathbf{\Phi} = diag\left[k_i\right] \tag{2.10}$$

Where:

- m_i, c_i and k_i are the *i-th* modal masses, damping and stiffness, respectively;
- ω_i is the *i-th* resonant frequencies (rad/s);
- ξ_i is the *i-th* modal damping ratios for i=1,2..N_n.

$$\omega_i = \sqrt{\frac{k_i}{m_i}} \;\; ; \;\; \xi_i = \frac{C_i}{2m_i\varpi_i} \tag{2.11}$$

$$\mathbf{D} = diag\left[2\xi_i\omega_i\right] \tag{2.12}$$

$$\mathbf{\Omega}^2 = diag\left[\omega_i^2\right] \tag{2.13}$$

Substituting Eqs. 2.8-2.10 and 2.13 in Eq. 2.7 and applying a normalization to the modal masses, yields to:

$$\mathrm{I}\ddot{q}(t) + \mathrm{D}(t) + \Omega^2\mathrm{q}(\mathrm{t}) = diag[\tfrac{1}{m_i}]\Phi^T f(t) \tag{2.14}$$

where I $\in \Re^{N_n \times N_n}$ is the Identity matrix. Using the Laplace transform and neglecting the initial conditions, Eq. 2.14 results in the following equation:

$$\left[\mathbf{I}s^2 + \mathbf{D}s + \mathbf{\Omega}^2\right]\mathbf{Q}(s) = diag\left[\frac{1}{m_i}\right]\mathbf{\Phi}^T\mathbf{F}(s) \tag{2.15}$$

so that the following input-output relation can be written:

$$\mathbf{Q}(s) = \left[\mathbf{I}s^2 + \mathbf{D}s + \mathbf{\Omega}^2\right]^{-1} diag\left[\frac{1}{m_i}\right]\mathbf{\Phi}^T\mathbf{F}(s) \tag{2.16}$$

The inverse matrix in Eq. 2.16 can be formulated in its modal form and further simplified considering the expression of poles:

$$\begin{aligned}\left[\mathbf{I}s^2 + \mathbf{D}s + \mathbf{\Omega}^2\right]^{-1} &= diag\left[\frac{1}{s^2 + 2\xi_i\omega_i s + \omega_i^2}\right] \\ &= diag\left[\frac{1}{s-\lambda_i} + \frac{1}{s-\lambda_i^*}\right]\end{aligned} \tag{2.17}$$

where (•)* denotes the complex conjugate operator and i are the poles related to resonant frequencies and modal damping ratios:

$$\lambda_i\,;\lambda_i^* = -\xi_i\omega_i \pm i\omega_i\sqrt{1-\xi_i^2} \tag{2.18}$$

Applying the Laplace transform to Eq. 2.6, yields to:

$$\mathbf{Y}(s) = \mathbf{\Phi}\mathbf{Q}(s) \tag{2.19}$$

Finally, substotuting Eq. 2.16 in Eq. 2.19 yields to the formulation of the transfer matrix H(s) in its modal form:

$$\begin{aligned}\mathbf{Y}(s) &= \boldsymbol{\Phi}\, diag\left[\frac{1}{s-\lambda_i}+\frac{1}{s-\lambda_i^*}\right] diag\left[\frac{1}{m_i}\right]\boldsymbol{\Phi}^T\,\mathbf{F}(s) \\ &= \sum_{k=1}^{N_n}\left[\frac{\boldsymbol{\phi}_k\,\boldsymbol{\gamma}_i^T}{s-\lambda_i}+\frac{\boldsymbol{\phi}_i\,\boldsymbol{\gamma}_i^T}{s-\lambda_i^*}\right]\mathbf{F}(s) \\ &= \mathbf{H}(s)\mathbf{F}(s)\end{aligned} \tag{2.20}$$

being $\boldsymbol{\gamma}_i$ the line vector of the modal participation factors for mode *i*. In Eq. 2.20 the transfer matrix **H**(*s*) is a square matrix $\in C^{N_n \times N_n}$. However, a transfer matrix more close to the experimental world should relate only the N_i *DOFs* excited by the input and the N_o DOFSs wherein the output is actually measured. Hence, generally **H**(*s*) should be a rectangular matrix $\in C^{N_o \times N_i}$. In addition, since not all the N_n modes are generally observable, the sum in Eq. 2.20 should be limited to a subset of such modes (Magalhães & Cunha 2011).

2.5 Modal Identification

2.5.1 OMA in the frequency domain

2.5.1.1 The Peak-Picking technique

The Peak-Picking (PP) techniques was developed by Bendat & Piersol in the 1970s (Bendat & Piersol 1993) and it is so called since the eigenfrequencies are identified as the peaks of an appropriate spectral plot. PP is still widely used nowadays in the modal identification of Civil Engineering structures because of its simplicity and capability to generally provide modal parameters with enough accuracy.

Notwithstanding its simplicity, however, the techniques rely on well defined assumptions whose violation usually leads to erroneous results. In short, two basic assumptions govern a successful use of PP technique (Bendat & Piersol 1993, Peeters 2000):

a) Low structural damping;

b) Mode shapes well-separated in the frequency domain;

In fact, PP identifies operational deflection shapes (ODS) instead of mode shapes and

for closely spaced modes ODS are in practice the superposition of multiple modes. ODS is defined as the deformation of a structure when a pure harmonic excitation is acting; theoretically ODS is a combination of all mode shapes, but in practice only modes having eigenfrequencies close to the excitation frequency contribute significantly.

The basic idea can be presented as follow. Firstly, any system response vector $\underline{\mathbf{y}}(t)$ can be expressed in terms of modal coordinates vector $\underline{\mathbf{q}}(t)$ as:

$$\underline{\mathbf{y}}(\mathrm{t}) = \phi_1 q_1(t) + \phi_2 q_2(t) + \cdots = \boldsymbol{\Phi}\underline{\boldsymbol{q}}(t) \tag{2.21}$$

where $\boldsymbol{\Phi}$ is the matrix containing the N_n mode shapes of the dynamic system. Afterwards, the covariance matrix of the responses $\mathbf{C}_{yy}$ is considered:

$$\mathbf{C}_{yy}(\tau) = E[\mathbf{y}(t+\tau)\mathbf{y}(t)^T] \tag{2.22}$$

Substituting Eq. 2.21 in Eq. 2.22 yields to:

$$\mathbf{C}_{yy}(\tau) = E[\boldsymbol{\Phi}\mathbf{q}(t+\tau)\mathbf{q}(t)^T\boldsymbol{\Phi}^H] \quad \Leftrightarrow \quad \mathbf{C}_{yy}(\tau) = \boldsymbol{\Phi}\mathbf{C}_{qq}(\tau)\boldsymbol{\Phi}^H \tag{2.23}$$

For a white noise input and low damped well-separated modes, the spectrum at any eigenfrequency ω_i is dominated by a single mode, so that the following approximated expression for $\mathbf{C}_{yy}(\omega)$ can be considered (Peeters 2000):

$$C_{yy}(iw_i) \approx \frac{\Phi_i\, g_i^T\, R_{uu}\, g_i\, \Phi_i^H}{(\xi_i w_i)^2} \tag{2.24}$$

Afterwards, if a complex scalar α_i is defined as:

$$\alpha_i = \frac{1}{(\xi_i\omega_i)^2}\mathbf{g}_i^T\mathbf{R}_{uu}\mathbf{g}_i^* \tag{2.25}$$

Eq. 2.24 can be rewritten as:

$$C_{yy}(iw_i) \approx \alpha_i\Phi_i\Phi_i^H \tag{2.26}$$

The interpretation of Eq. 2.26 is that at a resonant frequency ω_i, each column of the spectral matrix (or equivalently each row) can be considered as an estimation of the observed mode shape Φ_i up to a scaling factor. Of course, if a column (or a row) corresponds to a DOF of the structure placed at a node of a certain mode, this mode

cannot be identified.

In addition, in Bendat & Piersol (1993) a strategy for a damping estimation was proposed. It is based on the classic half-power bandwidth concept (Bendat & Piersol . 1993), hence assuming ω_1 and ω_2 as the two frequency values left and right from the eigenfrequency ω_i as close as possible to ω_i where the magnitude of a certain element of the spectrum matrix is half the resonance magnitude, an estimation of damping is given by the following:

$$\xi_i \approx \frac{\omega_2 - \omega_1}{2\omega_i} \tag{2.27}$$

However damping estimation by Eq. 2.27 is usually not very accurate as reported in Peeters (2000) wherein some numerical evaluations of values resulting from Eq. 2.27 were performed.

Some refinements of PP or variant of the classical technique have been presented in literature. Main proposals have been the following:

a) In Bendat & Piersol (1993) it is suggested the inspection both of coherence functions (which should be close to one at the resonant frequencies because of the high signal-to-noise ratio at these frequency values) and of the phase angle of cross spectra (which should be really close to either 0 or π radiant at resonant frequencies) in order to select the structural modes;
b) In Felber (1993) it is suggest to get a "global picture" of the eigenfrequencies by the computation of an Averaged Normalized Power Spectral Density (ANPSD) function. More specifically, the diagonal elements of the spectral matrix Gyy(f) namely the Auto Power Spectral Density (APSD) functions are firstly considered. Then, these functions are normalized and finally they are averaged so that an ANPSD function summarizing the information contained in the APSDs. However, when signals from symmetric points of the structure have been measured, in averaging the APSDs different strategies might be useful: adding the APSDs usually lead to highlight bending modes; whereas, subtracting the APSDs,

torsion modes usually can be better identified;

c) Finally, as reported in Peeters (2000), if a reference sensor can be properly positioned on the structure so that its auto-spectrum contains all the physical information (modes) of a certain structure, then, only the cross-spectra between all the other sensors and the reference sensor can be estimated so that the computational work is reduced. In other words, it is assumed that by a properly positioned reference sensor, only one column (or one row) of the spectral matrix Gyy(f) becomes sufficient to estimate the mode shapes.

Concerning the accuracy of the technique, it relies on the estimation procedure of spectral density functions starting from digital signals. Of course, as a technique in the frequency domain the accuracy is related to the frequency resolution Δf (or resolution bandwidth B_e) adopted which depends on the frequency bandwidth B and the number of frequency lines or bins. Estimation errors are widely discussed in literature (see e.g. Bendat & Piersol 1993) and can also affect the accuracy of the procedure known as Welch's method (or modified periodogram method) commonly used to estimate the spectral density functions.

2.5.1.2 The Frequency Domain Decomposition technique

The technique known as Frequency Domain Decomposition (FDD) originally presented in (Brincker *et al.* 2000, Brincker *et al.* 2001) can be considered as an evolution of PP technique and its practical implementation. The idea of the Frequency Domain Decomposition technique is to perform an approximate decomposition of the system response into a set of independent, single degree of freedom (SDOF) systems, one for each mode.

The basic idea of FDD is similar with that of Peak Picking method, let us refer to Eq. 2.23, the covariance matrix of the measurements is related to the covariance matrix of the modal coordinates through the mode shape matrix. The equivalent relation in the frequency domain is obtained by applying the Fourier transform:

$$\mathbf{G}_{yy}(f) = \mathbf{\Phi}\mathbf{G}_{qq}(f)\mathbf{\Phi}^{H} \tag{2.28}$$

where contains the basic idea of FDD if the following assumptions are satisfied:

a) modal coordinates are uncorrelated;

b) the spectral matrix in modal coordinates $\mathbf{G}_{qq}(f)$ is diagonal;

c) mode shapes are orthogonal;

As a consequence of (a)-(c) Eq. 2.28 has the meaning of SVD of the response spectral matrix $\mathbf{G}_{yy}(f)$. Hence, the basis equation of FDD becomes the following:

$$\mathbf{G}_{yy}(f) = \mathbf{U}(f)\mathbf{S}(f)\mathbf{U}(f)^{H} \tag{2.29}$$

where $\mathbf{U}(f)$ are the left and right matrices of the singular vectors and $\mathbf{S}(f)$ is a diagonal matrix containing the singular values (SVs).

The FDD technique is therefore based on the estimation of the spectral density matrix $\mathbf{G}_{yy}(f)$ and its subsequent SVD. Afterwards, the identification of structural modes by a manual approach is essentially based on the investigation of the peaks of the first singular value function (SV_1). In other words, around each well separated resonant peak the SV_1 function represents an accurate approximation of the transfer function which reaches, at resonance, a local maximum wherein only one mode is important in Eq. 2.20. Hence, a rank-one problem leads to an accurate identification of such a mode. Finally, when a structural mode is identified, say at frequency f_0, an accurate estimation of the associated mode shape is given by the corresponding first singular vectors at the same frequency line namely:

$$\phi = \mathbf{u}_1(f_0) \tag{2.30}$$

On the contrary, if two or more modes have closely spaced eigenfrequencies, the problem rank will be two or more around those frequencies, so that the SV_1 is not enough for the modal identification (Peeters 2000).

Finally, concerning the FDD techniques the following general comments can be made:

- FDD technique is based on using frequency lines coming from the FFT analysis, that the accuracy of the estimated natural frequency depends on the FFT

resolution adopted in estimating the spectral matrix;

- modal damping is not estimated;
- FDD generally allows the modal identification of closely-spaced modes. Thus, FDD is a significant enhancement of the PP technique which is not capable in accurately identifying closely modes;
- the technique works well even when significant noise is present (Brincker 2007);
- If a rank-one problem governs the modal identification (well separated modes) of a certain mechanical system, then SV1 is generally enough to identify modes, since it concentrates information from all spectral density functions;
- Generally, SV_1 is more effective than the corresponding "global picture" given by the ANPSD since the latter may lead to loss information when one torsion mode is placed between two bending modes and close to them.

2.5.2 OMA in the time domain (SSI)

The stochastic subspace identification technique is a time domain method that directly works with time data, without the need to convert them to correlations or spectra. The stochastic subspace identification algorithm identifies the state space matrices based on the measurements by using robust numerical techniques. Once the mathematical description of the structure (the state space model) is found, it is straightforward to determine the modal parameters. The SSI methods are based on the discrete-time stochastic state-space form of the dynamics of a linear – time - invariant system under unknown excitation:

$$\begin{aligned} \underline{\mathrm{x}}(\mathrm{k}+1) &= \underline{\underline{A}}\,\underline{x}(k) + \underline{w}(k) \\ \underline{\mathrm{y}}(\mathrm{k}) &= \underline{\underline{C}}\,\underline{x}(k) + \underline{v}(k) \end{aligned} \tag{2.31}$$

where k is the generic time step, $x \in \mathrm{R}^{\mathrm{n}}$ is the state vector, $A \in \mathrm{R}^{\mathrm{n}\times\mathrm{n}}$ is the system matrix, $w \in \mathrm{R}^{\mathrm{n}}$ is the external input, modeled as a white noise vector process, $y \in \mathrm{R}^{\mathrm{l}}$ is the vector containing the l out-put measurements, $C \in \mathrm{R}^{\mathrm{l}\times\mathrm{n}}$ is the corresponding output matrix and $v \in \mathrm{R}^{\mathrm{l}}$ is another white noise vector process representing the noise

content of the measurements. The total number of available time samples is equal to s.

After estimation the model matrices A and C, with the convariance driven SSI algorithms, the modal parameters of the structural system can be idenfied. The natural frequencies f_i, modal damping ration ξ_i and mode shapes ϕ_i of the structural system are calculated from:

$$A = \Psi\Lambda\Psi^{-1}, \Lambda = \mathrm{diag}(\lambda_i) \in C^{n\times n}, i = 1, \dots, n \tag{2.32}$$

$$\lambda_i^c = \frac{\ln \lambda_i}{\Delta t}, i = 1, \dots, n \tag{2.33}$$

$$f_i = \frac{|\lambda_i^c|}{2\pi}, i = 1, \dots, n \tag{2.34}$$

$$\xi_i = \frac{real(\lambda_i^c)}{|\lambda_i^c|}, i = 1, \dots, n \tag{2.35}$$

$$\Phi = C\Psi, \Phi = (\phi_1, \dots, \phi_n) \tag{2.36}$$

Data-driven SSI consists of the following steps: (a) construction of the block Hankel matrix of the measurements, H_i; (b) computation of the projection matrix, $P_i \in R^{li\times j}$; (c) estimation of the observability matrix, Γ_i; (d) extraction of the modal parameters estimates from matrix Γ_i.

The block Hankel matrix is defined as:

$$H_i = \begin{bmatrix} y(0) & y(1) & \cdots & y(j-1) \\ y(1) & y(2) & \cdots & y(j) \\ \vdots & \vdots & \ddots & \vdots \\ y(i-1) & y(i) & \cdots & y(i+j-2) \\ \hline y(i) & y(i+1) & \cdots & y(i+j-1) \\ y(i+1) & y(i+2) & \cdots & y(i+j) \\ \vdots & \vdots & \ddots & \vdots \\ y(2i-1) & y(2i) & \cdots & y(2i+j-2) \end{bmatrix} = \begin{bmatrix} Y_p \\ \hline Y_f \end{bmatrix} \tag{2.37}$$

where 2i and j, with $j \le s - 2i + 1$, are user-defined quantities representing the number of output block rows and the number of columns of matrix Hi, respectively.

The block Hankel matrix of the measurements, in Eq. (2.37), is subdivided into two sub-matrices, named as Y_p and Y_f, which are usually referred to as past and future output block matrices. The orthogonal projection of the row space of Y_f onto the row

space of Y_p, which is denoted by Y_f/Y_p, can be directly calculated yielding a matrix, $P_i \in R^{li\times j}$, which is known as projection matrix. The main result of SSI yields $P_i = \Gamma_i \hat{X}_i$, where Γ_i is the observability matrix of the system and $\hat{X}_i$ is a matrix containing Kalman filter estimates of the state vector at different time steps. Hence, matrix Γ_i can be estimated from the singular value decomposition of matrix $W_1 P_i W_2$, where W1 and W2 are convenient weight matrices. The available SSI-data algorithms essentially differ for the expressions of the weight matrices. The modal parameters estimates are then readily extracted from matrix Γ_i.

2.6 Application of Software Programmes

2.6.1 DADiSP Program

DADiSP (Data Analysis and Display) is a computer program developed by DSP Development Corporation which allows to display and manipulate data series, matrices and images in an environment similar to a spreadsheet.

The DADiSP program contains a graphical software tool for displaying and analyzing data from virtually any source (Timm & Priest. 2004). The DADiSP Worksheet applies key concepts of spreadsheets to the often-complex task of displaying and analyzing entire data series, matrices, data tables and graphic images. Data from an individual section can be read from the DATAQ file and displayed in DADiSP where different functions can then be applied to the signal (i.e., moving average, Fourier Transform, etc.).

Because it is often easier to interpret data visually rather than as a column or table of numeric values, DADiSP's default presentation mode is usually a graph within a Worksheet Window. A Worksheet Window in DADiSP serves two purposes at once—it provides a place to store data and serves as a tool for viewing data.

Plenty of functions can be realized by DADiSP, including (DADISP. 2003):

- Acquire and/or import data using DADiSP's easy-to-follow pop-up menus

- Reduce and edit data and save the intermediate results
- Transform data by a variety of matrix and other mathematical operations
- Analyze data or digital signals by extensive signal processing tools
- Produce quality output using a variety of annotation features.

Furthermore, DADiSP is completely customizable to create specific menus, macros, functions and command files.

A brief description of the basic analysis and spreadsheet paradigm is presented here to give a sketch of DADiSP worksheet.

The first task generally performed is to read/import data (from data files in various formats) and visualize the data in graphical windows. According to the view of data, some functions can be realized such as zoom in, add grid, expend or compress the data series horizontally or vertically and so on.

Then, according to the purpose of analysis, some formulas can be written in the window with Function wizard. For example, the average value of the data from window 1 can be analyzed.

On the basis of the former steps, more functions can be introduced. For example, over plotting is a simple way to visually compare original data to the averaged data.

According to the simple example, the basic use of DADISP program is drawed. The application of this software for modal identification is presented in chapter 4.

a) 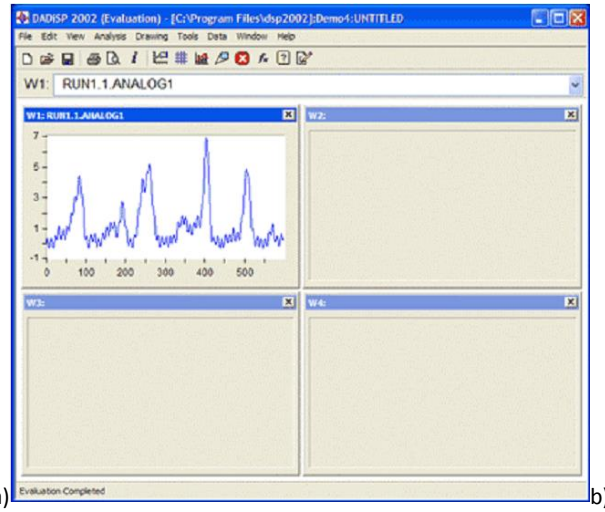

b) 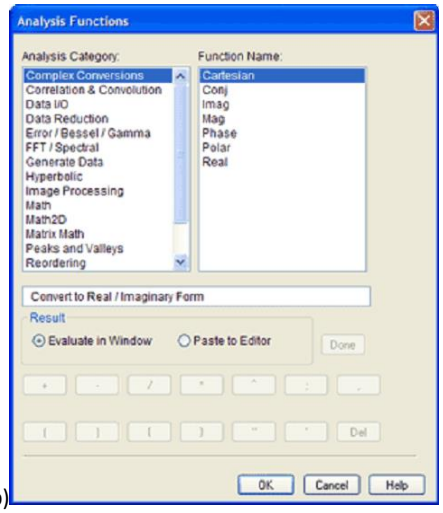

Figure 2-3 Order window of DADISP a)read data; b)analysis function

2.6.2 ARTEMIS Program

The ARTeMIS Extractor is the effective tool for modal identification from ambient vibration data. The software allows the user to accurately estimate natural frequencies of vibration and associated mode shapes and modal damping of a structure from measured responses only.

In all versions of the ARTeMIS Extractor, one can generate geometry information and perform measurements in any standard measurement system and then perform modal identification and validation (SVS. 2012). Response data files can be provided in a flexible ASCI format or by making use of the standard Universal File Format (UFF). All versions include powerful and efficient signal processing tools, capabilities for 2D displaying of spectral densities and correlation functions and for 3D geometry validation and mode shape animation. All plots and tables can easily be exported to other Windows programs such as Word and Excel using copy/paste commands. This also helps producing complete documentation with a minimum amount of work involved.

Some more details are presented following:

Data input

1) ARTeMIS Extractor configuration file and data file (ASCII). Data file format is the MATLAB /ASCII file format, stored as a matrix, time series stored column by column.
2) Maximum number of channels and data is unlimited by the software.

Data output

1) Copy/Paste and Print functions for all graphics and tables.
2) Modal results: Universal File Format (ASCII) including geometry, one or more modes in each file.
3) Modal results: ARTeMIS Extractor output files, one or more modes in each file (ASCII) .

4) Modal results: Interface to FEMtools updating software through UFF.
5) Animations: export of AVI movie files to e.g. Windows MPlayer or PPT

Signal processing

1) Decimation, 1-1000 times, digital anti-aliasing filter, cut-off at 0.8 times Nyquist frequency.
2) Filtering: low-pass, high-pass, band-pass, band-stop Butterworth, filter order 1-50 poles, arbitrary cut-off frequencies, test for filter stability Spectral estimation using FFT and Welch's averaged periodogram method.
3) Data Plotting: Spectral magnitude and phase, singular value decomposition of spectral matrix, average of full spectral matrix, average of diagonal elements of spectral matrix, coherence of spectral matrix, filter characteristic, correlation functions. Cursor read out on all curves

Frequency domain decomposition

1) User choices: Peak picking
2) Frequency resolution: defined by frequency lines in spectral density function
3) Mode shape estimation: Immediate animation
4) Damping: None

Enhanced frequency domain decomposition

1) User choices: Peak picking, MAC level for identification of spectral peak, time interval for identification of damping
2) Frequency resolution: Not limited by frequency resolution
3) Mode shape animation: Immediate animation, mode shape estimate improved by frequency domain averaging
4) Damping: Estimated from free decays corresponding to identified spectral Peak

Time domain identification

1) Basic Method: Data driven Stochastic Subspace Identification
2) User choices:
   a) Unweighted Principal components, Principal Components or Canonical

Variate Analysis;

b) Model orders: from one mode to the size defined by the common SSI input matrix;

c) Stabilization criteria: natural frequency, damping, mode shape

3) Select and link: Modes from the models chosen from each data set is selected and linked in a separate window with snap functions and editing facilities

4) Uncertainty estimation: In case of several data sets, the empirical standard deviation is calculated for natural frequencies and damping ratios

Validation

1) Comparison: Modal model vs. FFT based auto- and cross-spectra

2) Comparison: Modal model vs. unbiased (zero-padded FFT) auto- and cross-correlation functions

3) Modal Assurance Criterion, MAC plots for comparison of mode shapes between same or different estimation techniques as well as between same or different projects

4) Simultaneous animation of different mode shapes

5) Animation of differences between mode shapes

Chapter 3

Investigation performed on the “Gabbia” Tower, Mantua

3.1 Introduction

The "Gabbia" Tower, about 54.0 m high and surrounded by an important historic building, is a symbol of the cultural heritage in Mantua, northern Italy. Up to few years ago, the seismic risk of this area was not considered high and the last catastrophic earthquake was far in time. The local building techniques, then, evolved without seismic protection details and at present the historic structures, particularly if decayed and without continuing maintenance, are highly vulnerable.

Two severe earthquakes happened in May 2012. Damages were reported on several historic buildings mainly in the south area of the province of Mantua, where Politecnico di Milano has a large campus. Consequently, “Polo Territoriale di Mantova” and the VIBLAB (Laboratory of Vibration and Dynamic Monitoring of Structures) of Politecnico di Milano were committed to assess the structural condition and to evaluate the seismic performances of the "Gabbia" Tower. The fall of small masonry pieces from its upper part, reported after the earthquake, provided strong motivations for extensively investigating the seismic vulnerability of the building.

After the earthquakes of May 2012, the access to the inner structure of the tower - originally provided by wooden stairs – was not available due to lack of maintenance.

Consequently, in August 2012 geometric survey and visual inspection of the external

fronts of the tower were carried out by using a mobile platform. In the same days an ambient vibration test was performed: 4 cross sections were instrumented at several levels along the height of the tower and 3 accelerometers were mounted in each section.

These investigations clearly showed the poor structural condition of the upper part of the tower and the need of a repair intervention.

Hence, a metallic scaffolding and a light wooden roof were installed inside the tower, with the objectives of allowing the inspection of the inner bearing walls and providing the inner access needed for the forthcoming strengthening intervention.

Subsequently, the geometric survey and visual inspection of inner walls were carried out in October and November 2012, together with some slight and non-destructive tests on the materials. Furthermore, a second ambient vibration test (with the same arrangement of the first one) was carried out in November 27th 2012. The comparison of the results obtained from the two dynamic tests showed the same variations of the natural frequencies. In order to survey the structure condition of the tower, a long-term dynamic monitoring system was installed in December 2012.

In paragraph 3.2, some information about the earthquakes of May 2012 is presented, and the “Gabbia” Tower is described in Paragraph 3.3. In Paragraph 3.4, the results of visual inspection and geometric survey are summarized. The tests on the materials are presented in Paragraph 3.5. Details of the two ambient vibration tests are presented in Paragraph 3.6, together with the arrangement of the tests and the discussion of the results.

3.2 Information about earthquakes

In May 2012, two major earthquakes occurred in Northern Italy, causing 26 deaths and widespread damage.

The first earthquake of magnitude 6.1 hit Northern Italy, on May 20th, 2012 at 02:03 UTC, in the region of Emilia Romagna. This event was largely felt in Northern Italy.

Important damages are reported in the province of Ferrara, Modena, Mantova and Reggio Emilia where significant cultural heritage buildings have been affected.

9 days later, on May 29th, 2012 at 07:00 UTC, a second magnitude 5.8 earthquake occurred 15 km west from the May 20th event. The mechanisms involved in both events are similar. The region, already affected by the previous event, is experiencing important damages and causalities. This strong earthquake damaged several historic buildings, such as churches, bell-tower, castles, palaces, and many of the factories in the area. The main shock could be felt as far away as Switzerland. The focal mechanism indicates that the earthquake was a result of thrust faulting, with a north-south direction of compression, on a fault plane trending west-east. This type of faulting is consistent with the regional tectonic setting.

The acceleration of the two earthquakes was recorded by the sensors installed in Mantua (Figure 3-1). In Figure 3-2 examples of damaged buildings are shown.

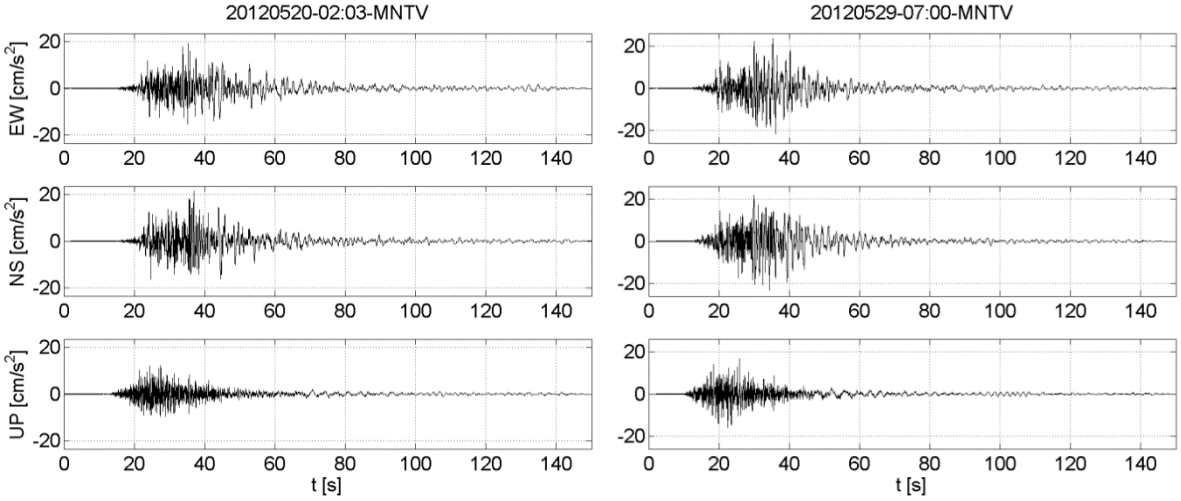

Figure 3-1 The acceleration of earthquakes recorded in Mantua

Figure 3-2 Buildings damaged by the earthquakes of the spring 2012

3.3 Description of the tower

The "Gabbia” Tower, about 54.0 m high, located in Via Cavour 102, is the tallest tower in Mantua. Construction techniques, materials, geometry and some document would confirm the building in late XII century (and no later than the early years of the next century).

An important palace surrounds the tower but, even if this building dates back nearly the same period of the tower, the load bearing walls of the palace are not effectively linked. Precious frescoes, dating back to XIV and XVI centuries, decorate the tower’s fronts embedded in the palace (Gentile et al. 2012).

Figure 3-3 gives the location and views of the tower from four directions. Figure 3-4 shows the tower in some historical drawings.

The tower’s plan is almost squared and the load bearing walls are about 2.4 m thick until the upper levels; the upper part of the building has a two level lodge, which hosted in XIX century the observation and telegraph post.

Figure 3-3 a) West view; b) East view; c) South view; d) North view e) Location of the tower

Figure 3-4 a) Expulsion of Bonacolsi, Oil on canvas by Domenico Morone, 1494; b) Urban description map the city of Mantua, particularly with the “Gabbia” Tower by G. Bertazzolo (1628)

The “Gabbia”, with the meaning of “cage”, was installed in 1576 when Duke William decided to punish the criminals by not only prisoning them but also exposing them to the public in the cage as a warning to bad people. The front with the cage (Gabbia) is shown in Figure 3-5.

Figure 3-5 Views of the tower front with the cage

Maintenance works were carried out in 1811 (Zuccoli, 1988), including the painting of refined decorations on the inner walls, along the wooden staircases leading to the upper levels. Those staircases have not been practicable since several years and the inner access to the tower was re-established only recently (October 2012) through provisional scaffoldings; it should be noticed that the entrance is at 17.7 m from the

ground level (Figure 3-6) but the entrance to the lower portion and the base of the tower is still not accessible. The tower was used in the XVI century as open-air jail and the hanged cage on the S-W front (Figure 3-6) gives the building its name of "Gabbia” Tower.

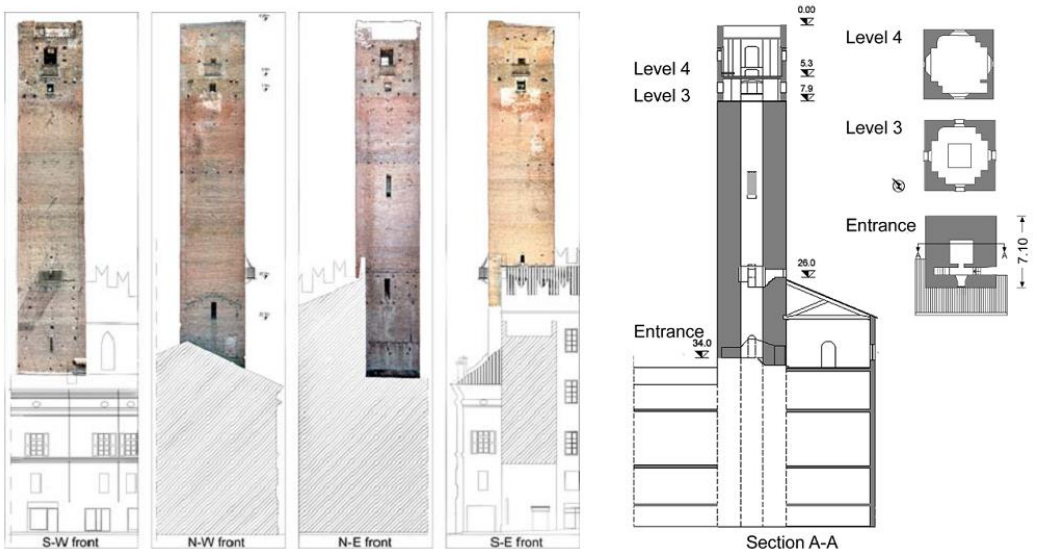

Figure 3-6 Fronts and section of the tower

3.4 Geometric survey

Geometric survey is the first step in the tower diagnosis.

The geometric survey and visual inspection was carried out in two phases: in August 2012, the external fronts were examined; whereas in October and November 2012, the inner walls of the tower were investigated.

The survey operations were facilitated by the placement of a reference metric tape on the several fronts. In this way it was possible to complete the survey in limited time by the inspection and the localization of the major discontinuity. The crack pattern and the several discontinuities detected on the fronts of the tower was accurately mapped and superimposed on the photo rectification of the external fronts. The survey was carried out by identifying the cracks as well as the structural discontinuities related to the evolution of the building.

3.4.1. Inspection of North-east front

Discontinuities are the main problems of the tower, which is detected from the visual inspection. The reasons of the discontinuities are reported in (Saisi & Gentile. 2013). There are numerous discontinuities due to the different phases of constructions in the upper part of the wall (Figure 3-7). By observing the changes of the masonry texture of the upper part of the north-eastern side, with staggered courses and not continuous, merlon shaped discontinuities can be recognized. These discontinuities are concentrated from about 5.50 m from the top. Settlement of the interventions and of the opening infillings coupled with the highly disordered masonry and mortar erosion causes lack of horizontality of the joints of the crowing and the development of cracks. In such a situation it is possible to get a fast evolution of the phenomenon with significant local collapses.

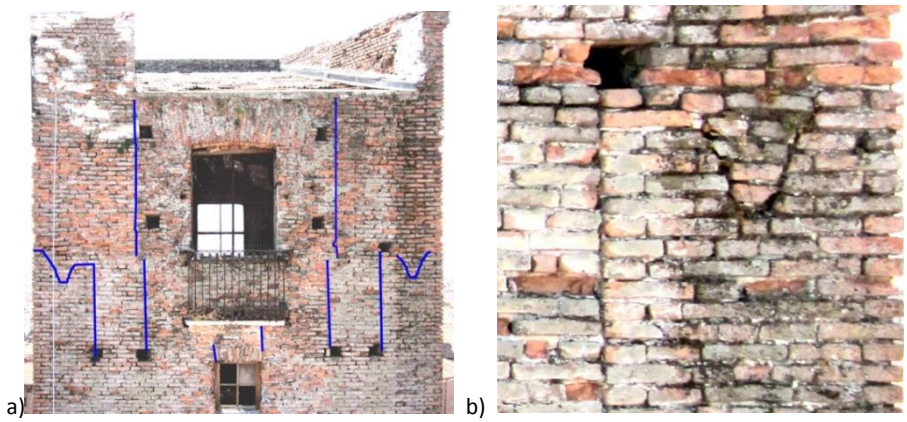

Figure 3-7 Detail of a) top of the N-E side b) changes in the texture of the upper part

Another important thing to highlight is the general state of decay of the joints and brick of the upper part of the tower and in particular between the openings (Figure 3-8a). The walls between two openings are very irregular. The erosion of the mortar joints partially hides the presence of the cracks starting from the end of the stone slab of the upper opening. The flat arch above the window (Figure 3-8a) is damaged and not effectively supported by the masonry wall.

Accurate observations should be directed to the crowning. Despite the presence of

metallic angular support that strengthens locally the masonry on the corners, the erosion of the mortar joints is extensive and deep. In addition, local repair mortar with a white color is easily recognized. The presence of the strengthening tieing, apparently passive, may not be effective, not adhering to the wall (Figure 3-8 b) and c)). Furthermore, the walls of the crown seem very vulnerable and decayed, with disintegration of the joints and lack of bricks. At the moment of the summer survey, debris were present, removed after the roof replacement.

At about 6.80 m from the top (Figure 3-9), a clear change appeared in the masonry texture, size and surface treatment of bricks. This change is underlined the presence of a series of holes of great size and with a band of about 2.00 -2.50 m of reddish color brickwork masonry The color change is due to the absence of the grey patina. In the transition zone to about 6.80m, the erosion of mortar joints are observed, and the presence of vegetation with a root system creeping in the mortar (Figure 3-9).

Figure 3-8 a)Walls between two openings; b),c)The degradation of bricks and repair mortar

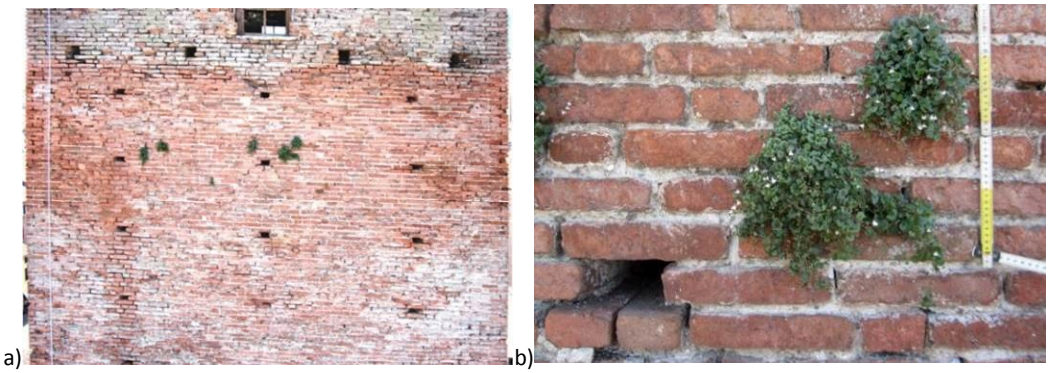

Figure 3-9 a)Change in the texture of walls, size and the surface treatment of bricks; b)Presence of vegetation with a root system that penetrates deep into the mortar.

3.4.2 Inspection of South-east front

The observations are similar to what was found from Northeast front. In fact, in the upper part of the tower the same masonry discontinuity (Figure 3-10) attributable to changes in the building with infilling masonry elements with poor connection or without connection to the side masonry. These discontinuities are concentrated from about 5.50 m from the top.

The discontinuities are sharp, without effective links to the side wall portions. In addition, the masonry is irregular and with mortar joint erosion and surface decay of the bricks and with non-horizontal courses. There are also several scaffolding holes, even passing-through the wall section

This situation may be the cause of cracks in the area next to the left corner, which extend from a height of about 3.5 m up to the top (Figure 3-11a) and b)). In addition, the masonry crowning is irregular, with a wide and deep decay of the mortar joints that causes the loss of horizontality of the joints themselves. The degradation is particularly evident in correspondence of the right corner (Figure 3-11 c) and d)).

a)  b) 

Figure 3-10 a)Top of the Southeast front ;b) Details of the discontinuities

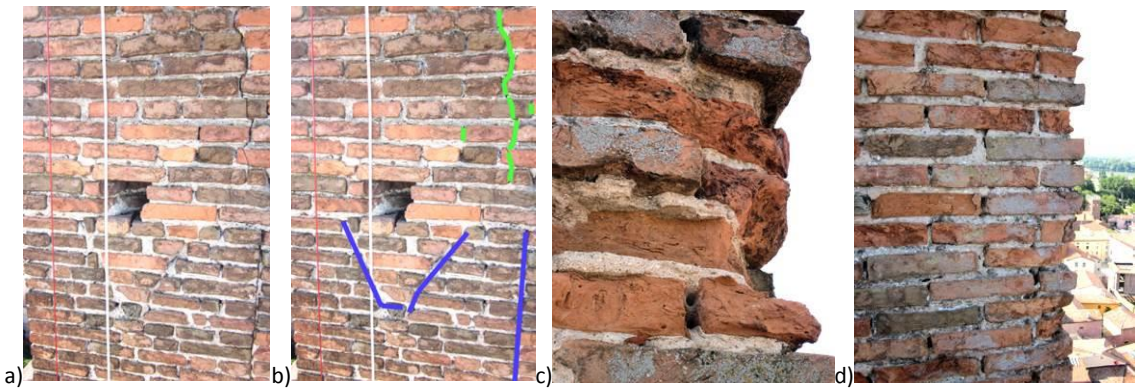

Figure 3-11 a),b) Several cracks near the left corner from around 3.5 m up to the top; c)d)Particularly pronounced decay at the right corner

3.4.3 Inspection of North-West front (with the cage)

The observations are similar to what was found in the North-East and South-East fronts. In the upper part, the same number of discontinuity of the wall (Figure 3-12) attributes to changes in the building with infilling masonry portion or poorly link without any connection to the side masonry. The similarity of the observations for all the fronts clearly indicates the similarity of the morphology and construction methods and its specific vulnerability, both in the choice of materials and the construction without effective structural connection between the masonry elements. These discontinuities are concentrated from about 5.50 m from the top.

Similar to other fronts, the discontinuities are always sharp, without effective connection with the side masonry portions even in the central part of the crown. In general, besides the various discontinuities, the upper part of the tower shows the loss of horizontality of the joints and the decay in depth of the mortar joints and of the brick surface. The brickwork appears irregular, with bricks of various sizes, color and state of preservation. The degradation is particularly evident in correspondence with the left corner. In Figure 3-12 b), the presence of two blocks of stone can be distinguished, one used as a lintel of the window and one inserted in the masonry.

At the level of the cage there are several discontinuities in the wall surface, probably related to structures that no longer exist (Figure 3-13).

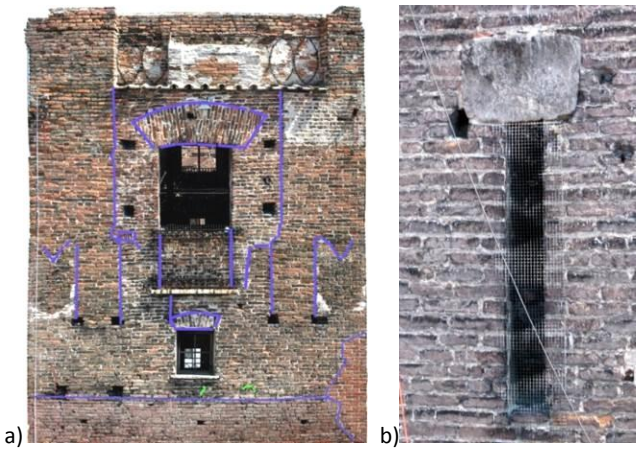

Figure 3-12 a) Top of the South-West front; b) The presence of a blocks of stone

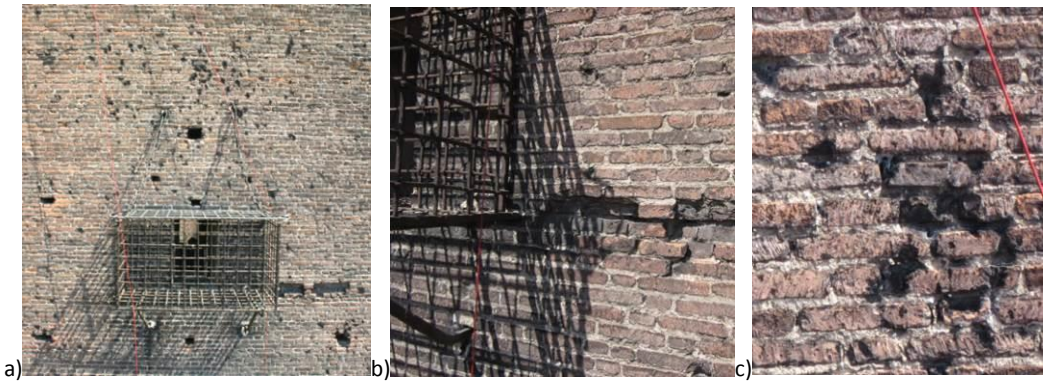

Figure 3-13 a),b) Details around the cage; c)Discontinuities in the wall surface around the cage

3.4.4 Inspection of South-west

The observations are quite similar to that of Northeast, Southeast and Southwest, with similar layout and disposal of the discontinuity of the wall (Figure 3-14a). These discontinuities are concentrated at about 5.50 m from the top.

The upper part of the tower shows over the loss of horizontality of the joints (Figure 3-14b) and the deterioration in depth of the mortar joints and bricks, and several cracks. The thickness of the wall is reduced at the level of the crown and not well connect to the other masonry portions. The decay of bricks placed around the corner is diffuse, particularly in the area of the crown.

At about 13.60 m, scaffolding holes are present. The side holes are very close to the corner. Local corner of the masonry is composed of 3, 4 courses that could easily become instable and drop off. In the lower part of the tower, it is recognized in the

wall surface the shape of a roof of a building leaning against the tower, which no longer exists any more (Figure 3-15a). As a reading of the discontinuity of the wall, this opening was obtained in a second time with respect to the construction of the tower (Figure 3-15b). The opening was then infilled with bricks apparently of recent production.

a) b)

Figure 3-14 a) Top of the front North-West with highlighting structural discontinuities; b) The loss of horizontality joints and the degradation in depth of mortar joints and brick.

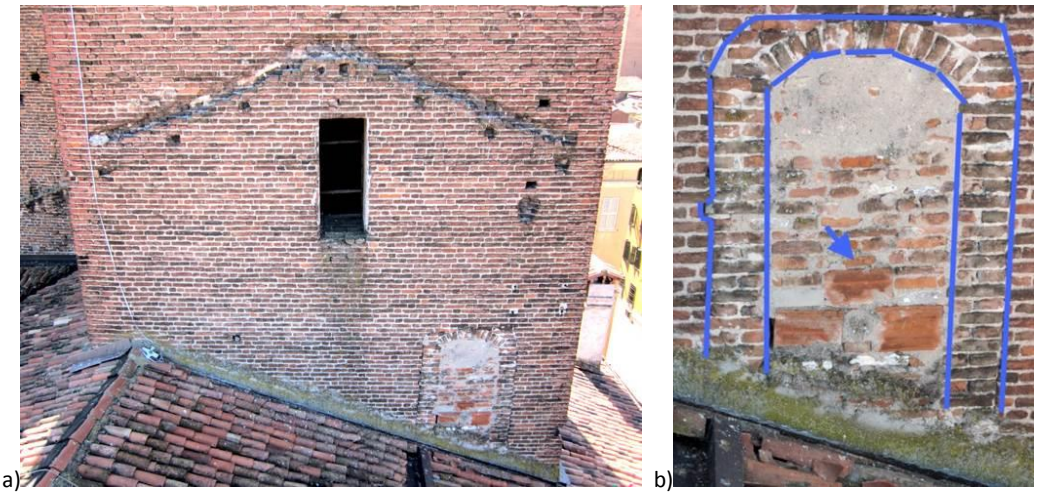

a) b)

Figure 3-15 a) Detail of the wall at about 29.50 m, a roof of a building leaning against the tower, b) Details of the infilled opening, formed in a second time with respect to the construction of the tower

3.4.5 Inner inspection of the tower

The interior of the tower is largely covered with a fine decorated plaster which

prevents a general overview of the characteristics masonry walls. Up to the third level (about 43.8 m) in the area without plaster because of the decay, the masonry is apparently intact, with a mortar with a good consistency (Figure 3-16). The deterioration of the plaster was probably determined by the percolation of water from the previous roof.

In the upper part, however, the masonry is characterized by high constructive and material inhomogeneities and a noticeable degradation of the surfaces. See as an example (Figure 3-17a) on the inner fronts Southwest and West to level 4. The top end of the tower has a number of interventions and discontinuities, often passing through the wall section, confirming the observations of the outside front.

Figure 3-16 Detail of wall texture in correspondence with gaps render (about 16 m from the top). The equipment is ordered and the mortar of good consistency.

At level 3, the lack of plaster show irregular masonry, with repairs and discontinuity, as well. Details of the wall texture of the corner at the third level are shown in Figure 3-17 b). The angular elements are easily recognized, and the geometry of the corner North is differentiated with respect to the other corners being rounded. At the fourth level the configuration of the corners of North and South is highly complicated (Figure 3-18).

a)  b) 

Figure 3-17 a) Detail of the opening of the interior elevation view corner Southwest and West; b) Details of the wall texture of the corner pieces to the third level



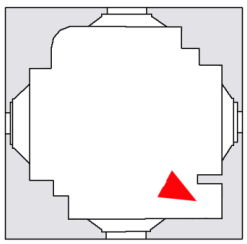

Figure 3-18 Fronts Southeast and South of the corner detail.

3.5 Local material characteristic identification

3.5.1 Flat jack tests

The tests were performed on two locations and each one of them both single and double flat jacks tests were carried out for the relief of the state of compressive stress agent in the walls and the deformability of the masonry (Tiraboschi & Cantini. 2013).

Location 1: Front of Via Cavour, 1.10 m height from the floor (street level), 11 m approx. from the north-west wall of the room.

Testing area were found including two areas.

Table 3-1 Results from the 1st flat jack test

Reference Range $\Delta\sigma$ (N/mm²)		Elastic Modulus (N/mm²) $\Delta\sigma / \Delta\varepsilon_v$	Expansion coefficient of transverse $\Delta\varepsilon_h / \Delta\varepsilon_v$
0.2	1.1	5200	0.21
1.2	2.5	3050	0.17

Observations: The test was interrupted due to the formation of cracks at the sides of the upper jack, to a level of pressure equal to 28 bar.

The deformation of the jack during the test (initial thickness = 4 mm, the final variable from 7 to 12 mm) should be considered for the possibility of reduction of the constant parameters used.

Location 2: South West Side, inside the tower, height 32.8 m from Via Cavour. The arrangement is similar with the first one.

Table 3-2 Results from the 2nd flat jack test

Reference Range $\Delta\sigma$ (N/mm²)		Elastic Modulus (N/mm²) $\Delta\sigma / \Delta\varepsilon_v$	Expansion coefficient of transverse $\Delta\varepsilon_h / \Delta\varepsilon_v$
0.2	1.0	3300	0.39
1.0	1.3	1300	0.87

3.5.2 Sonic surveys

The instruments used for the sonic survey and the arrangement of the test are shown in Figure 3-19. And the results are presented in Table 3-3. Generally, the masonry of the crowning appears poor, both as regards the mortar joints and the surface of the bricks. This decay appears to be very advanced, leading to loss horizontality of the mortar courses, which aggravate the conservation status of an area already characterized by considerable discontinuity (Saisi & Gentile. 2013).

In addition to what was already mentioned, it is important to emphasize the various phases of construction recognizable around openings, with corner piers not connected to the coplanar masonry or to the openings. These masonry walls are also thin, simply

placed alongside the wall elements, with many passing through scaffolding holes, as shown in the outside front. The connection of the unfilled wall portions is definitely one of the priorities for action for the structure.

The inspections have confirmed the high vulnerability of the upper zone of the tower, both as regards the sharp discontinuity of the load-bearing masonry, both for the poverty of the masonry organization and the wide decay, both for the geometry of the structure, especially the corners South and North.

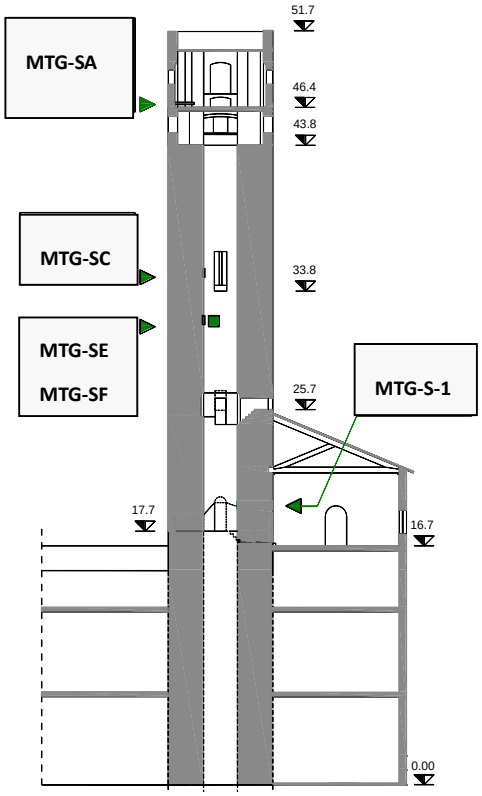

Figure 3-19 The arrangement of sonic survey instruments

Table 3-3 Summary of the results obtained by the sonic sensors

unit [m/s]	MTG-S-1	MTG-SA	MTG-SB	MTG-SC	MTG-SE	MTG-SF
velocity MIN.	1101.04	269.08	297.61	833.70	1014.28	982.98
velocity MAX	1592.84	1418.98	1713.48	1907.10	1799.50	1527.67
standard deflection	101.39	401.23	420.30	236.63	190.06	135.19
velocity MEDIA	1387.81	685.47	610.33	1448.14	1382.19	1317.51

3.6 Ambient vibration tests

3.6.1 Arrangement of dynamic test

The “Gabbia” Tower has been subjected to a campaign of dynamic studies performed on days 31 July, 1-2 August 2012 and 27 November 2012 by technicians of VIBLAB, Politecnico di Milano.

The measuring equipment consisted of:

(a) data acquisition system (Figure 3-20a) with 6 NI 9234 (resolution: 24 bit, sampling rate: up to 50 kHz / channel);

(b) Wilcoxon Research piezoelectric accelerometers 731A (nominal sensitivity 10 V/g, resolution: 0.5 g peak acceleration: ± 0.5 g), with power supply modules Wilcoxon Research P31 (Figure 3-20b);

(c) Temperature sensors.

As shown in Figure 3-21, 4 cross sections were instrumented and 3 accelerometers were mounted in each section. The positions of the sensors on the vertical direction were: 1) on the top of the tower, about 2m below the crown; 2) 7.30 m from the crown; 3) 18.00 m from the crown; 4) 26.00 m from the crowning and in line with the lower support of the cage.

It should also be noted that the accelerometers 1-2, 4-5, 7-8, 10-11 were placed at opposite corners of the south-west front, parallel to Via Cavour, while the sensors 3, 6, 9, and 12 were mounted on the south-east wall. 3 sensors were used for the measurement of temperature. All of the sensors were installed on the wall at the same level as the cage. There were two sensors arranged on the Southwest wall both inside and outside, while on the Southeast wall, the sensor was on the outside only.

The response in terms of acceleration was acquired with the time step t=0.005s. The identification of modal parameters was conducted using the techniques described in chapter 2, with reference to time windows of 3600 s.

a)  b) 

Figure 3-20 a) PC and data acquisition system; b) Mounting of accelerometers and on the tower




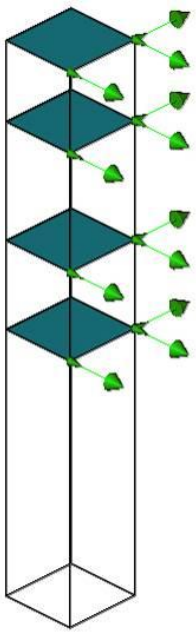

Figure 3-21 Arrangement of measuring sensors on the walls of the “Gabbia” Tower

3.6.2 Dynamic characteristics of the tower

3.6.2.1 The first dynamic test (31 July – 2 August 2012)

In order to identify the dynamic characteristics, the response of the structure to ambient vibration was acquired for over 24 hours: from 16:00 to 23:00 on July 31th, 2012 and from 10:00 am on August 1st to 06:00 am on August 2nd, 2012. Notwithstanding the very low level of ambient excitation of the tests, the application of both FDD and SSI techniques to all data sets generally was used to identify 5 vibration modes in the frequency range of 0-10 Hz.

Typical results in terms of natural frequencies and mode shapes are shown in Figure 3-22 and Figure 3-23, respectively. The plots refer to the acceleration data recorded in the time on 31/07/2012, 16:00-17:00. The first Singular Values (SV) of the spectral matrix resulting from the application of the FDD technique is shown in Figure 3-22a, whereas Figure 3-22b shows the stabilization diagram obtained by using the SSI method; the corresponding mode shapes, identified via SSI, are shown in Figure 3-23. The inspection of Figure 3-22 and Figure 3-23 allows the following comments on the dynamic characteristics of the "Gabbia" Tower:

(a) two closely spaced modes were identified around 1.0 Hz, which are dominant bending (B) and involve flexure in the two main planes of the tower, respectively. The mode B1 is dominant bending in the N-E/S-W plane whereas the modal deflections of B2 belong to the orthogonal N-W/S-E plane;

(b) The third mode B3 involves bending in the N-E/S-W plane, with slight (but not negligible) components in the orthogonal plane;

(c) Just one torsion mode (T) was identified and the corresponding natural frequency was 4.77 Hz (in the examined time window);

(d) The last identified mode is local (L) and only involves deflections of the upper portion of the tower. The mode shape looks dominant bending, with significant components along the two main planes of the structure. The presence of this local

vibration mode provides further evidence of the structural effect of the change in the masonry quality and morphology observed on top of the tower during the preliminary visual inspection. On the other hand, both visual inspection and operational modal analysis confirm the concerns about the seismic vulnerability of the building and explain the fall of small masonry pieces from the upper part of the tower, reported in the earthquake of 29/05/2012.

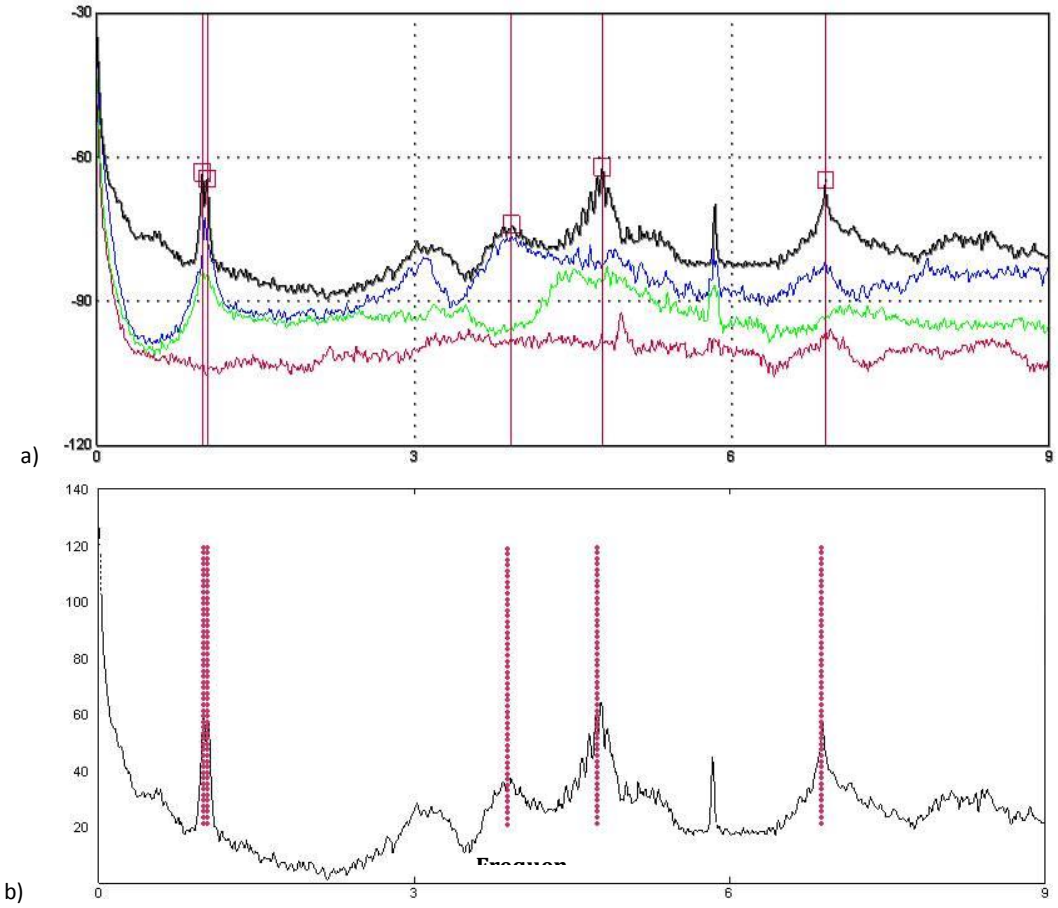

Figure 3-22 Vibration modes generally identified from ambient vibration data (SSI, 31/07/2012, 16:00-17:00).

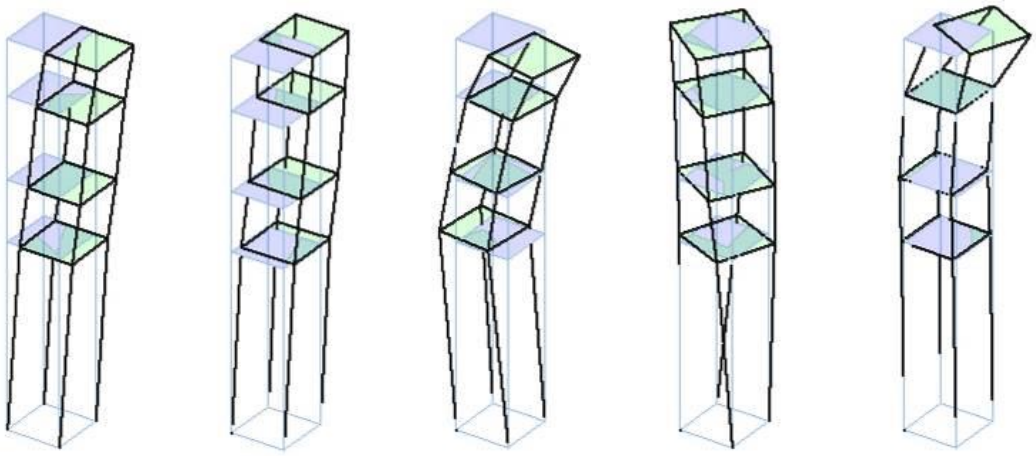

B1)f_{SSI} =0.957Hz B2) f_{SSI} =1.002Hz B3) f_{SSI} =3.887Hz T1) f_{SSI} = 4.746Hz L1) f_{SSI} =6.885Hz

Figure 3-23 The mode shape of the first five natural frequency

Statistics of the natural frequencies that were identified between 31/07/2012 and 02/08/2012 are summarized in Table 3-4 through the mean value, the standard deviation, the extreme values and the coefficient of variation of each modal frequency. It should be noticed that the natural frequencies of all modes exhibit slight but clear variation, with the standard deviation ranging between 0.011 Hz (mode B2) and 0.037 Hz (mode L1).

Table 3-4 Statistics of the natural frequencies identified (SSI) during 28 hours of dynamic testing

Modal	f_{media} (Hz)	f_{min} (Hz)	f_{max} (Hz)	σ_f (Hz)	CV (%)
1	0.981	0.957	1.014	0.018	1.826
2	1.026	1.006	1.052	0.011	1.093
3	3.891	3.857	3.936	0.025	0.654
4	4.763	4.714	4.802	0.022	0.462
5	6.925	6.849	6.987	0.037	0.528

Due to the very low amplitude of ambient excitation that existed during the 28 hours of continuous acquisition, the variation of natural frequencies is conceivably related to the environmental (i.e. temperature) effects. The analysis performed in order to investigate the possible relationships between natural frequencies and temperature suggests that:

1. the natural frequencies of the lower modes (global modes B1-B3 and T1) increase with increased temperature;
2. for the highest mode (i.e. the local mode of vibration), the variation in time of

the natural frequency seems quite different;

3. the oscillation in time of natural frequencies of lower modes seems almost perfectly in-phase with the outdoor temperature on the S-W front.

This result suggests that the thermal expansion of materials in a very inhomogeneous area of the structure causes a general worsening of the connection between the masonry portions. This evidence, again in agreement with the main observation of the visual inspection and the presence of the local mode L1, confirms the poor state of preservation and the high seismic vulnerability of the upper part of the building, highlighting the need for further analysis and preservation actions to be performed.

3.6.2.2 The second dynamic test (27 November 2012)

The post-earthquake assessment performed by visual inspections and AVTs clearly highlighted the critical situation of the upper part of the tower, pointing out the need for structural interventions to be carried out. For this purpose, and to provide access to the inner walls of the tower in order to complete the on-site survey, a metallic scaffolding and a light wooden roof were installed. Even if both the additions have been designed to be as light as possible, variations of the dynamic characteristics are in principle unavoidable, especially considering the wooden roof's binding effect on the upper area of the building. Therefore, a second dynamic test was performed on 27 November 2012, aimed at detecting the possible effects of such installations on the dynamic behavior of the tower. The AVT was completed in few hours since the metallic scaffolding allowed to access quite easily the cross-sections to be instrumented along the height of the building. As previously pointed out, accelerometers were installed in the same cross-sections of the inner side of the walls; moreover, only two hours of data were collected in the second AVT, with the outdoor temperature being almost constant (10°C-11°C). After the test, a small permanent dynamic monitoring system was installed in the "Gabbia" Tower, with early warning purposes. The modal characteristics of the tower identified in the 2nd AVT are summarized in Figure 3-24.

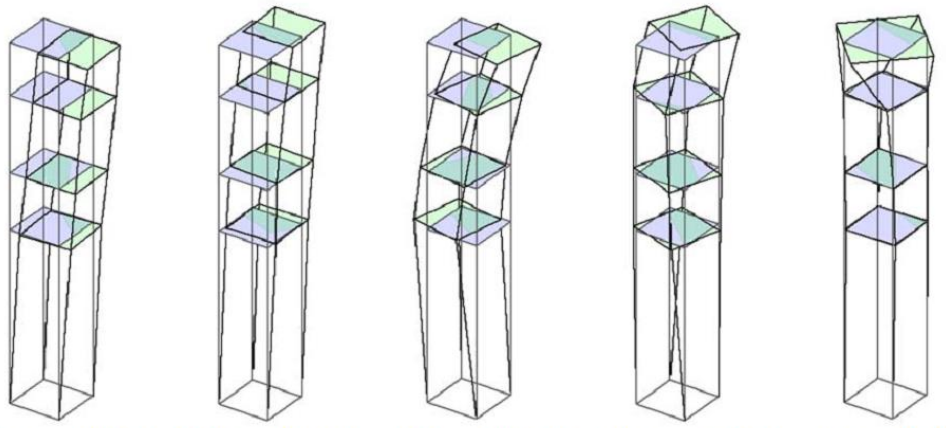

Figure 3-24 Vibration modes identified from ambient vibration data (SSI, 27/11/2012, 13:00-14:00).

The inspection and the comparison with the corresponding results obtained in the summer test (Figure 3-23) suggests the following comments:

(a) beyond the difference in terms of natural frequency, the mode shapes of lower bending modes B1-B3 did not exhibit significant changes (Figure 3-24 B1-B3 and Figure 3-23 B1-B3). Hence, the metallic scaffolding and the wooden roof practically do not affect those modes;

(b) on the contrary, the mode shape T1 (Figure 3-23 T1) now involves both torsion and bending. The identified frequency did not change appreciably with respect to the first dynamic survey, but the mode shape looks significantly different. The torsion component is dominant in the lower portion of the structure, while the upper part is characterized by dominant bending with significant components along the two main planes of the tower. In other words, after the installation of the wooden roof the deformed shape of mode T1 becomes a sort of superposition of previous modes T1 (Figure 3-23 T1, lower part of the structure) and L1 (Figure 3-23 L1, upper part of the structure). Furthermore, the previous mode L1 was no more detected;

(c) the previous local mode L1, shown in Figure 3-23 L1, has been "substituted" by another local mode, with higher frequency of 9.89 Hz and involving torsion of the upper part of the tower (Figure 3-24 L1). This "new" local mode, not identified in

the summer AVT, is probably related to the increase of connection between the masonry walls of the upper part of the tower induced by the new covering.

As a further comment, it seems that especially the wooden roof, even if very light, affects the dynamic characteristics of (the upper part of) the building. The main effect is that the roof acts as a mass added in a vulnerable area (so that a possible decrease of the natural frequency of previous local mode is generated).

The long-term dynamic monitoring is necessary, based the following considerations. First of all, both the two dynamic tests indicate the poor condition of the upper part of the tower, which calls for more and long-term attention, such as dynamic monitoring. And secondly, the structure condition needs to be carefully monitored before the essential strengthening intervention of the upper part. What’s more, the tower is located in the region facing high risk of earthquakes. Hence, the long-term monitoring can provide the responses of the structure due to earthquakes and these results will be helpful for prediction of the structure behavior in earthquakes. The last but not least, the forthcoming strengthening intervention also needs to be investigated to make sure that the retrofitting is successfully operated.

Chapter 4

Dynamic Monitoring of the "Gabbia Tower"

4.1 Introduction

As described in Chapter 3, the inspection carried out in August 2012 (Gentile et al. 2012, Saisi & Gentile 2013) mainly revealed the poor state of preservation of the upper part of the "Gabbia" tower and the need of a repair intervention.

For this reason and in order to allow to perform visual inspection of the inner walls, the Administration of Mantua installed metallic scaffolding and a light wooden roof inside the tower. As already pointed out, the wooden roof – even if very light – caused some changes in the dynamic characteristics of the structure.

Consequently and in order to collect further information during the preliminary design of retrofitting work, a long-term dynamic monitoring system was installed in the tower and has been active since December 17th, 2012. The monitoring system is described in Paragraph 4.2.

Two computer codes available on the market, namely DADiSP and ARTeMIS, were systematically used to manage the data collected on the tower (DADiSP) and to perform the modal identification (ARTeMIS). The computational procedures adopted and some typical results are presented in Paragraph 4.3.

Until June 30th 2013, more than 4700 datasets, of 1 hour each, were recorded by the monitoring system and the data analysis is summarized in Paragraph 4.4. The modal identification results obtained from ARTeMIS are collected in an Excel datasheet to summarize the evolution of the dynamic characteristics and to evaluate the correlation

between natural frequencies and environmental effects (i.e. temperature). Furthermore, during the examined monitoring period, several earthquakes occurred in Northern Italy and the effects of some seismic event were significantly felt on the tower. In particular, the earthquake occurred on June 21th, 2013 induced the remarkable acceleration of $20\mathrm{cm}/s^2$ on the tower.

Detailed analysis on the evolution of natural frequencies between December 17th, 2012 and June 30th 2013, the correlation between natural frequencies and temperature and the behavior of the structure under this seismic event are presented in Paragraph 4.4.

4.2 Description of the dynamic monitoring system

Few weeks after the execution of the second AVT, a simple dynamic monitoring system was installed on the "Gabbia Tower". The system is composed by a 4-channel data acquisition system (24-bit resolution, 102 dB dynamic range and anti-aliasing filters) with 3 piezoelectric accelerometers (WR model 731A, 10 V/g sensitivity and ±0.50 g peak). Furthermore, a temperature sensor is installed on the S-W front, measuring the outdoor temperature. (Gentile et al. 2013).

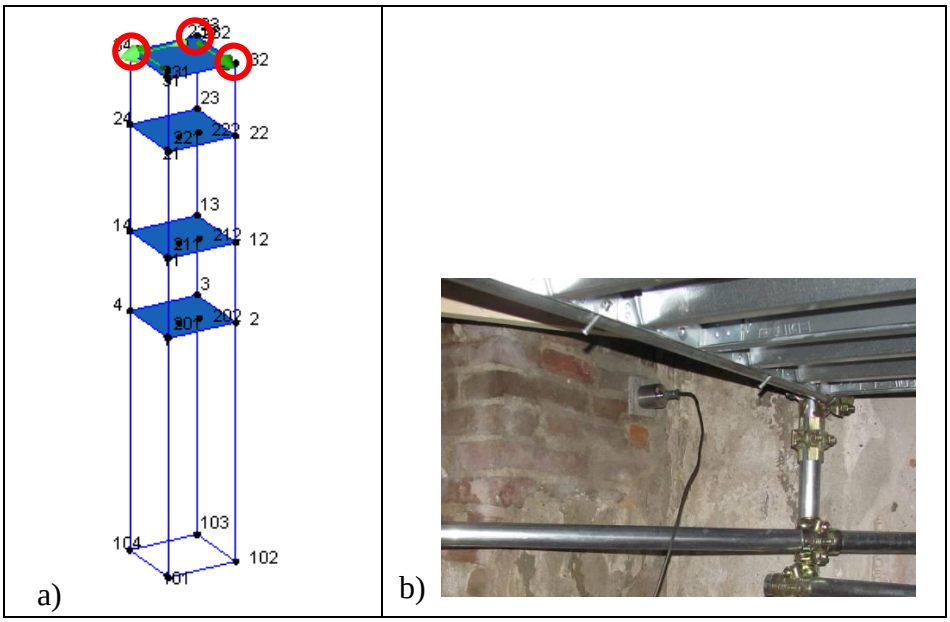

Figure 4-1 a) Location of the sensors in the monitoring system; b) WR 731A accelerometer

As shown in Figure 4-1a), the accelerometers of the long-term dynamic monitoring are fixed on the top of the “Gabbia Tower” (red circles). The digitized data are transmitted to an industrial PC on site. A binary file, containing 3 acceleration time series (sampled at 200 Hz) and the temperature data, is created every hour, stored on the local PC and transmitted to Politecnico di Milano for being processed.

This chapter deals with the analysis of the results collected in the dynamic monitoring between 17th December 2012 and 30th June 2013 (196 days and more than 4700 datasets acquired).

4.3 Data management and modal identification

Data management is carried out by DADISP program. Pre-processing and de-trending of each 1-hour dataset are firstly performed. Subsequently, for each dataset the following tasks have been programmed and automatically performed:

a) filtering and decimation of acceleration data;
b) evaluation of the hourly-averaged temperature;
c) estimation of the auto-spectral densities;
d) saving filtered and decimated data for modal identification.

Furthermore, the occurrence of possible seismic events is inspected.

Afterwards, the SSI technique available in the ARTeMIS program was used for modal identification. Details about the use of the two programs are described in the next sub-sections.

4.3.1 Data Management (DADISP)

In Figure 4-2, a typical worksheet of DADISP is shown. The worksheet consists of twenty windows and the function of each window is described in the following.

Analog signal of the sensor is transmitted to data acquisition board by cables and then transformed into digitized data, which are input data for DADISP.

Figure 4-3 shows the view of Window 1 (W1), which presents the input data (3 columns

of acceleration data and 1 column of temperature data, sampled at 200 Hz). By simply changing the name of the input data file, another dataset is uploaded by the program and the functions in each window are run automatically.

The acceleration obtained from the three accelerometers is presented in the worksheets of Windows 2, 3, 4 (W2, W3, W4) respectively. The data recorded by the sensors are proportional to the real acceleration. Here, the actual value of acceleration can be obtained by dividing the collected data by a constant factor (that characterizes each accelerometers) to obtain the unit of acceleration in m/s^2. An example (W4) of the recorded acceleration in m/s^2 is shown in Figure 4-4. Similarly to acceleration data, the evolution of temperature in ℃ is evaluated in W5, as shown in Figure 4-5.

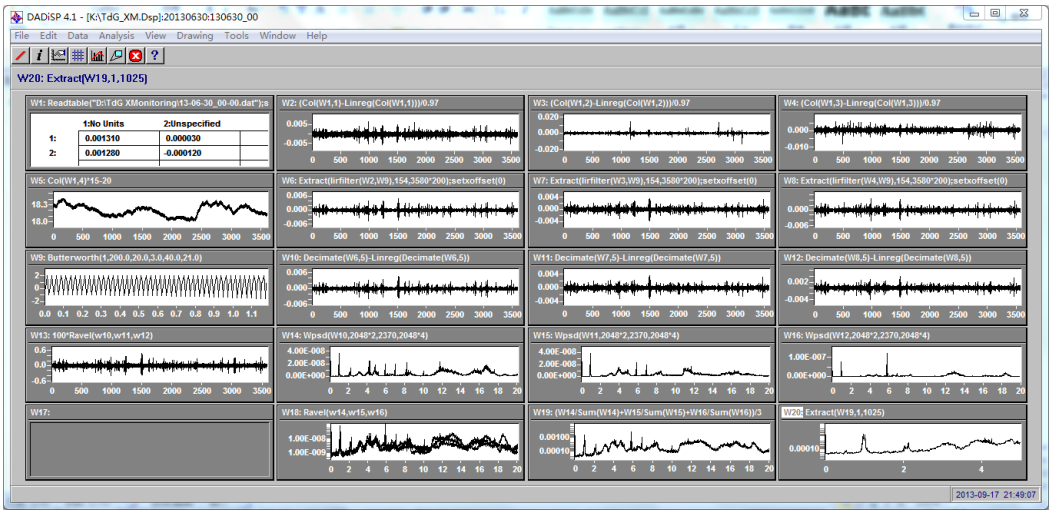

Figure 4-2 Typical DADISP worksheet for analysis

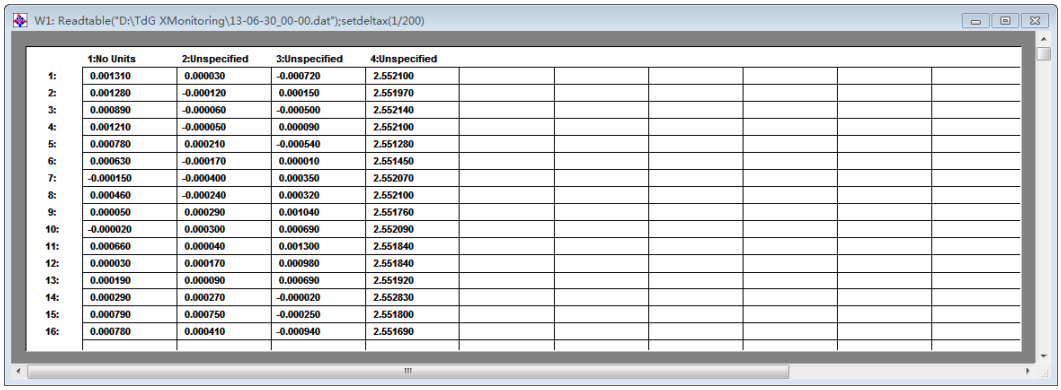

	1:No Units	2:Unspecified	3:Unspecified	4:Unspecified
1:	0.001310	0.000030	-0.000720	2.552100
2:	0.001280	-0.000120	0.000150	2.551970
3:	0.000890	-0.000060	-0.000500	2.552140
4:	0.001210	-0.000050	0.000090	2.552100
5:	0.000780	0.000210	-0.000540	2.551280
6:	0.000630	-0.000170	0.000010	2.551450
7:	-0.000150	-0.000400	0.000350	2.552070
8:	0.000460	-0.000240	0.000320	2.552100
9:	0.000050	0.000290	0.001040	2.551760
10:	-0.000020	0.000300	0.000690	2.552090
11:	0.000660	0.000040	0.001300	2.551840
12:	0.000030	0.000170	0.000980	2.551840
13:	0.000190	0.000090	0.000690	2.551920
14:	0.000290	0.000270	-0.000020	2.552830
15:	0.000790	0.000750	-0.000250	2.551800
16:	0.000780	0.000410	-0.000940	2.551690

Figure 4-3 Window 1 (W1): Input data

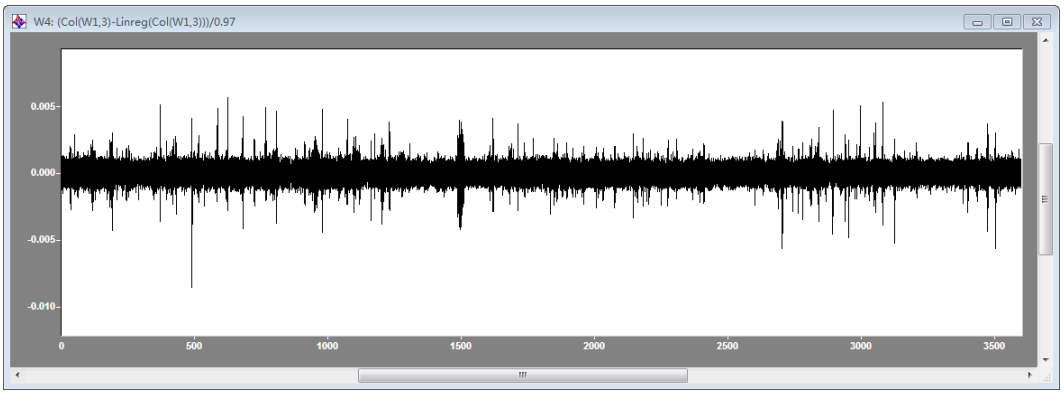

Figure 4-4 Window 4 (W4): sample of recorded acceleration

Since the sampling rate is 200Hz but only the lower frequencies are of interest in this study, filtering and decimation were carried out to speed up the computational work. For each dataset, a filter is firstly applied to remove the frequencies higher than 20Hz and then, data were decimated to reduce the sampling rate to 40Hz. The results of filtering and decimation applied to an acceleration time-history are exemplified in Figure 4-6 (Window 8) and Figure 4-7 (window 12), respectively.

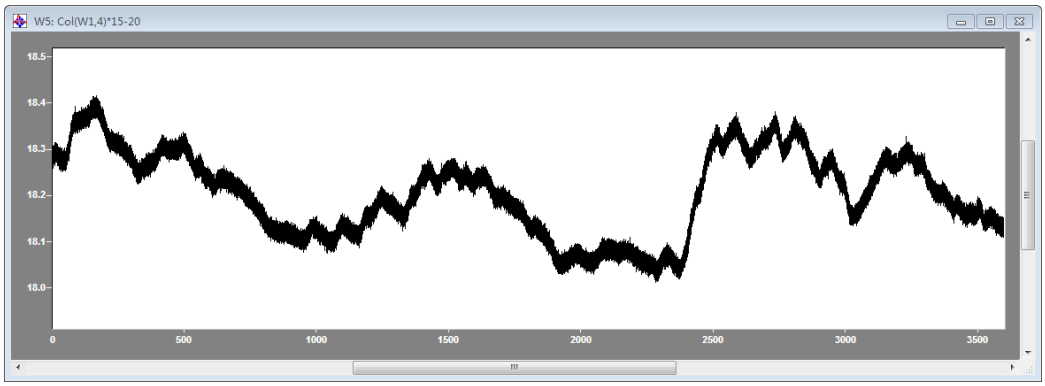

Figure 4-5 Window 5 (W4): sample of recorded temperature

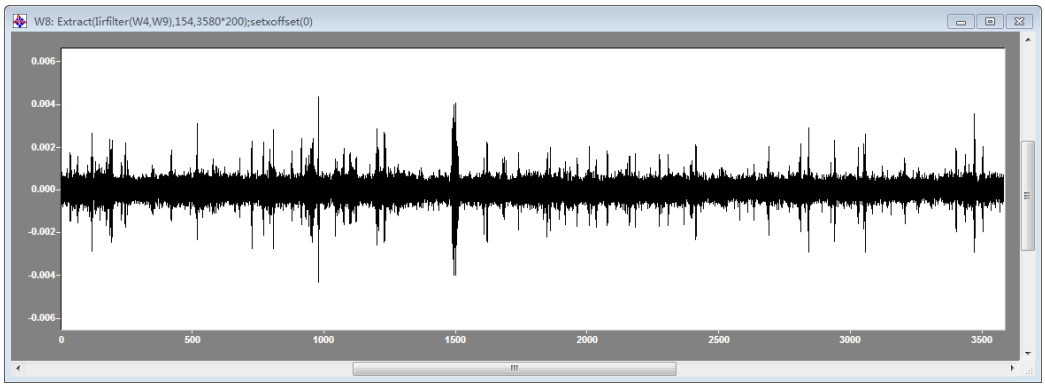

Figure 4-6 Window 8 (W8): typical results of the filter process

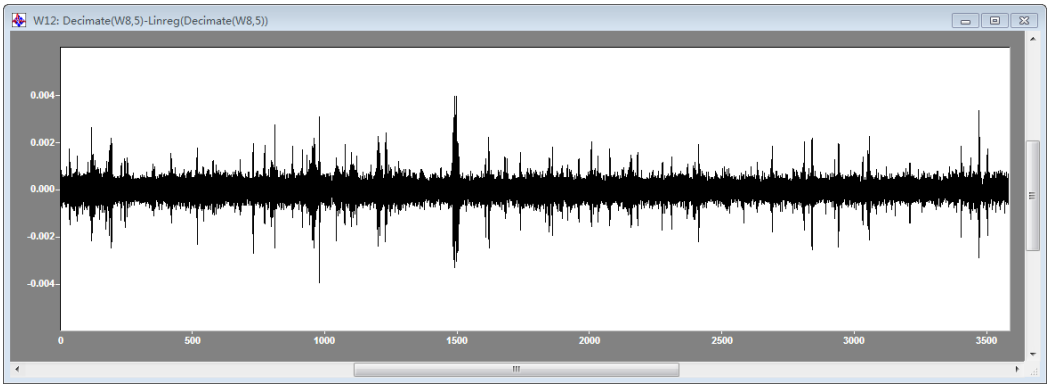

Figure 4-7 Window 12 (W12): typical results of the decimation process

Subsequently, the acceleration units are changed to "cm/s^2", as it is shown in Figure 4-8 (Window W13) for the 3 accelerations superposed, and exported in ".dat" file for the modal identification analysis in ARTeMIS.

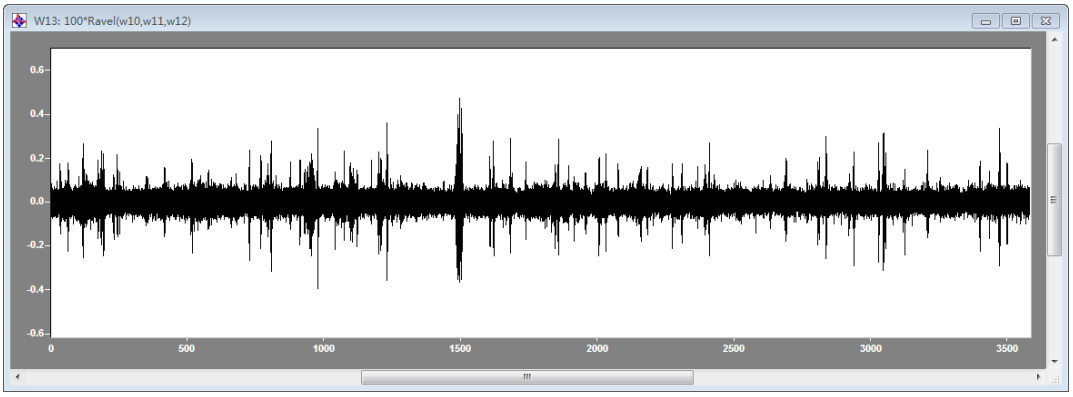

Figure 4-8 Window 13(W13): accelerations in *cm/s*²cm/ s□2□

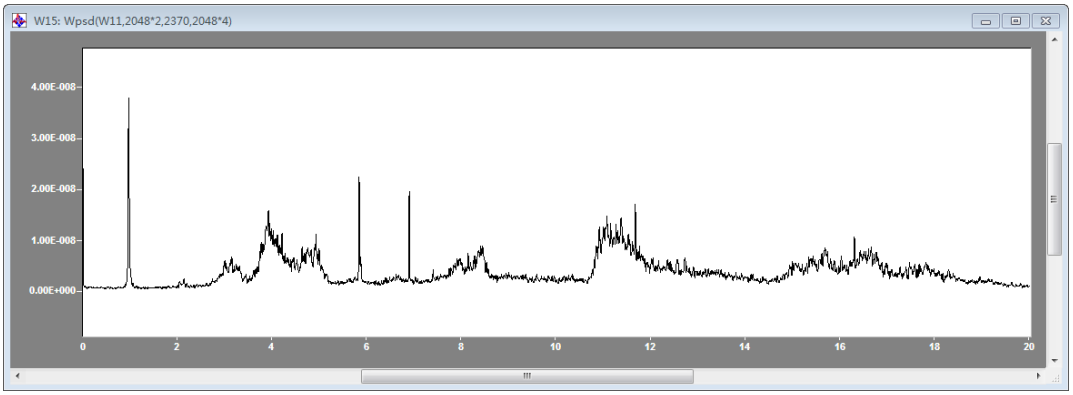

Figure 4-9 Window 15 (W15): typical plot of an auto-spectrum

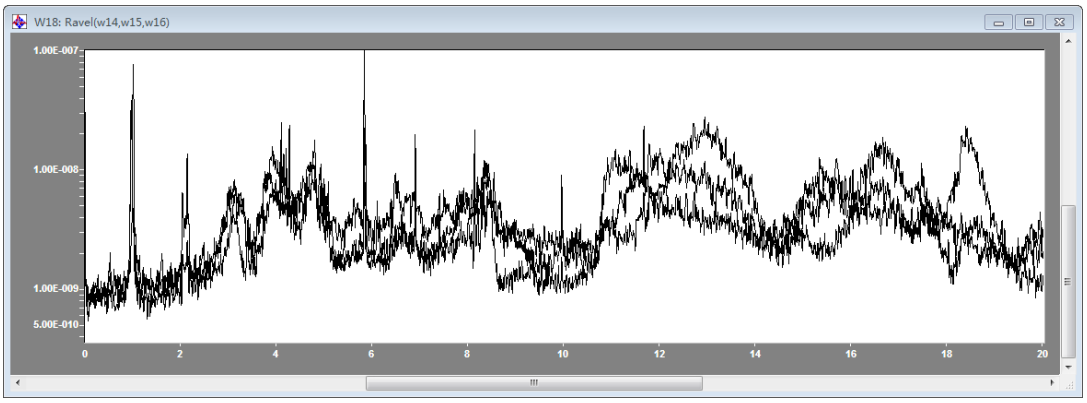

Figure 4-10 Window 18 (W18): typical plot of the superposed auto-spectra of all channels

The auto-spectra of each decimated signal are presented in windows W14-W16. An example of the Window 15 is shown in Figure 4-9. The diagrams of all three auto spectra are presented in Window 18 (Figure 4-10), whereas the Averaged Normalized Power Spectral Density (ANPSD) curve is shown in Window 19 (Figure 4-11). Zoom in the frequency in 0-5Hz and the diagram is shown in window 20.

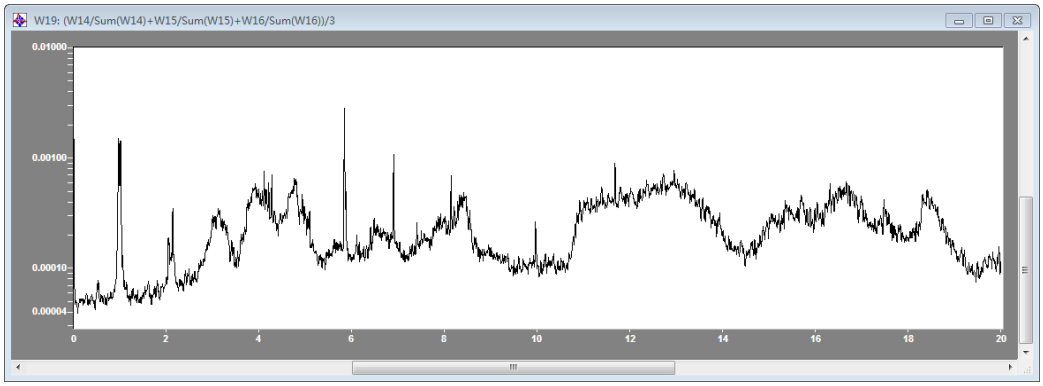

Figure 4-11 Window 19 (W19): typical plot of ANPSD curve

Hence, the different windows of a worksheet contain, for each 1-hour dataset, the following data:

-W1, the input data;

-W2-W4, acceleration, in m/s^2 , recorded by the three sensors;

-W5, the evolution of temperature in 1-hour;

-W6-W8, filtered accelerations;

-W9, characteristics of the adopted filter;

-W10-W12, decimation results of the three acceleration contents;

-W13, filtered and decimated accelerations, in cm/s^2;

-W14-W16, auto spectrum of each acceleration series;

-W18, all the three auto spectra results;

-W19, Averaged Normalized Power Spectral Density curve;

-W20, AVNPSD curve in the frequency interval 0-5Hz.

All datasets were analyzed by the proceeding procedures. It should be noticed that the above pre-processing is mainly aimed at the rough evaluation of the lower natural frequencies, the computation of hourly-averaged temperature and the generation of ".dat" files for the subsequent modal identification analysis.

A first rough identification of the lower frequencies is carried out by the Peak Picking procedure and the value of temperature is obtained by extracting the average value from W5. The results of Peak Picking the lower (five) natural frequencies are shown in Figure 4-12, where the selected dataset is the one recorded on January 28th 2013, 14:00-15:00. As it has to be expected at the low level of ambient excitation that generally existed during the monitoring, for some records (see e.g. Figure 4-13), the modal identification was not successful.

In this study, semi-automatic method was used to validate the results of more advanced automatic methods.

During the period of monitoring the "Gabbia Tower", one dataset related to an important seismic episode was recorded on 21 June 2013 and corresponded to a significant earthquake occurred near Massa, in the Tuscany region in north of Italy (Figure 4-14). The maximum amplitude of the earthquake-induced accelerations on the top of the tower ($20\mathrm{cm}/s^2$) was about 80 times larger than the ambient vibration responses.

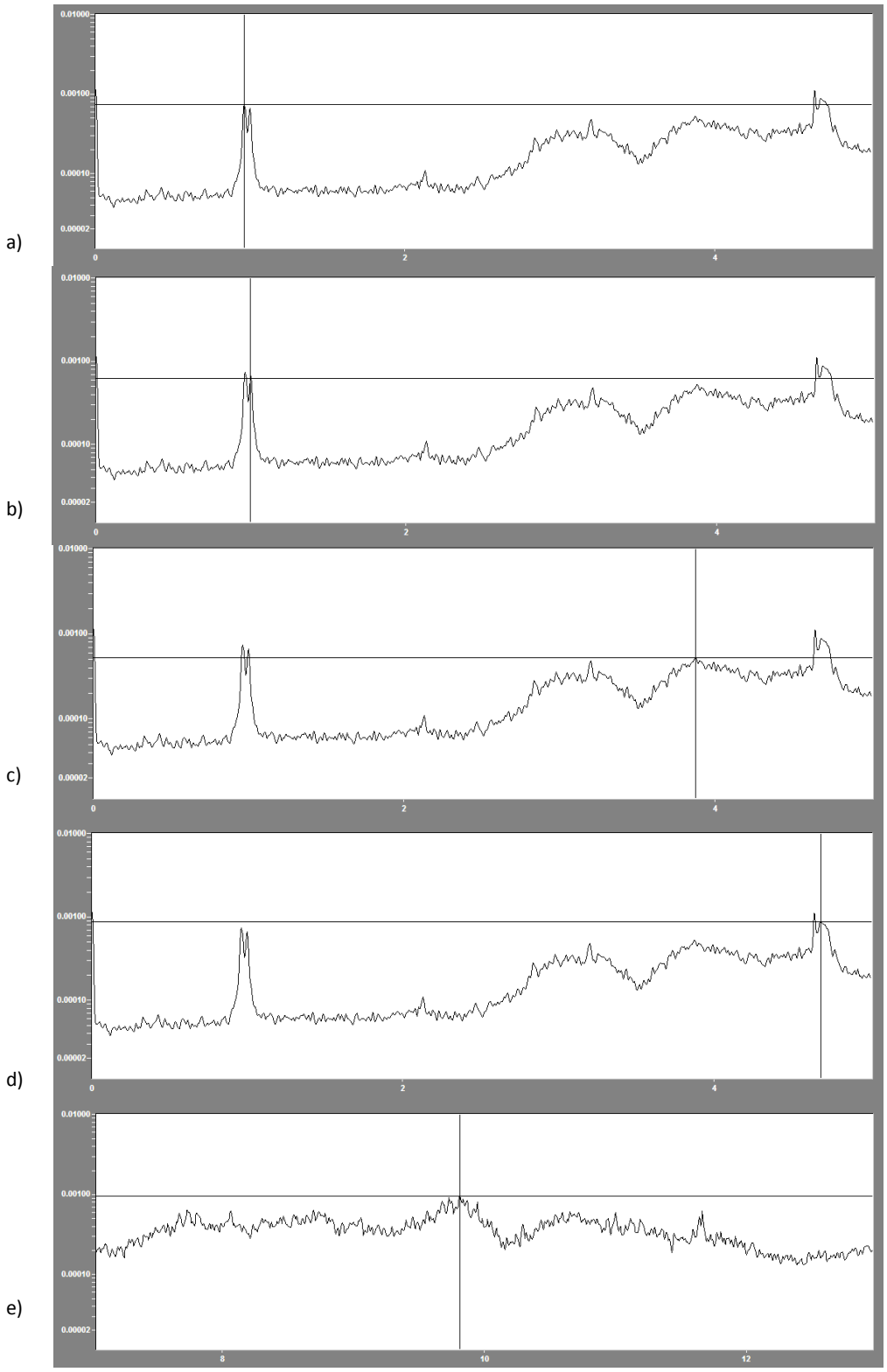

Figure 4-12 The natural frequencies identified using the Peak Pecking in DADiSP: a) 0.962 Hz; b) 0.996 Hz; c) 3.867 Hz; d) 4.678 Hz; e) 9.815 Hz

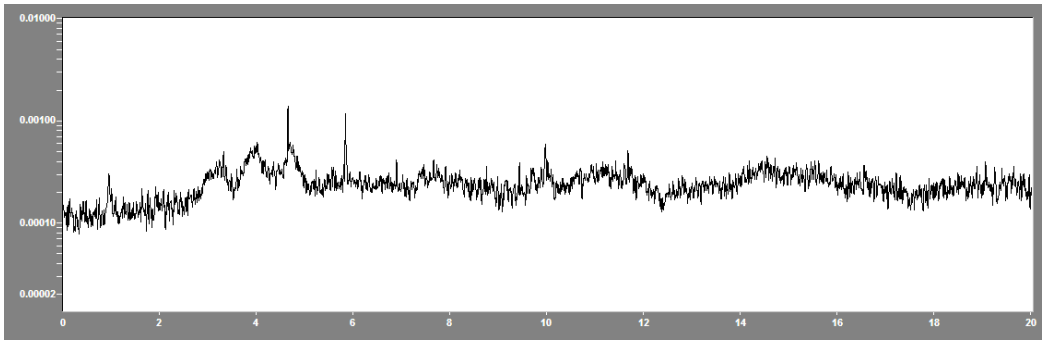

Figure 4-13 Typical ANPSD curve when the level of ambient excitation is too low

(January 1st 2013, 16:00-17:00)

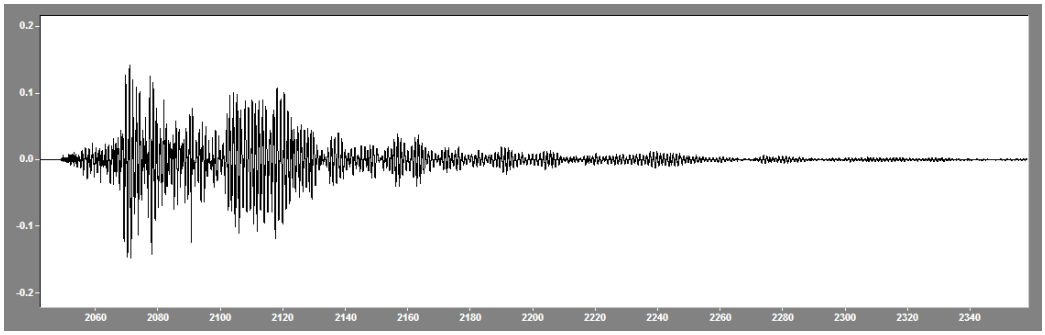

Figure 4-14 Acceleration recorded during the earthquake occurred on June 21th 2013

4.3.2 Modal identification (ARTeMIS)

The SSI method implemented in the ARTeMIS software was used to extract the modal parameters from each recorded dataset. The theory as well as the software program is described in Chapter 2. In this paragraph, the details of the application to each dataset are presented.

Some parameters are required during the processing of data in ARTeMIS, as shown in Figure 4-15. 4096 frequency lines were assumed to obtain the same frequency resolution adopted in the DADiSP software.

Let us refer to the result of the dataset recorded on January 28th 2013, 13:00-14:00 as an example. Typical results of the SSI analysis are shown in Figure 4-16. As it has to be expected, five stable modes can be generally identified (Figure 4-16a).

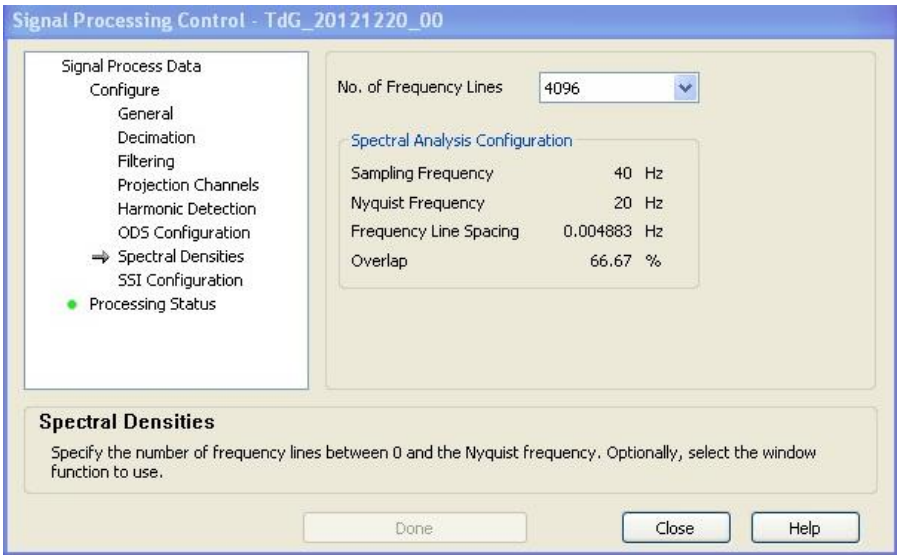

Figure 4-15 Parameters used in data processing

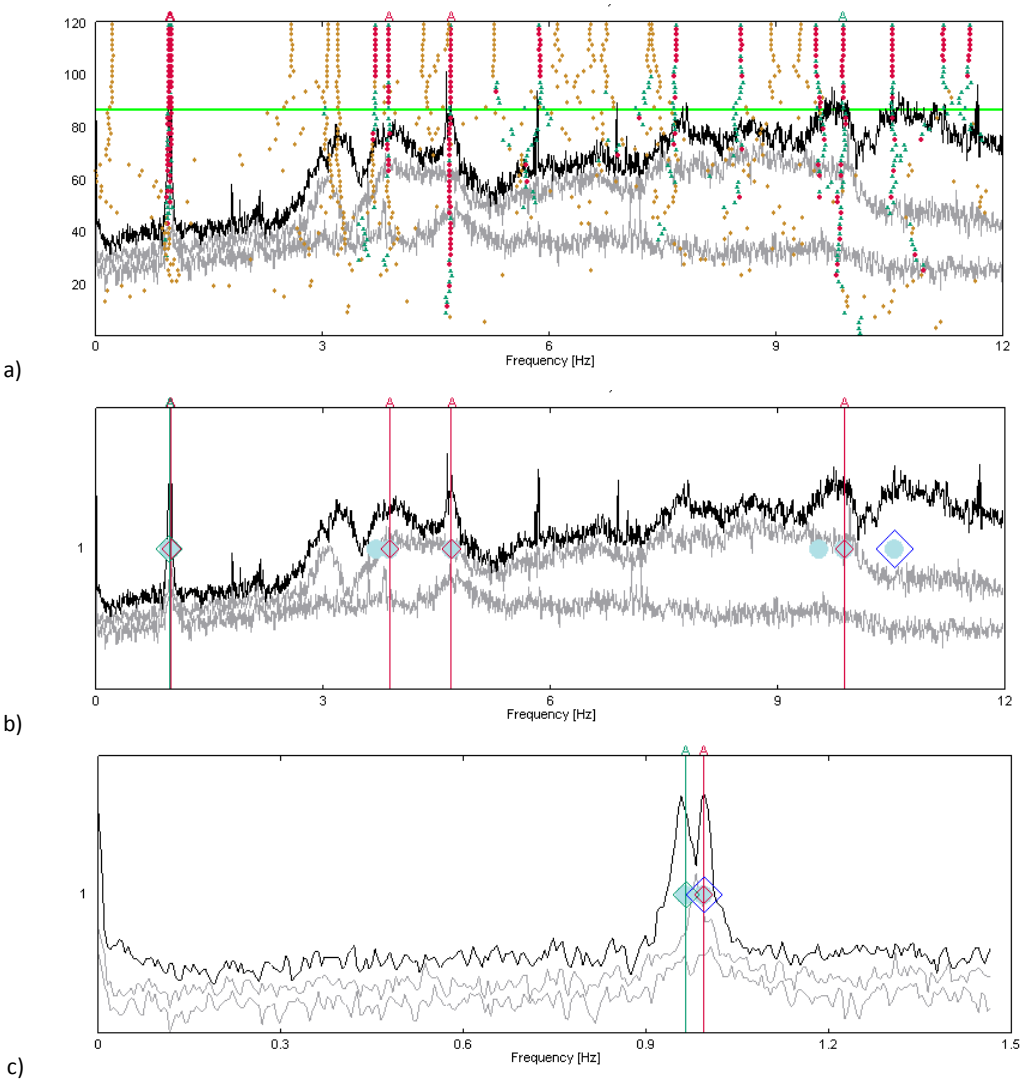

Figure 4-16 Jan 28th 2013, 13:00-14:00, a) SSI analysis results; b) first 5 frequencies; c) details around 1Hz

The mode shapes obtained from the second AVT of the entire structure are shown in Figure 4-17, whereas the typical modal deflections of the three sensors permanently installed on the top of the tower during the monitoring are shown in Figure 4-18.

Although the upper part of the tower was instrumented during the monitoring, the correspondence between natural frequencies and mode shapes ensures the consistency with previously identified dynamic characteristics.

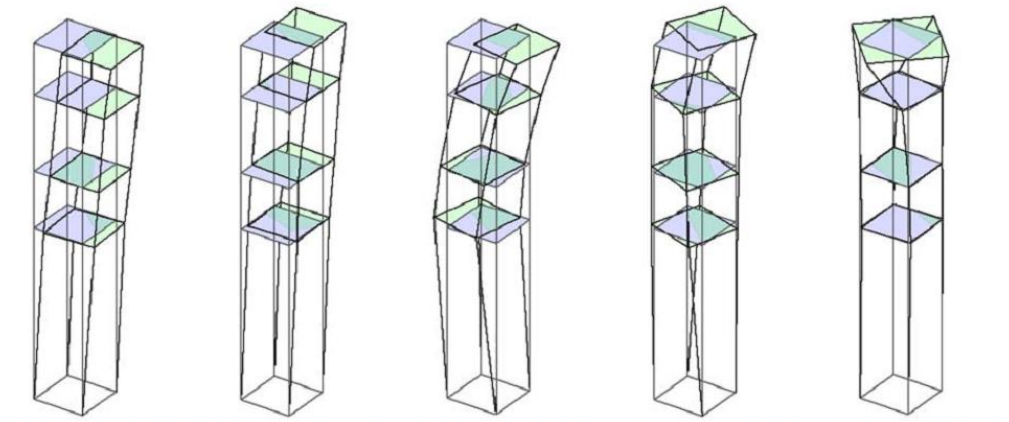

B1) f_{SSI} = 0.918 Hz B2) f_{SSI} = 0.986 Hz B3) f_{SSI} = 3.887 Hz T1) f_{SSI} = 4.648 Hz L1) f_{SSI} = 9.893 Hz

Figure 4-17 The mode shapes of the first five natural frequencies from the second AVT

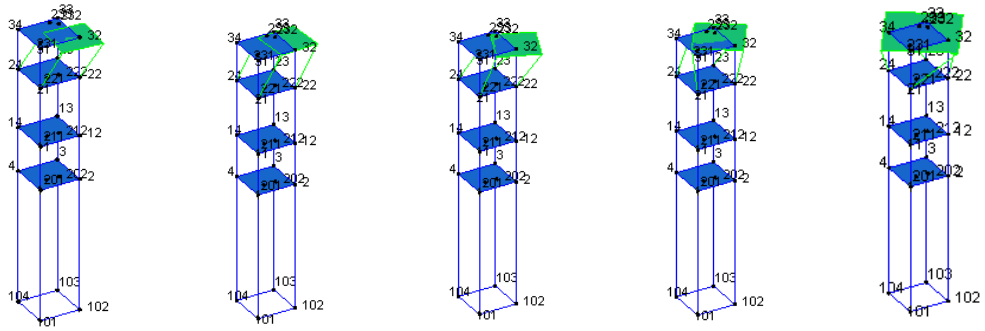

B1) f_{SSI}=0.9650Hz B2) f_{SSI} =0.9946Hz B3) f_{SSI} =3.877Hz T1) f_{SSI} =4.690Hz L1) f_{SSI} =9.875Hz

Figure 4-18 The mode shape of the first five natural frequencies from monitoring

As previously pointed out, in some cases, the amplitude of ambient vibrations was too low to allow the modal identification, shown in Figure 4-19 (that refers to the data recorded on February 2nd 2013, 03:00-04:00)

Typical results of modal identification from each month are presented in Figure 4-20 to show the variation of natural frequencies. The shift of frequencies is clear, especially for the local mode (L1); this variation suggests either a strong effect of temperature or

the occurrence of some damage mechanism. These aspects will be, of course, much better documented and addressed in the next paragraph.

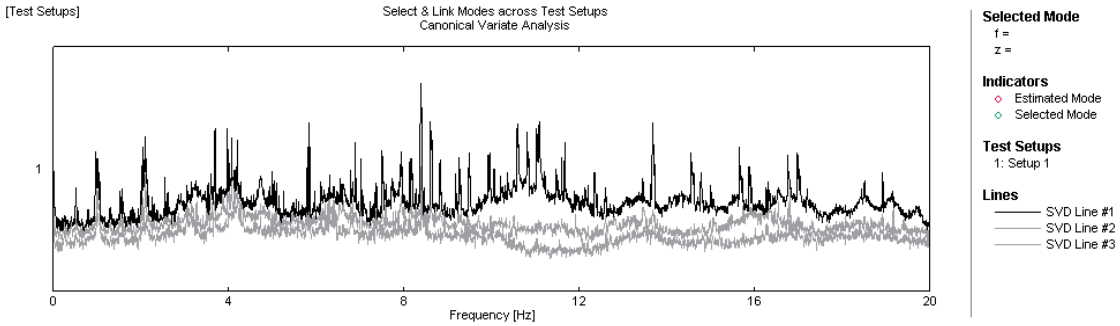

Figure 4-19 Bad result influenced by noises on Feb 2nd 2013, 03:00-04:00

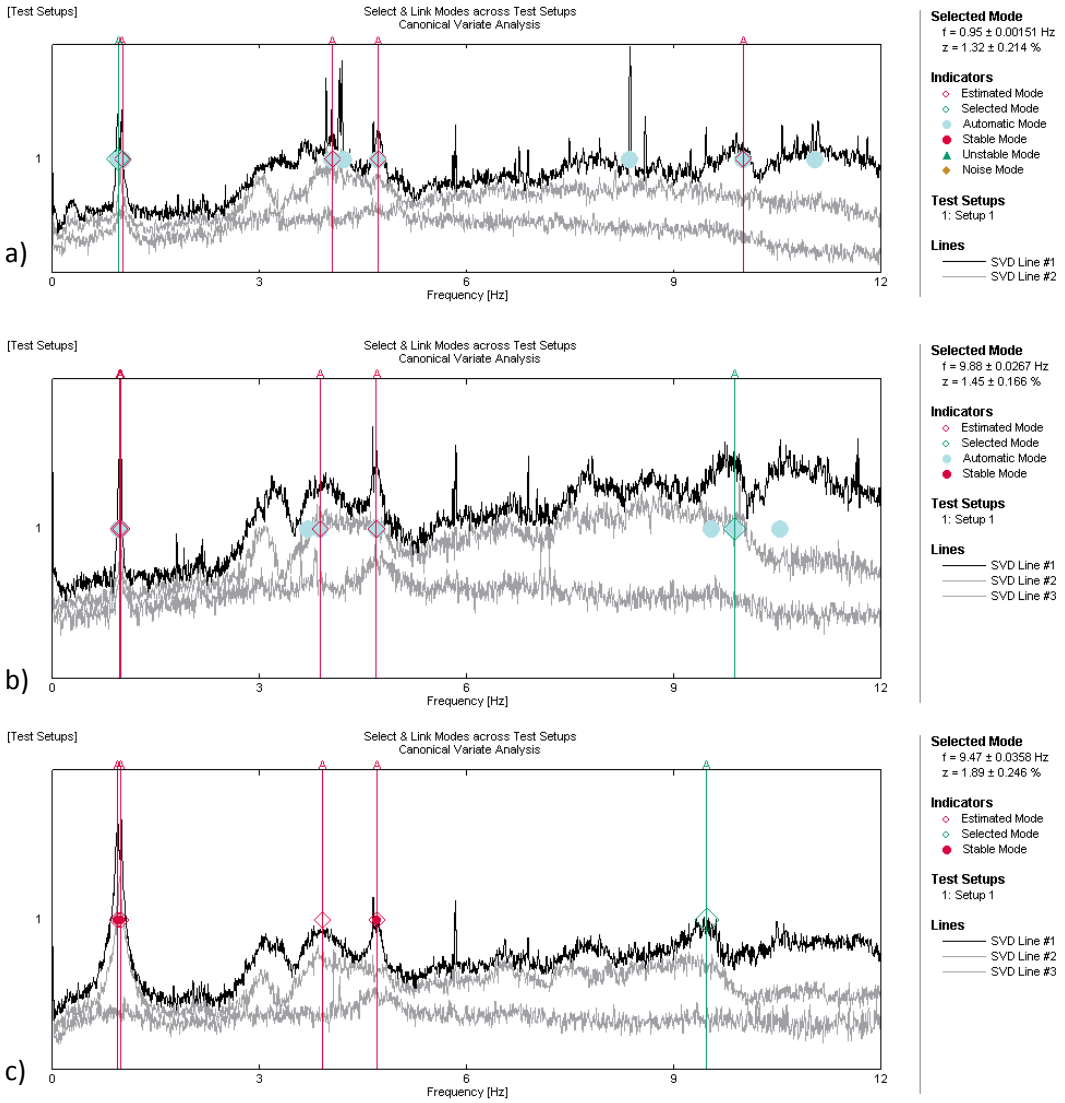

Figure 4-20 The variation of natural frequencies, a)11:00 on Dec 17th 2012; b)13:00 on Jan 28th 2013; c)17:00 Feb 6th 2013;

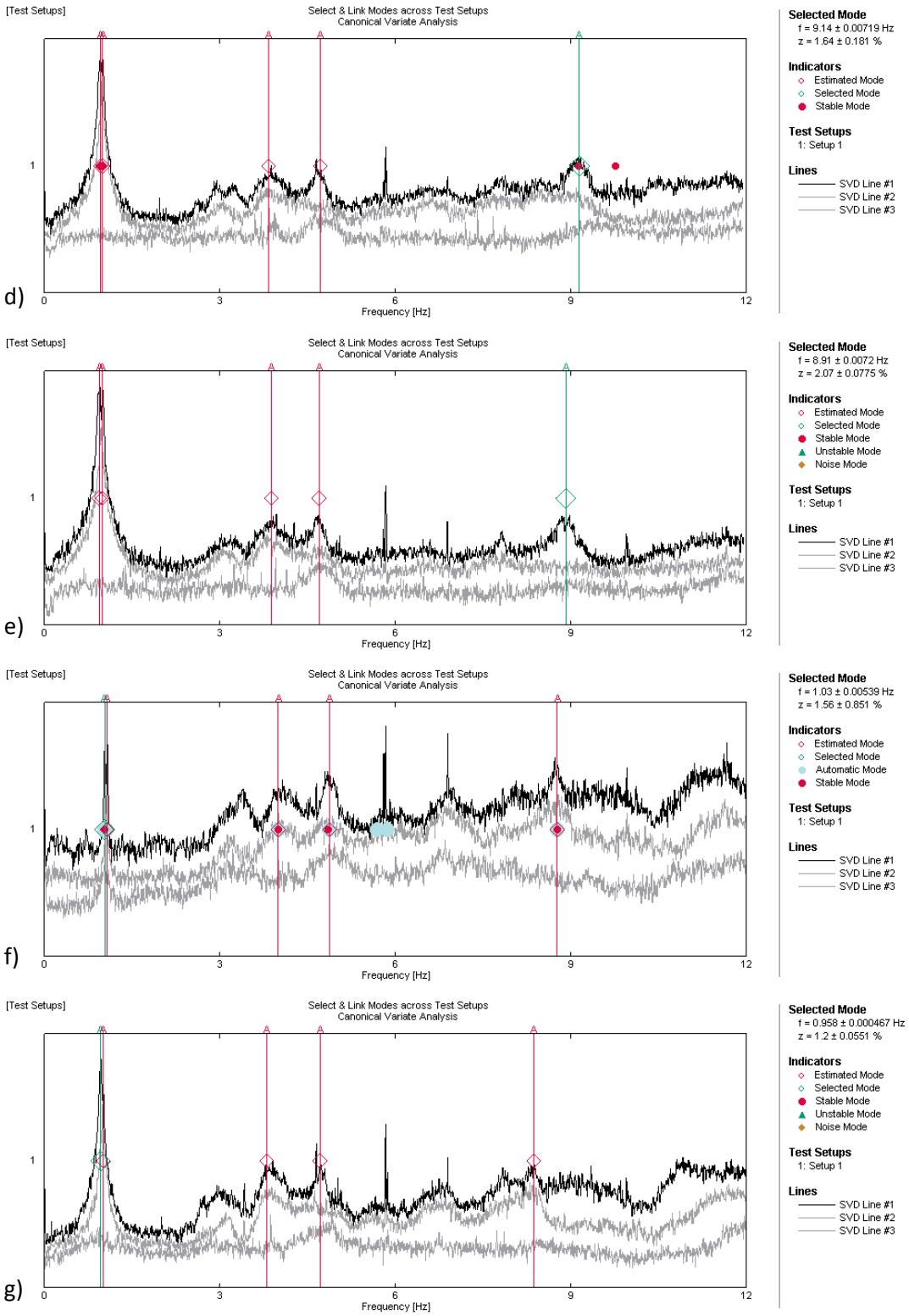

Figure 4-20 (cont’d) The variation of natural frequencies, d) 12:00 Mar 6th 2013; e) 23:00 Apr 4th 2013; f)13:00 May 5th 2013; g)18:00 Jun 27th 2013

Other important results − coming from the responses to the earthquake occurred on 12:33 June 21th, 2013 − are shown in Figure 4-21, illustrating the natural frequencies

identified before, during and after the earthquake. Figure 4-21 clearly highlights that the dynamic characteristics of the tower were significantly affected by the seismic events, as it will be more extensively discussed in the next section.

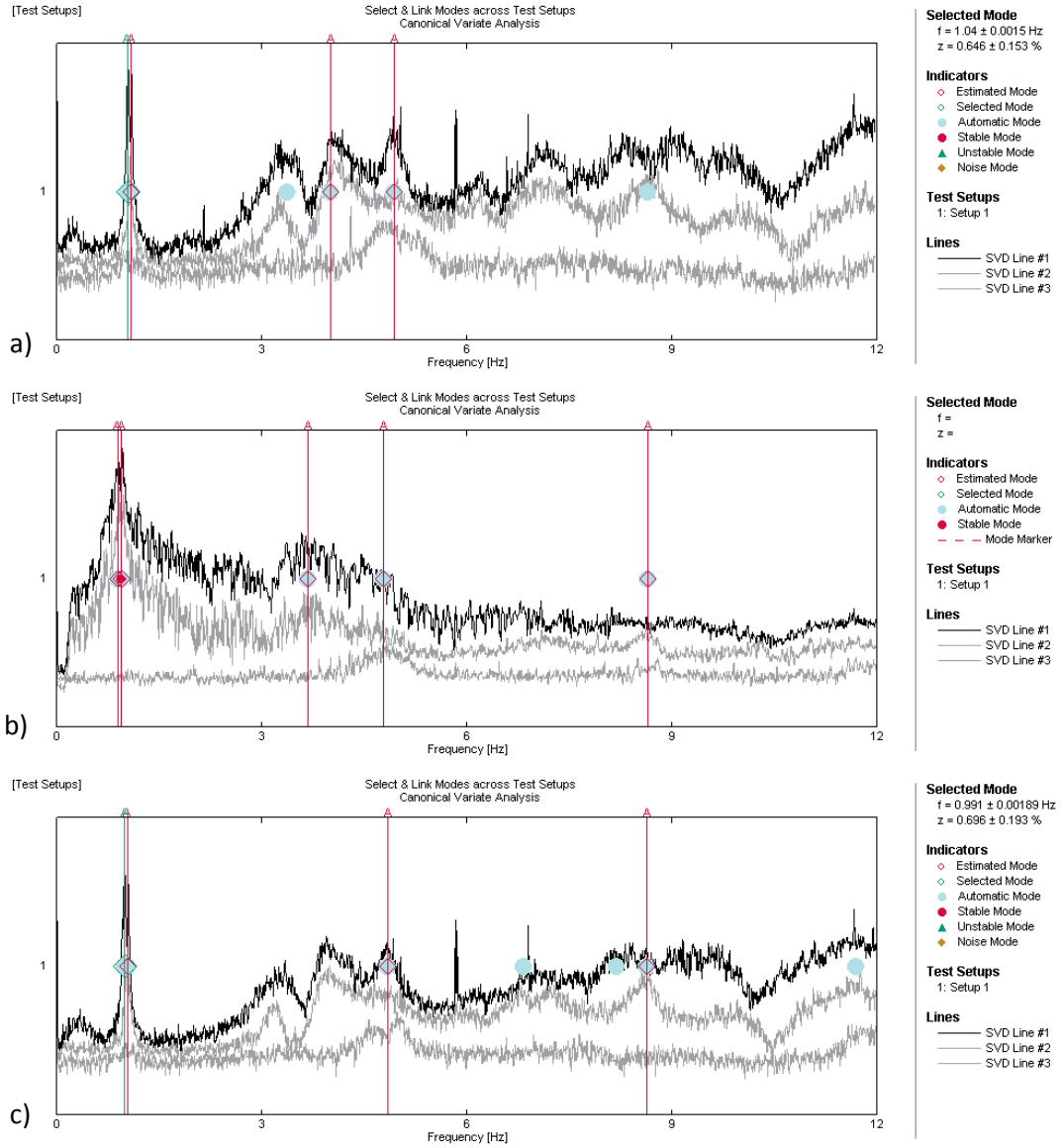

Figure 4-21 Identification of natural frequencies: a) before (11:00-12:00); b)during (12:00-13:00); c) after (13:00-14:00) the earthquake occurred on June 21th, 2013

4.4 Results of the dynamic monitoring

4.4.1 Evolution in time of natural frequencies and temperature

The identified natural frequencies and the corresponding temperature values were collected in an Excel datasheet.

The evolution of the outdoor temperature on the South West front in the period from 17/12/2012 to 30/06/2013 is shown in Figure 4-22. The temperature changed from −2°C to 50°C during the examined time interval. In sunny days, the curve showed significant daily variations. The daily highest temperature was below 25°C until the middle of April. And after then, both the daily variation and the highest daily temperature increased to a large value.

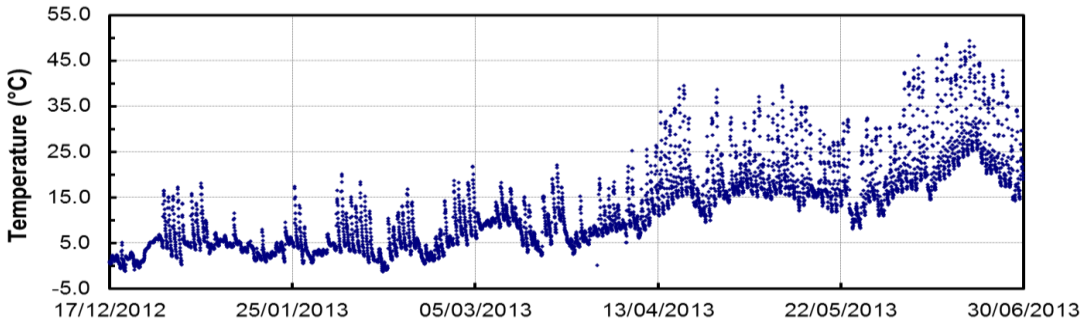

Figure 4-22 Time evolution of temperature between 17/12/2013 and 30/06/2013

The identification of the natural frequencies from the datasets collected in the same period provides the frequency tracking shown in Figure 4-23. The inspection of Figure 4-23 reveals that all identified natural frequencies were varying in a certain range during the examined monitoring period. The natural frequencies of global modes exhibited limited fluctuations, which are characterized by similar trends. It is worth noting that notwithstanding the lower rate of identification of the natural frequency of mode B3, also this frequency show a trend very similar to the ones of the other global modes.

On the other hand, the fluctuation of the last natural frequency, corresponding to the local mode, is more significant and exhibits different behavior.

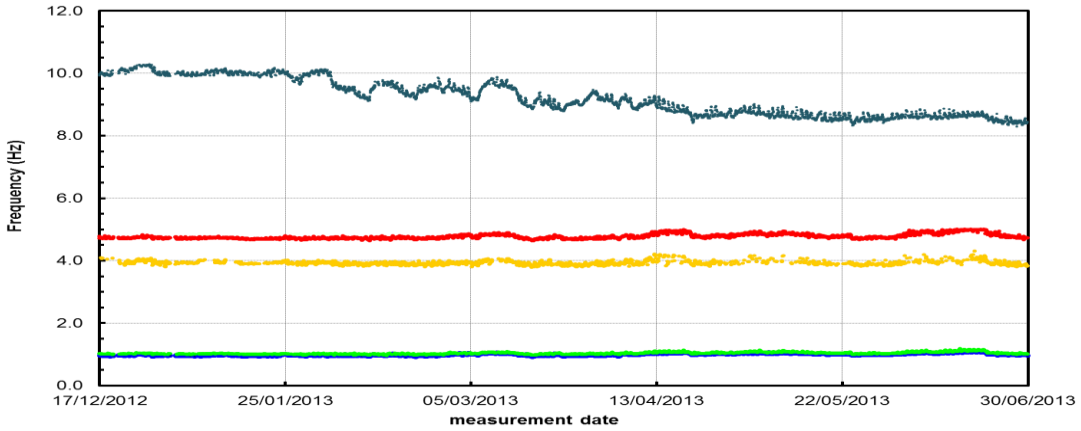

Figure 4-23 Time evolution of the natural frequencies identified between 17/12/2013 and 30/06/2013

In order to better show the fluctuation in time of the natural frequencies of each mode, zoomed diagrams are shown in Figure 4-25 and Figure 4-255, respectively.

Figure 4-25 shows that the time evolution of the natural frequencies of the global modes clearly follows the temperature (i.e. the frequencies increase with increased temperature and decrease with decreased temperature). A similar behavior was observed also in past experiences (Ramos et al. 2010) on masonry structures and can be explained through the closure of superficial cracks, masonry discontinuities or mortar gaps induced by the thermal expansion of materials. Hence, the temporary "compacting" of the materials induces a temporary increase of stiffness and modal frequencies, as well.

On the contrary, Figure 4-255 confirms that the time evolution of the natural frequency of the local mode significantly differs from the others and deserves much more attention.

Statistics of temperature and identified natural frequencies in the examined monitoring period are summarized in Table 4-1. Both Figure 4-255 and Table 4-1 show that the value of natural frequency of local mode varied from about 10 Hz to 8.5 Hz. This abnormal behavior suggests the possible activation and evolution of some damage mechanism.

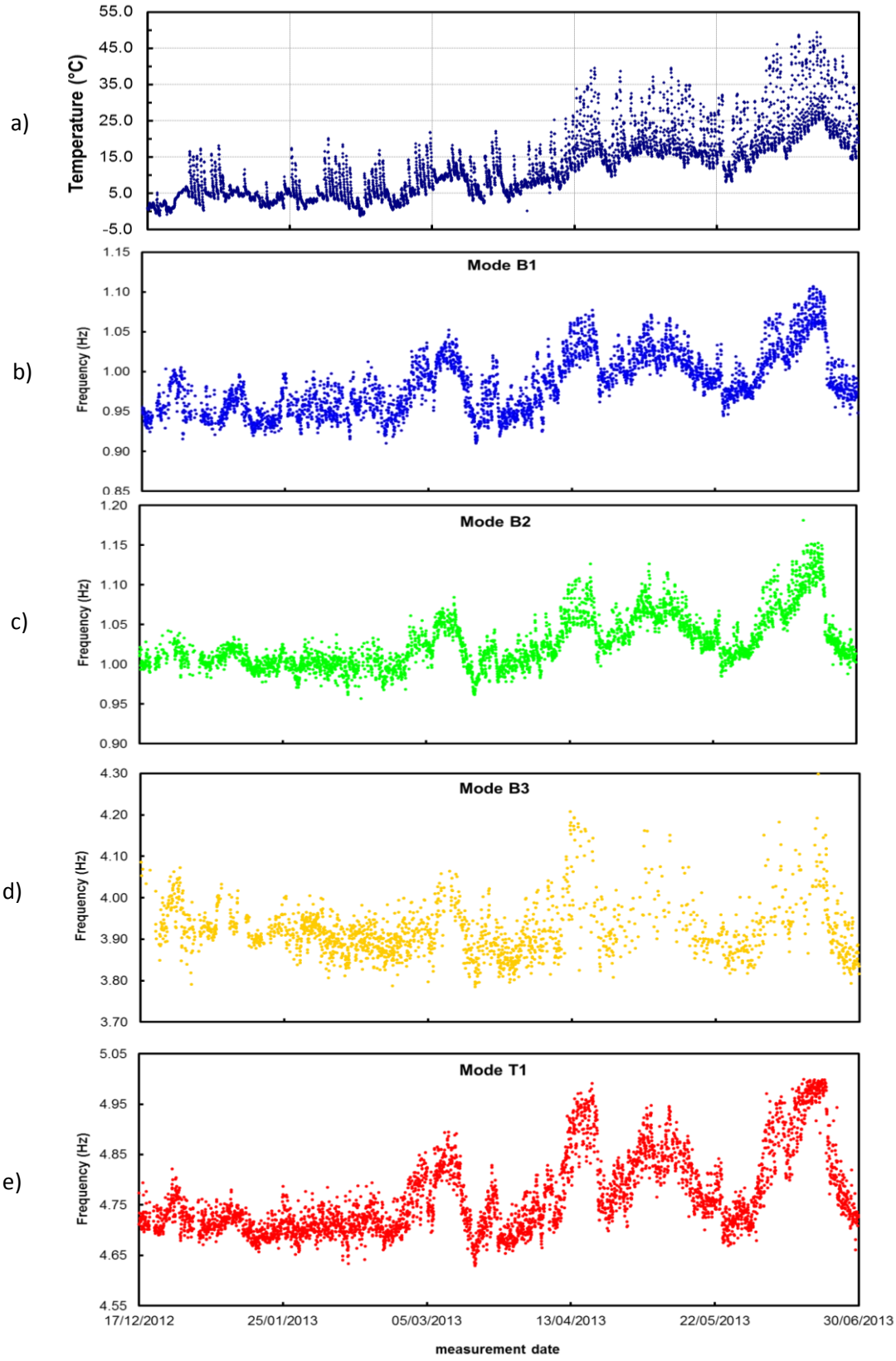

Figure 4-24 Evolution in time of: (a) temperature and (b-e) natural frequencies of global modes

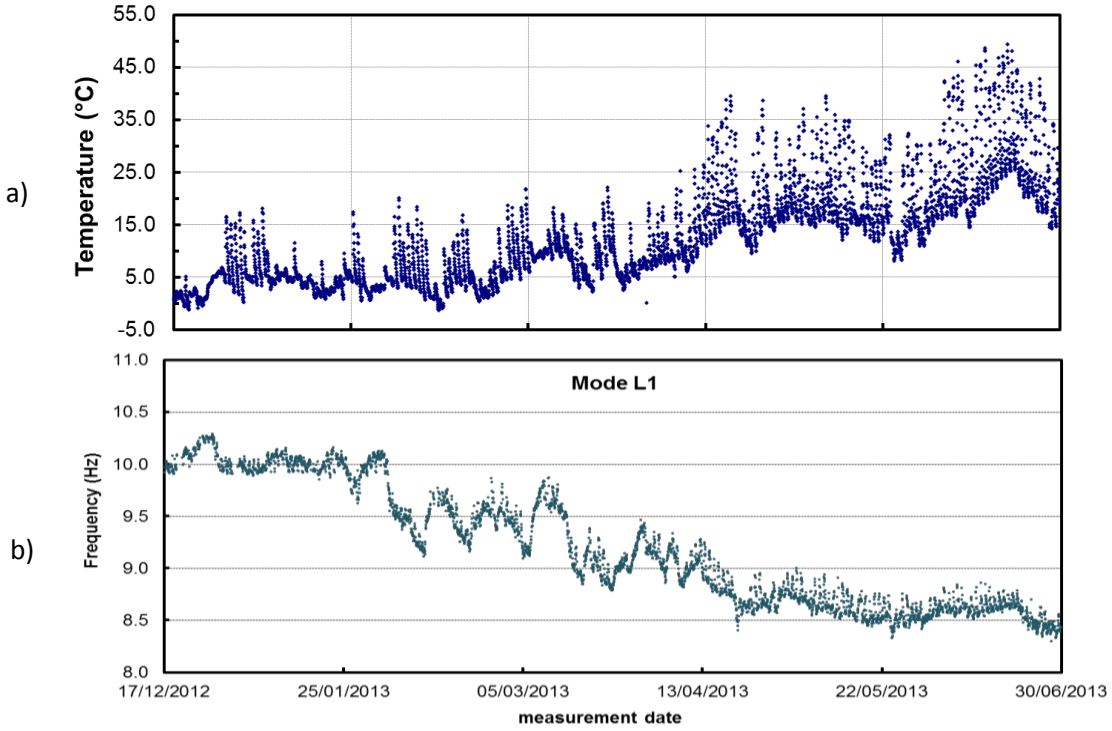

Figure 4-25 Evolution in time of: (a) temperature and (b) natural frequency of the global mode

Table 4-1 Statistics of the identified natural frequencies and temperature between 17/12/2013 and 30/06/2013

	Mode B1 (Hz)	Mode B2 (Hz)	Mode B3 (Hz)	Mode T1 (Hz)	Mode L1 (Hz)	Temperature (°C)
Max.	1.107	1.181	4.298	4.999	10.290	49.340
Min.	0.910	0.957	3.784	4.629	8.295	-1.450
Average	0.986	1.028	3.919	4.767	9.178	12.622
Sta_dev	0.038	0.035	0.065	0.079	0.558	9.591

4.4.2 Effects of temperature: global modes

4.4.2.1 Frequency-temperature correlation

As previously pointed out, the evolution of natural frequencies presents a clear correlation with temperature. In order to better explore the effects of temperature on the natural frequencies of the global modes, frequency-temperature curves are introduced in order to directly present the relationship between the two variables (Figure 4-26). The value of natural frequencies of global modes increases with increment temperature, as a consequence of the temporary increase of the local stiffness due to the thermal expansion of materials. Hence, linear regression line seems appropriate to describe this correlation, which can be written in a general equation as:

$$\mathrm{f_k(T_j)} = \mathrm{a_k} + \mathrm{b_k T_j} = \hat{\mathrm{f}}_\mathrm{k}(\mathrm{T_0} = 20℃) + \mathrm{c_k}(\mathrm{T_j} - \mathrm{T_0}) \tag{4.1}$$

Where,

$\mathrm{a_k}$ represents the natural frequency when $\mathrm{T} = 0℃$;

$\mathrm{b_k}$ is the slope of the regression line;

$\hat{\mathrm{f}}_\mathrm{k}(\mathrm{T_0} = 20℃)$ represents the natural frequency when $\mathrm{T} = 20℃$;

$\mathrm{c_k} = \mathrm{b_k}$.

According to the linear fitting results, the dependence of each modal frequency on temperature can be expressed as follows:

$$f_{\mathrm{B1}}(T_j) = 0.9442 + 0.0032T_j \tag{4.2}$$

$$f_{B2}(T_j) = 0.9904 + 0.0029T_j \tag{4.3}$$

$$f_{B3}(T_j) = 3.8931 + 0.0025T_j \tag{4.4}$$

$$f_{T1}(T_j) = 4.6887 + 0.0061T_j \tag{4.5}$$

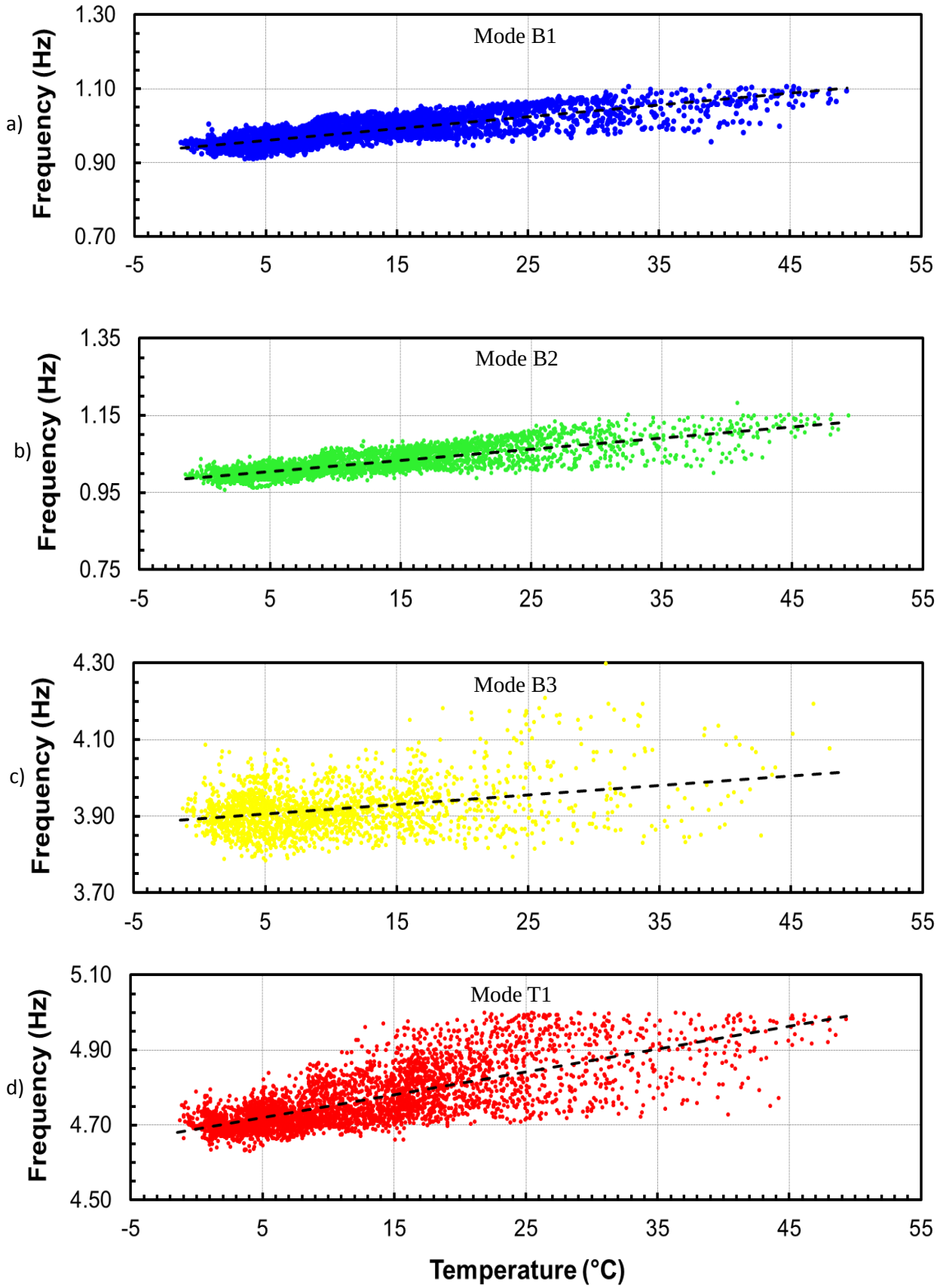

Figure 4-26 Natural frequency of mode: (a) B1, (b) B2, (c) B3 and (d) T1 plotted with respect to the temperature in the period between 17/12/2013 and 30/06/2013

It should be noticed (Figure 4-26) that the linear fitting equations of Mode B1, Mode B2 and Mode T1 fit better than that of Mode B3, probably as a consequence of the lower rate of identification met in the frequency of Mode B3.

The comparison between the identified modal frequencies (from ARTeMIS analysis) and the corresponding estimated values (from linear fitting equations) is exemplified in Figure 4-27, referring to a period of 20 days (from 26/05/2013 to 15/06/2013).

In the Figure 4-27, the black lines refer to the estimated values and the color dots refer to the experimental values.

During the selected time period (from 26/05/2013 to 15/06/2013), the temperature had a relative high value and significant daily variation. Generally speaking, the estimation values of the natural frequencies are consistent with that of the experimental results. The linear fitting equation of Mode B3, as previously stated, exhibits less accurate approximation so that the prediction analysis was limited to Modes B1, B2 and T1 in Figure 4-27.

The inspection of Figure 4-27 indicates that the estimated values show better fitting behavior with higher temperatures. Around 01/06/2013, there was a small drop of the daily highest temperature and the experimental results were stable at a lower value than the estimated ones. On the other side, between 11/06/2013 and 15/06/2013, the temperature was high and the estimated results were almost coincident with the experimental ones.

As a further comment, the estimated frequencies of Mode B1 and Mode B2 seem to exhibit better fit the ones of Mode T1.

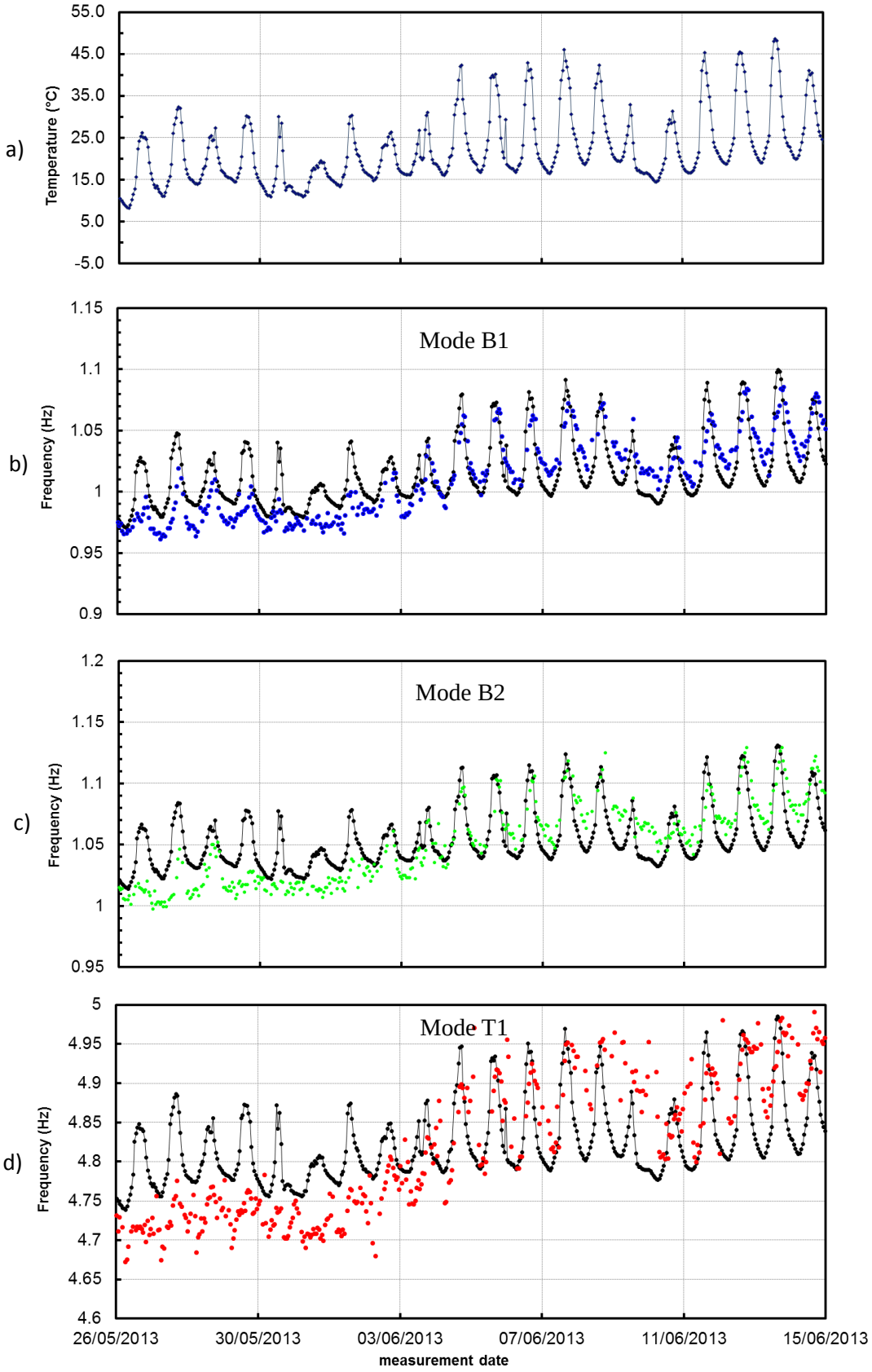

Figure 4-27 (a) Evolution of temperature and comparison between experimental and estimated natural frequencies of (b) mode B1; (c) mode B2; (d) mode T1 from 26/05/2013 to 15/06/2013

4.4.2.2 Prediction error analysis

As previously exemplified in Figure 4-27, using the measured temperatures and applying the linear regression lines (4.2)-(4.5), it is possible to approximately predict the evolution of natural frequencies. The difference between estimated and actual (experimentally identified) value of natural frequencies is called prediction error.

The prediction error is supposed to be varying stably in a certain range when the structure does not exhibit changes. On the contrary, the prediction error should increase as a consequence of structural changes, such as temporary anomalies, deterioration or the occurrence of damage.

Hence, the evolution in time of prediction error may provide a visual and fast diagnosis of possible anomaly or damage. The prediction error related to the natural frequency of the global modes B1, B2 and T1 is shown in Figure 4-28.

The inspection of the curve of Mode B1 indicates that the error was stable at the beginning with the value in the range (-0.4, 0.4). Around 07/03/2013, the value increased to almost -0.6 suddenly. Another increment took place on 21/06/2013 with the value up to 0.8, when the earthquake occurred. A similar trend can be observed in the diagram of the normalized error of the second mode (Mode B2) and the fourth mode (Mode T1).

Beyond these two increments observed in the three diagrams, the evolution of mode T1 shows another increase around 14th April 2013 with the value enlarged up to almost -1. Since the linear fitting result gets worse with increased temperature, this increment should result from the inaccurate estimated values at high temperatures rather than damage.

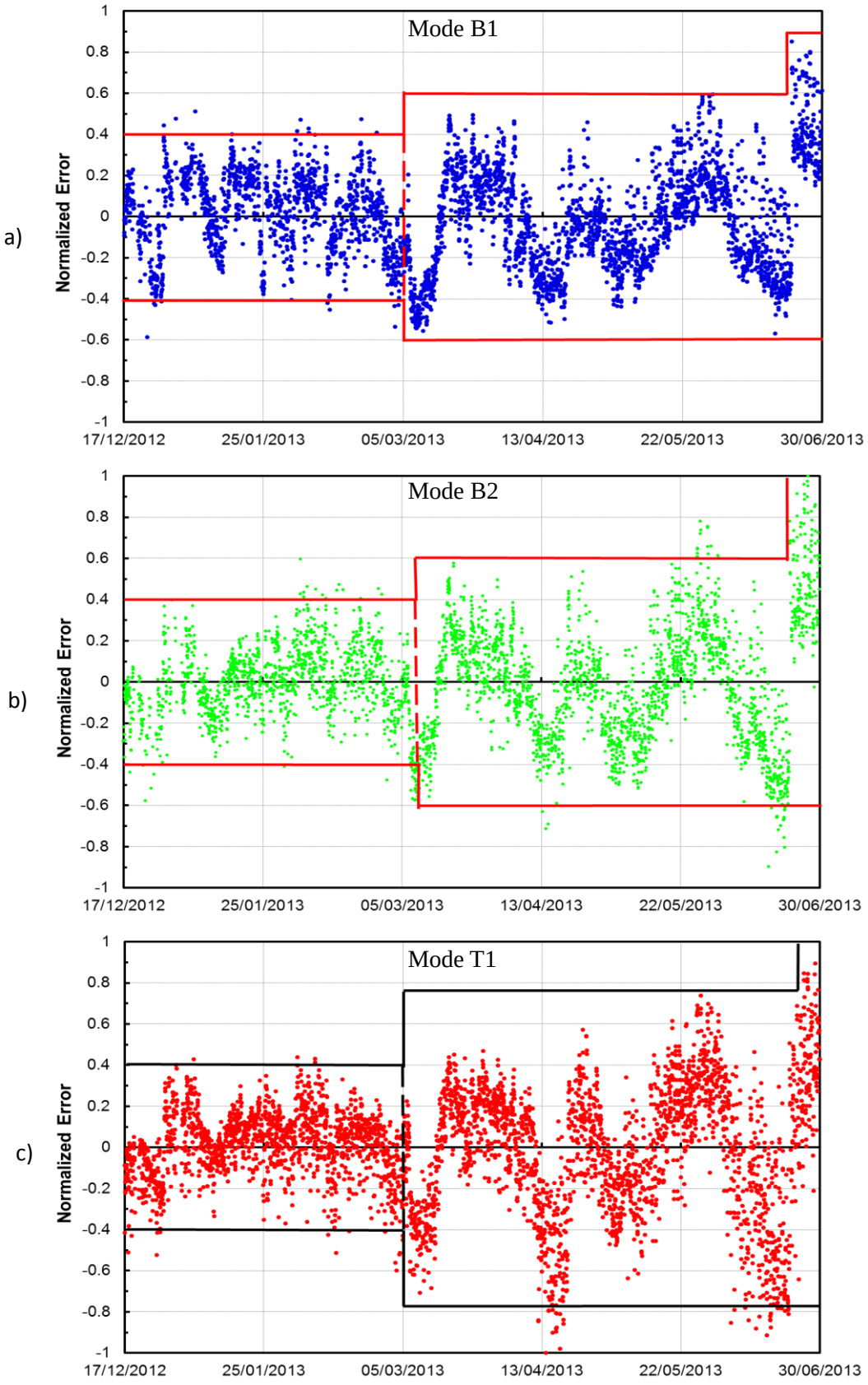

Figure 4-28 Prediction error of global modes

4.4.2.3 Global damage assessment

According to the normalized prediction error diagrams of global modes in Figure 4-28, an abnormal behavior can be observed around March 6th 2013. For mode B1, the value of normalized error increased from ∓ 0.4 to ∓ 0.6 and the same trend was observed also be in mode B2 and mode B1. This behavior of normalized error of global modes suggests that there may be some damage occurred around March 6th 2013. The diagrams of the evolution of temperature and the natural frequencies of global modes from 03/03/2013 to 11/03/2013 are shown in Figure 4-29, respectively.

Comparing the evolution of temperature and natural frequencies in this short period, this drop behavior of the natural frequencies didn't coincident with that of the temperature.

Firstly, the observation of the temperature diagram suggests that the daily variation was from 5℃ to 23℃ before March 5th and the daily highest temperature dropped to a stable value at 10℃ from March 5th to 9th. Afterwards, the temperature variation again ranged from 5℃ to 20℃

Then, let us refer to the diagrams of natural frequencies time history of global modes. During the period from 05/03/2013 to 09/03/2013, the value of natural frequency of mode B1 decreased with a slight drop observed around March 6th. Similar behavior was observed both in the curve of mode B2 and mode T1, with the decrease of the three modal frequencies being practically simultaneous, on 06/03/2013.

Furthermore, the decrease of natural frequencies does not show correlation with the temperature (since the temperature was almost constant). Hence, conceivably some slight damage or deterioration or structural change occurred in the tower.

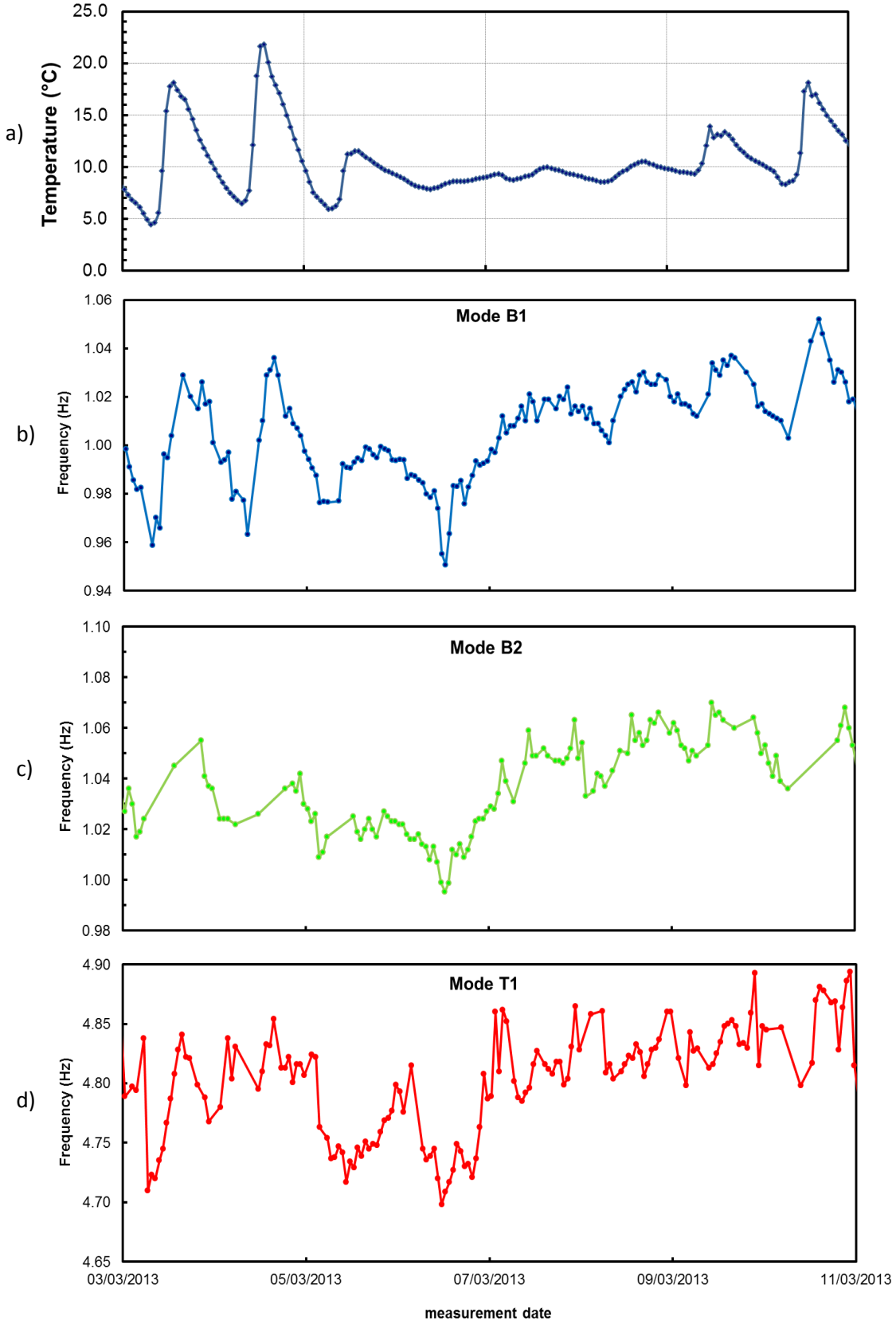

Figure 4-29 Evolution of a) temperature; b) mode B1; c) mode B2; d) mode T1 in the period from 03/03/2013 to 11/03/2013

4.4.4.4 Effects of the earthquake on June 21th 2013

As previously pointed out, during the monitoring of the “Gabbia Tower”, one dataset related to a seismic episode was recorded on 21th June 2013, 12:33 and corresponded to a significant earthquake occurred near Massa, in the Tuscany region in north of Italy. The acceleration of this earthquake was recorded by the monitoring system. One example of the acceleration from the three sensors is shown in Figure 4-30.

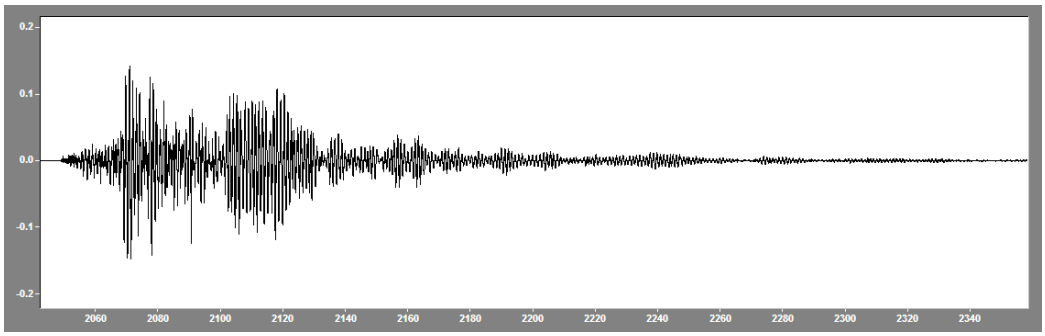

Figure 4-30 Acceleration response associate to the earthquake on June 21th 2013

The evolution in time of temperature and natural frequencies of global modes (B1, B2 and T1) are shown in Figure 4-31 respectively.

The temperature varied normally around the period of earthquake. The daily temperature varied from 22℃ to 40℃. Nevertheless, the fluctuation of the natural frequencies behaved abnormally before and after the earthquake.

The value of the 1st natural frequency (mode B1) decreased from 1.038Hz in the dataset recorded in 11:00-12:00 21th June 2013 to 0.9905Hz in 13:00-14:00 of the same day. And the value of natural frequencies of 2nd (mode B2) and 4th (mode T1) changed from 1.086Hz to 1.041Hz and 4.930Hz to 4.836Hz respectively.

The decrease of natural frequencies of global modes strongly suggests that some damage was caused by the earthquake.

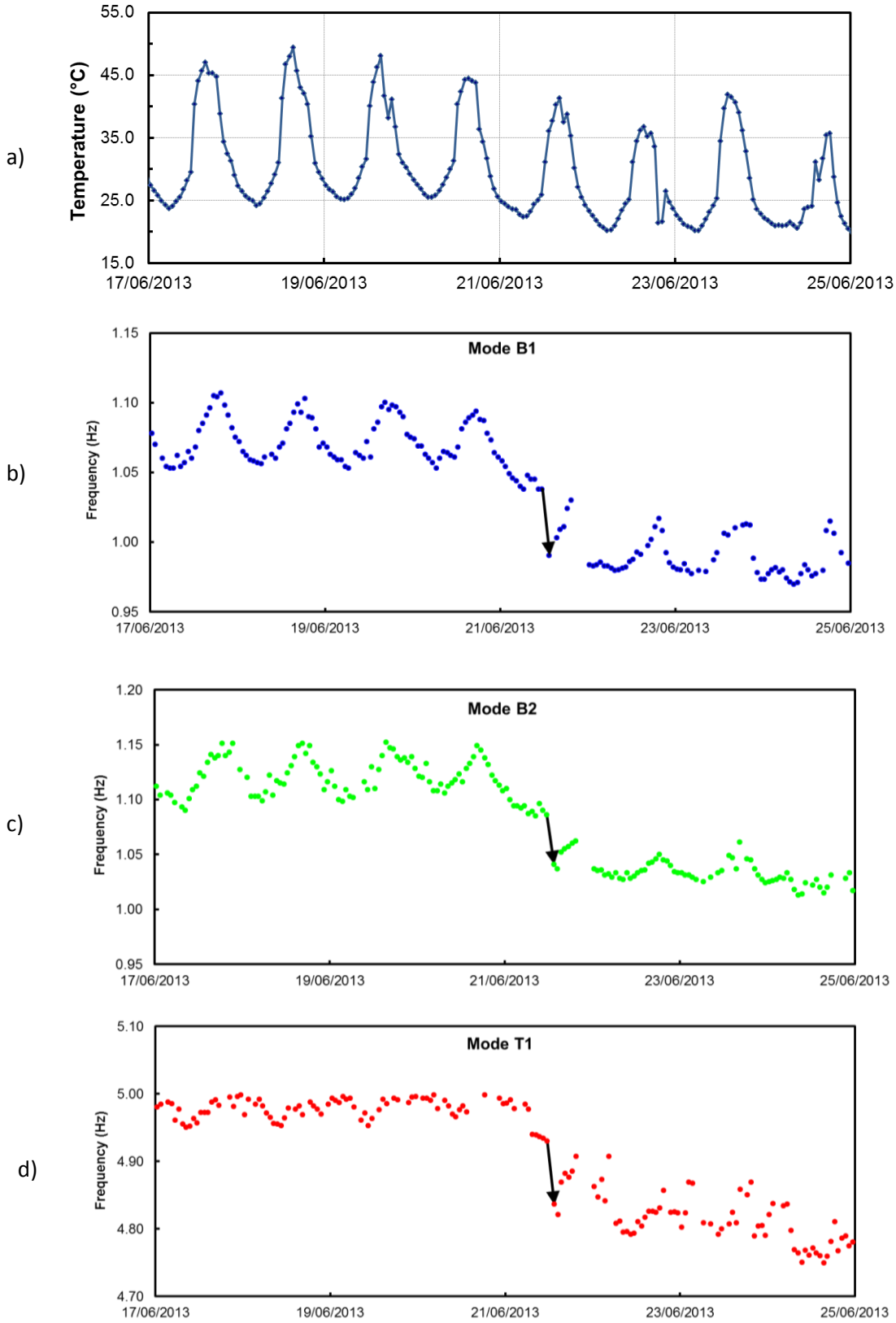

Figure 4-31 Evolution in time of a) temperature; b-d) global modes around the earthquake (21/06/2013)

4.4.3 Effect of temperature: local mode (and structural deterioration)

As already stated in Paragraph 4.4.1, the evolution in time of the natural frequency of the local mode, deserves more concern because the trend of this curve is quite different from the others. More specifically, the modal frequency exhibits significant fluctuations and clearly decreases in time, from an initial value of about 10.0 Hz (17/12/2012) to a final value of about 8.2 Hz at the end of the analyzed period (30/06/2013).

The diagram shown in Figure 4-32 presents the fluctuation curve of the local mode as well as the location of some drops in natural frequency. The inspection of this figure reveals that 4 clear decrement of the modal frequency took place:

(a) between 03/02/2013 and 04/02/2013;

(b) between 14/03/2013 and 15/03/2013;

(c) between 13/04/2013 and 15/04/2013;

(d) around 21/06/2013.

The natural frequency of the local mode is plotted versus temperature in Figure 4-33. Let us refer to this frequency-temperature plot. Generally, it is clear that the natural frequency of the local mode decreased dramatically during the monitoring. In addition, it seems that 4 different “clouds” of frequency-temperature points are identifiable in Figure 4-33 and that the correlation between frequency and temperature is linear in each cloud. The inspection of this diagram provides a new idea of the analysis of the frequency – temperature correlation: drawing the frequency – temperature curves in divided parts to better extract the correlation between the two variables.

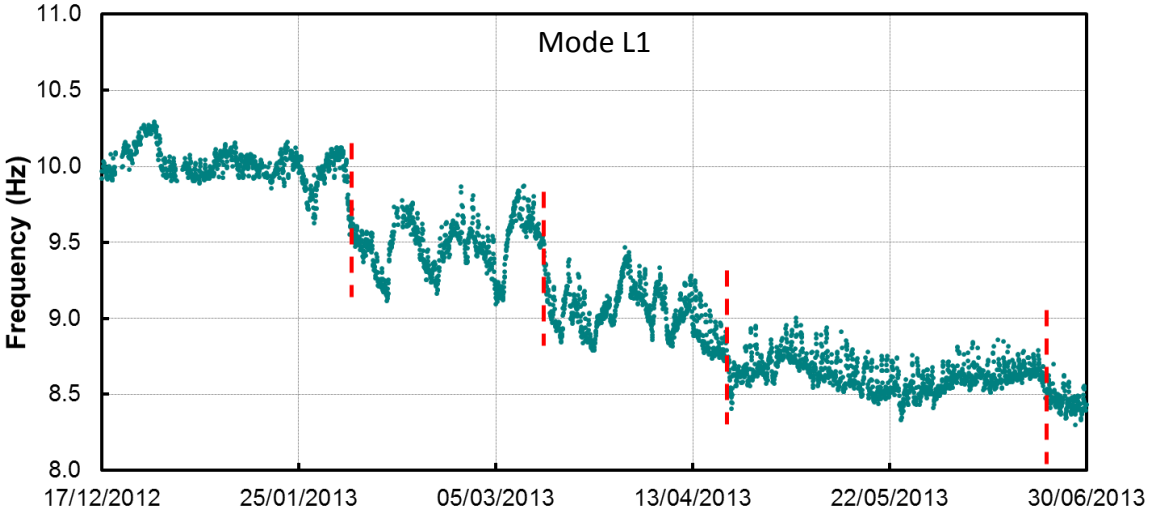

Figure 4-32 Evolution of natural frequency with 4 frequency decrements

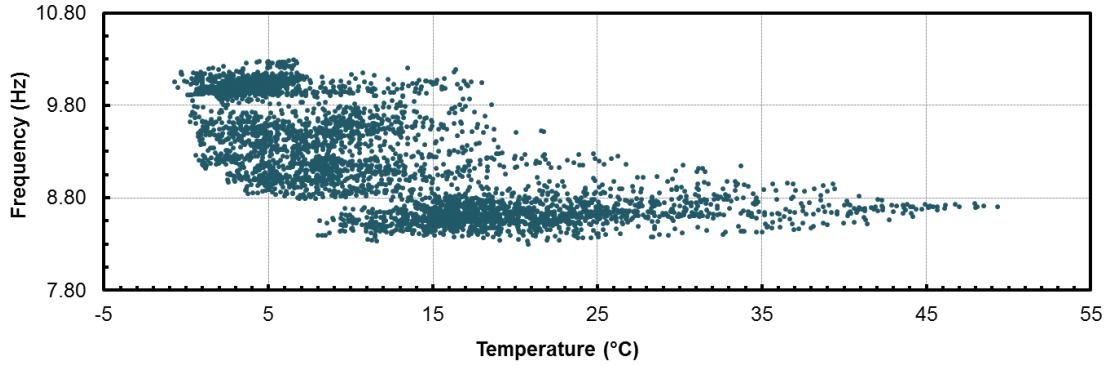

Figure 4-33 Frequency-temperature curve of local mode

In order to better present the evolution of local mode, the period of the results from 07/01/2013 to 12/06/2013 is considered; the evolution in time of the natural frequency of local mode in this period is shown in Figure 4-34, where:

P 01 – Period from 07/01/2013 to 02/02/2013;

P 02 – Period from 05/02/2013 to 14/03/2013;

P 03 – Period from 16/03/2013 to 12/04/2013;

P 04 – Period from 16/04/2013 to 12/06/2013;

According to the divided 4 parts of data, a much clear graph of the correlation between the natural frequency of the local mode and the temperature can be drawn and shown in Figure 4-35. Linear fitting procedure is applied to each part respectively.

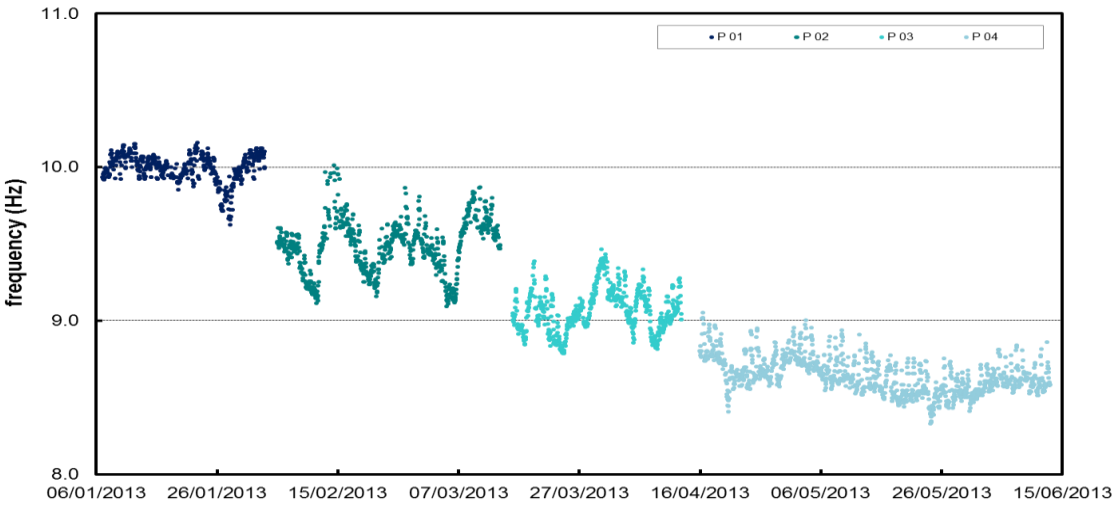

Figure 4-34 time evolution of local mode in 4 periods

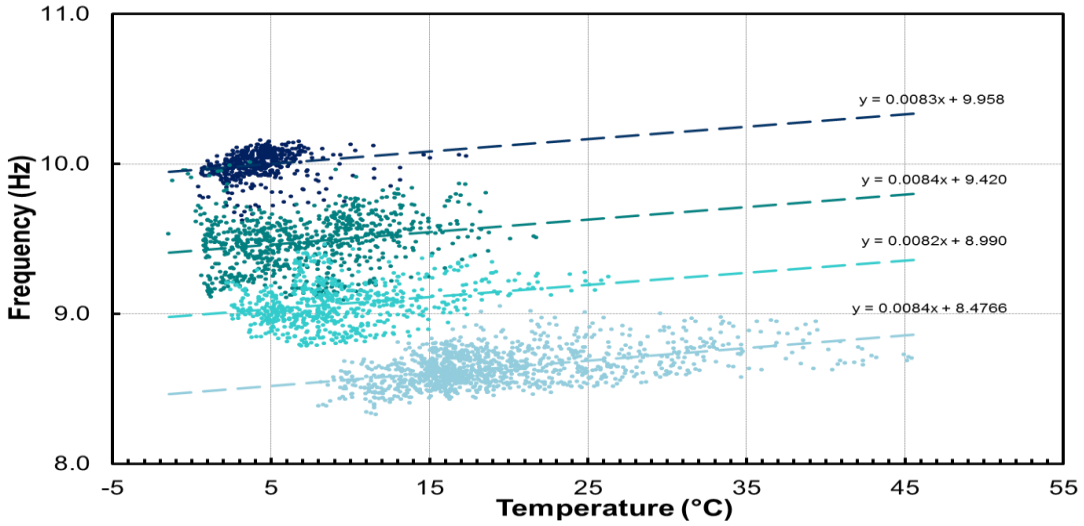

Figure 4-35 linear fitting results of the frequency-temperature curves

The linear fitting equations of the four parts are,

$$f_{\mathrm{P1}}(T_j) = 9.958 + 0.0083T_j \tag{4.2}$$

$$f_{P2}(T_j) = 9.420 + 0.0084T_j \tag{4.3}$$

$$f_{P3}(T_j) = 8.990 + 0.0082T_j \tag{4.4}$$

$$f_{P4}(T_j) = 8.477 + 0.0084T_j \tag{4.5}$$

According to results, some comments can be done:

a) In each part of the diagram, the linear fitting shows that the natural frequency of

the local mode increases with increment temperature. This behavior is coincident with that of the global mode;

b) the slopes of the four linear fitting results are almost the same but the intercept of the four linear fitting results decreased from period 01 to period 04 gradually. The value of the decrement between two adjacent intercepts represents the decrement of natural frequency of local mode between two periods.

The comments drawn from the frequency-temperature diagram suggest the quick progress of a local damage mechanism, conceivably related to the worsening of the binding effect exerted by the wooden roof, and confirms once more the poor structural condition and the high seismic vulnerability of the upper part of the tower, highlighting the urgent need for preservation actions to be performed.

Conclusions

The Thesis presents the results of a continuous dynamic monitoring program carried out on the tallest historic tower in Mantua, Italy. The dynamic monitoring follows an extensive diagnostic investigation carried out by Politecnico di Milano (Polo Territoriale di Mantova), between July and October 2012, to assess the state of preservation of the tower after the seismic events of May 2012. The diagnostic procedures included detailed visual inspections and geometric survey, single and double flat jack tests, pulse sonic tests, laboratory tests on sampled materials and preliminary AVTs (28 hours of almost continuous acquisition).

The results of the post-earthquake investigation highlighted the poor structural condition and the high vulnerability of the upper part of the tower, pointing out the need for structural interventions to be carried out. In order to make possible the planned strengthening, a metal scaffolding and a light wooden roof have been installed inside the tower; furthermore, it was decided to install a simple dynamic monitoring system in the building, as a part of the health monitoring process helping the preservation of the historic structure.

The instrumentation installed inside the tower consists of a 4-channel data acquisition board, with 3 piezoelectric accelerometers and 1 temperature sensor. A binary file, containing 3 acceleration time series (sampled at 200 Hz) and the temperature data, is created every hour, stored in an industrial PC on site and transmitted to Politecnico di Milano for being processed.

The Thesis summarizes the results of the semi-automatic analysis performed by using the DADiSP and ARTeMIS computer codes to identify the modal parameters of the tower in the time period between 17/12/2012 and 30/06/2013.

The time evolution of the modal frequencies identified in the examined time interval (196 days, 470 datasets of 1 hour each) clearly highlights:

i) the effect of temperature on natural frequencies of the vibration modes. More

specifically, the modal frequencies increase with increased temperature;

ii) the quick progress of a damage mechanism, involving the upper part of the tower, and clearly identified through the remarkable fluctuations and the significant decrease (about 15% in 6 months) of the natural frequency corresponding to a local mode;

iii) the decrease of the natural frequencies of the fundamental modes detected after the occurrence of a far-field seismic event, demonstrated by the comparison of the modal peaks identified before and after the earthquake, and confirmed by the subsequent frequency tracking;

iv) the suitability of the prediction error (defined as the difference between the natural frequencies predicted by a simple linear regression model and the actual experimental values) to identify the occurrence of anomalies in the structural behavior (natural frequency) as well as the time of anomaly occurrence.

As a further and more general conclusion, the results indicate that continuous dynamic monitoring and damage detection methods based on natural frequency shifts are sustainable and highly effective tools in the diagnosis of historic masonry towers, providing remarkable evidence of the possible key role of permanent dynamic monitoring in the assessment of Cultural Heritage structures.

References

ASTM. 1991a. Standard test method for in situ compressive stress within solid unit masonry estimated using the flat-jack method. ASTM C 1196-91, Philadelphia: ASTM.

ASTM. 1991b. Standard test method for in situ measurement of masonry deformability properties using flatjack method. ASTM C 1196-91, Philadelphia: ASTM.

Aerojet General Corporation. 1967. Investigation on sonic testing of masonry walls. Final Report to the Dept. of General Services of Architecture and Construction, State of California.

L. Binda, A. Saisi, C. Tiraboschi. Investigation procedures for the diagnosis of historic masonries. Construction and Building Materials 14 2000 199]233

L. Binda & C. Tiraboschi 1999b. Flat-Jack Test as a Slightly Destructive Technique for the Diagnosis of Brick and Stone Masonry Structures. Int. Journal for Restoration of Buildings and Monuments, Int. Zeitschrift fur Bauinstandsetzen und Baudenkmalpflege, Zurich. 449-472.

L. Binda, L. Cantini, G. Cardani, A. Saisi & C. Tiraboschi, 2007b. Use of Flat-Jack and Sonic Tests for the qualification of Historic Masonry. 10th Tenth North American Masonry Conference (10NAMC), St. Louis, Missouri. 791-803.

L. Binda, A. Saisi & C.Tiraboschi, 2001. Application of Sonic Tests to the Diagnosis of Damage and Repaired Structures, Non Destructive Testing and Evaluation Int. 34(2). 123-138.

L.Binda, A. Saisi & L. Zanzi, 2003a. Sonic Tomography and Flat Jack Tests as Complementary Investigation Procedures for the Stone Pillars of the Temple of S.Nicolo' L'Arena (Italy). Non Destructive Testing and Evaluation Int 36(4). 215-227.

L. Binda, L. Cantini, G. Cardani, A. Saisi & C. Tiraboschi, 2007b. Use of Flat-Jack and Sonic Tests for the qualification of Historic Masonry. 10th Tenth North American Masonry Conference (10NAMC), St. Louis, Missouri. 791-803.

L. Binda, A. Saisi, C. Tiraboschi. Investigation procedures for the diagnosis of historic masonries. Construction and Building Materials 14 2000 199]233

F. Benedettini, C. Gentile. Operational modal testing and FE model tuning of a cable-stayed bridge. Engineering Structures 33 (2011) 2063–2073

C. Blasi, F. Ottoni, New studies on Brunelleshi's Dome in Florence from historical to modern monitoring data analysis. The effect of encircling scaffoldings on crack evolution, Domes in the world, 19-23 March 2012, Florence, Italy

R. Brincker, C.E. Ventura, P. Andersen, (2001b), Damping estimation by frequency domain decomposition, Proc. 19th International Modal Analysis Conference (IMAC), in IMAC XIX, Kissimmee, Florida, USA, CD-ROM.

R. Brincker, L. Zhang, P. Andersen, (2001a), Modal identification of output-only systems using frequency domain decomposition, Smart Material and Structures, 10(3): 441-445.

R. Brincker, (2010a), Special issue in Operational Modal Analysis, Editorial, Mechanical Systems and Signal Processing, 24(5): 1209-1212.

R. Brincker, (2010b), Ideas and concepts of OMA. Lecture at course "Monitoring, Control and Identification of Bridges by Dynamic Methods", CISM, Udine, Italy.

R. Brincker, P. Andersen, N.J. Jacobsen, (2007), Automated Frequency Domain Decomposition for Operational Modal Analysis, Proc. 24th International Modal Analysis Conference (IMAC), in IMAC XXIV, Orlando, Florida, USA, CD-ROM.

J. Bendat, A. Piersol, (1993), Engineering Applications of Correlation and Spectral Analysis, 2nd Edition, John Wiley & Sons Ltd.

Á. Cunha, E. Caetano, C. Moutinho, F. Magalhães, W.H. Hu, F. Marques, (2011), Dynamic Monitoring of Bridges at ViBest/FEUP, Proc. 4th International Conference on Experimental Vibration Analysis of Civil Engineering Structures (EVACES), in EVACES 2011, C. Gentile & F. Benedettini (eds.), Varenna, Italy, pp. 97-105.

DADISP. The DADiSP™ Worksheet-Data Analysis and Display Software: Function Reference Manual 2003

A. Dura, M. Boquera, L. Pulido, M. Puchalt, Structural Behaviour analysis of the dome of the cathedral of Valencia, 2012DWE, Wroctaw, Poland, ISSN 0860-2395, ISBN 978-83-7125-216-7

D.J. Ewins, (2000), Modal Testing: Theory and Practice, Research Studies Press, UK.

A. Giuffrè A, (editor), (1993), Sicurezza e conservazione dei centri storici in area sismica, il caso Ortigia, Laterza, Bari, (in Italian).

C. Gentile, A. Saisi . Ambient Vibration Testing of Historical Masonry Tower for Structural Identification and Damage Assessment. Constr Build Mater 2007;21:1311–21.

C. Gentile, A. Saisi, M. Guidobaldi, Torre della Gabbia, Mantova: Esecuzione di indagini sperimentali post-sima. Indagini di caratterizzazione dinamica. Politecnico di Milano, Polo Territoriale di Mantova, 2012.

A. Felber, (1993), Development of a Hybrid Bridge Evaluation System, Ph.D. Thesis, University of British Columbia, Vancouver, Canada.

P. Moser, B. Moaveni. Environmental effects on the identified natural frequencies of the Dowling Hall Footbridge. Mechanical Systems and Signal Processing 25 (2011) 2336–2357

N.N. Minh, H. Yamada, T. Miyata, H. Katsuchi, Aeroelastic complex mode analysis for coupled gust response of the Akashi Kaikyo bridge model, Journal of Wind Engineering and Industrial Aerodynamics 88 (2–3) (2000) 307–324.

F. Magalhães, Á. Cunha, E. Caetano, (2012), Vibration based structural health monitoring of an arch bridge: From automated OMA to damage detection, Mechanical Systems and Signal Processing, 28: 212-228.

F. Magalhães, Á. Cunha, (2011), Explaining operational modal analysis with data from an arch bridge, Mechanical Systems and Signal Processing, 25(5): 1431-1450.

F. Ottoni, C. Blasi, The role of structural monitoring in historical building conservation, Structural Analysis of historical construction, 2012

Van Overschee, P., DeMoor, B. (1996), Subspace Identification for Linear Systems –

Theory, Implementation, Applications, Kluwer Academic Publishers.

F. J. Pallarés, S. Ivorra , L. Pallarés , J. M. Adam. State of the art of industrial masonry chimneys: A review from construction to strengthening. Construction and Building Materials 25 (2011) 4351–4361

B. Peeters, H. Van der Auweraer, (2005a), Vibration-based structural monitoring: Measurements and data processing, Proc. 6th European Conference on Structural Dynamics (EURODYN), in EURODYN 2005, C. Soize & G.I. Schuëller (eds.), Paris, France, pp. 275-280.

B. Peeters, H. Van der Auweraer, (2005b), POLYMAX: a revolution in operational modal analysis, Proc. 1st International Operational Modal Analysis Conference (IOMAC), in IOMAC 2005, R. Brincker & N. Møller (eds.), Copenhagen, Denmark, pp. 41-51.

B. Peeters, (2000), System Identification and Damage Detection in Civil Engineering, Ph.D. Thesis, Dept. of Civil Engineering, Katholieke Universiteit, Leuven, Belgium.

P.P. Rossi, 1982. Analysis of mechanical characteristics of brick masonry tested by means of in situ tests, 6th IBMaC, Rome, Italy.

L.F. Ramos, L. Marques, P.B. Lourenco, G. De Roeck, A. Campos-Costa, J. Roque. Monitoring historical masonry structures with operational modal analysis: Two case studies. Mechanical Systems -and Signal Processing 24 (2010) 1291–1305

L.F. Ramos, R. Aguilar, P.B. Lourenco, S. Moreira. Dynamic structural health monitoring of Saint Torcato church. Mechanical Systems and Signal Processing 35 (2013) 1–15

C. Rainieri, G. Fabbrocino, E. Cosenza, (2011), Near real-time tracking of dynamic properties for standalone structural health monitoring systems, Mechanical Systems and Signal Processing, 25(8): 3010-3026.

SVS. ARTeMIS Extractor Maual 2012. http://www.svibs.com

A. Saisi, C. Gentile, Torre della Gabbia, Mantova: Esecuzione di indagini sperimentali post-sima. Rilievi diagnostici dei paramenti murari. Politecnico di Milano, Polo Territoriale di Mantova, 2013.

D. H. Timm, A. L. Priest, DYNAMIC PAVEMENT RESPONSE DATA COLLECTION AND

PROCESSING AT THE NCAT TEST TRACK, NCAT Report 04-03 2004;

C. Tiraboschi, L. Cantini, Torre della Gabbia, Mantova: Prove con martinetti piatti sulle strutture murarie e prove di laboratorio sui materiali prelevati. Politecnico di Milano, Laboratorio Prove Materiali, 2013.

N. Zuccoli,1988. Historic research on the Gabbia tower (in Italian). Internal Report, Municipality of Mantua.